

---

Report No. K-TRAN: KSU-06-2  
FINAL REPORT

## **EFFECTS OF AMBIENT TEMPERATURE CHANGES ON INTEGRAL BRIDGES**

Bhavik R. Shah, M.S.  
Dunja Peric, Ph.D.  
Asad Esmaeily, Ph.D., P.E.  
Kansas State University  
Manhattan, Kansas

September 2008

A COOPERATIVE TRANSPORTATION RESEARCH PROGRAM  
BETWEEN:

KANSAS DEPARTMENT OF TRANSPORTATION  
KANSAS STATE UNIVERSITY  
UNIVERSITY OF KANSAS



<b>1 Report No.</b> K-TRAN: KSU-06-2	<b>2 Government Accession No.</b>	<b>3 Recipient Catalog No.</b>	
<b>4 Title and Subtitle</b> <b>EFFECTS OF AMBIENT TEMPERATURE CHANGES ON INTEGRAL BRIDGES</b>		<b>5 Report Date</b> September 2008	
		<b>6 Performing Organization Code</b>	
<b>7 Author(s)</b> Bhavik R. Shah, M.S., Dunja Perić, Ph.D., Asad Esmaeily, Ph.D., P.E.		<b>8 Performing Organization Report No.</b>	
<b>9 Performing Organization Name and Address</b> Department of Civil Engineering Kansas State University 2118 Fiedler Hall Manhattan, Kansas 66506		<b>10 Work Unit No. (TRAIS)</b>	
		<b>11 Contract or Grant No.</b> C1579	
<b>12 Sponsoring Agency Name and Address</b> Kansas Department of Transportation Bureau of Materials and Research 700 SW Harrison Street Topeka, Kansas 66603-3745		<b>13 Type of Report and Period Covered</b> Final Report August 2005 - January 2008	
		<b>14 Sponsoring Agency Code</b> RE-0403-01	
<b>15 Supplementary Notes</b> For more information write to address in block 9.			
<b>16 Abstract</b>  <p>Integral Bridges (IBs) are joint-less bridges whereby the deck is continuous and monolithic with abutment walls. IBs are outperforming their non-integral counterparts in economy and safety. Their principal advantages are derived from the absence of expansion joints and sliding bearings in the deck, making them the most cost-effective system in terms of construction, maintenance, and longevity. The main purpose of constructing IBs is to prevent the corrosion of structure due to water seepage through joints. The simple and rapid construction provides smooth, uninterrupted deck that is aesthetically pleasing and safer for riding. The single structural unit increases the degree of redundancy enabling higher resistance to extreme events.</p> <p>However, the design of IBs not being an exact science poses certain critical issues. The continuity achieved by this construction results in thermally induced deformations. These in turn introduce a significantly complex and nonlinear soil-structure interaction into the response of abutment walls and piles of the IB. The unknown soil response and its effect on the stresses in the bridge, creates uncertainties in the design.</p> <p>To gain a better understanding of the mechanism of load transfer due to thermal expansion, which is also dependent on the type of the soil adjacent to the abutment walls and piles, a 3D finite element analysis is carried out on a representative IB using state-of-the-art finite element code ABAQUS/Standard 6.5-1. A literature review focusing on past numerical studies of IBs is presented, followed by details of the numerical model developed in this study using the interactive environment ABAQUS/CAE 6.5-1 along with the analysis details. A discussion of results of the analysis of the IB with three different soil conditions, each experiencing three different temperature change scenarios is presented. Conclusions of the study and recommendations for future research wrap up the report. The advancement of knowledge enabled by this research will provide a basis for introduction of new guidelines in Kansas Bridge Design Manual.</p>			
<b>17 Key Words</b> Integral bridge, IB, thermal expansion, Kansas Bridge Design Manual		<b>18 Distribution Statement</b> No restrictions. This document is available to the public through the National Technical Information Service, Springfield, Virginia 22161	
<b>19 Security Classification (of this report)</b> Unclassified	<b>20 Security Classification (of this page)</b> Unclassified	<b>21 No. of pages</b> 187	<b>22 Price</b>



# **EFFECTS OF AMBIENT TEMPERATURE CHANGES ON INTEGRAL BRIDGES**

**Final Report**

Prepared by

Bhavik R. Shah, M.S.  
Dunja Perić, Ph.D.  
Asad Esmaily, Ph.D., P.E.

Kansas State University  
Department of Civil Engineering  
2118 Fiedler Hall  
Manhattan, Kansas 66506

A Report on Research Sponsored By

THE KANSAS DEPARTMENT OF TRANSPORTATION  
TOPEKA, KANSAS

September 2008

© Copyright 2008, **Kansas Department of Transportation**

## **PREFACE**

The Kansas Department of Transportation's (KDOT) Kansas Transportation Research and New-Developments (K-TRAN) Research Program funded this research project. It is an ongoing, cooperative and comprehensive research program addressing transportation needs of the state of Kansas utilizing academic and research resources from KDOT, Kansas State University and the University of Kansas. Transportation professionals in KDOT and the universities jointly develop the projects included in the research program.

## **NOTICE**

The authors and the state of Kansas do not endorse products or manufacturers. Trade and manufacturers' names appear herein solely because they are considered essential to the object of this report.

This information is available in alternative accessible formats. To obtain an alternative format, contact the Office of Transportation Information, Kansas Department of Transportation, 700 SW Harrison, Topeka, Kansas 66603-3745 or phone (785) 296-3585 (Voice) (TDD).

## **DISCLAIMER**

The contents of this report reflect the views of the authors who are responsible for the facts and accuracy of the data presented herein. The contents do not necessarily reflect the views or the policies of the state of Kansas. This report does not constitute a standard, specification or regulation.

## **ABSTRACT**

Integral Bridges (IBs) are joint-less bridges whereby the deck is continuous and monolithic with abutment walls. IBs are outperforming their non-integral counterparts in economy and safety. Their principal advantages are derived from the absence of expansion joints and sliding bearings in the deck, making them the most cost-effective system in terms of construction, maintenance, and longevity. The main purpose of constructing IBs is to prevent the corrosion of structure due to water seepage through joints. The simple and rapid construction provides smooth, uninterrupted deck that is aesthetically pleasing and safer for riding. The single structural unit increases the degree of redundancy enabling higher resistance to extreme events.

However, the design of IBs not being an exact science poses certain critical issues. The continuity achieved by this construction results in thermally induced deformations. These in turn introduce a significantly complex and nonlinear soil-structure interaction into the response of abutment walls and piles of the IB. The unknown soil response and its effect on the stresses in the bridge, creates uncertainties in the design.

To gain a better understanding of the mechanism of load transfer due to thermal expansion, which is also dependent on the type of soil adjacent to the abutment walls and piles, a 3D finite element analysis is carried out on a representative IB using state-of-the-art finite element code ABAQUS/Standard 6.5-1. A literature review focusing on past numerical studies of IBs is presented, followed by details of the numerical model developed in this study using the interactive environment ABAQUS/CAE 6.5-1 along with the analysis details. A discussion of results of the analysis of the IB with three

different soil conditions, each experiencing three different temperature change scenarios is presented. Conclusions of the study and recommendations for future research wrap up the report. The advancement of knowledge enabled by this research will provide a basis for introduction of new guidelines in Kansas Bridge Design Manual.

# TABLE OF CONTENTS

Abstract .....	iii
Table of Contents .....	v
List of Figures .....	viii
List of Tables .....	xi
Acknowledgements .....	xvi
Chapter 1 - Introduction .....	1
1.1 Background .....	1
1.2 Integral Bridge Concept .....	1
1.2.1 What are Integral Bridges? .....	1
1.2.2 History of Integral Bridges .....	3
1.2.3 Advantages of Integral Bridges .....	3
1.2.4 Critical Design Issue – Soil-Structure Interaction .....	4
1.3 Objectives and Scope of Research .....	5
1.4 Contents of Report .....	6
Chapter 2 - Literature Review .....	7
2.1 Introduction .....	7
2.2 Past Finite Element Studies on IBs .....	9
2.2.1 “Nonlinear Analysis of Integral Bridges: Finite-Element Model” .....	9
2.2.2 “Analysis of Soil-Pile Interaction in Integral Abutment” .....	12
2.2.3 “Field Monitoring and 3D FE Modeling of an Integral Bridge in West Virginia” .....	17
Chapter 3 - Numerical Modeling .....	23
3.1 The Bridge Model .....	23
3.2 Loads .....	26
3.3 Concrete and Steel properties .....	27
3.4 Soil Model and its Properties .....	28
3.4.1 Springs Behind Abutment .....	28
3.4.2 Springs Behind Piles .....	36
3.4.3 Convergence of Iterations .....	39
3.5 Bridge Model Including Approach Slab .....	39

3.5.1 Temperatures .....	40
3.5.2 Springs .....	41
Chapter 4 - Results and Discussion .....	45
4.1 Nomenclature .....	45
4.2 Results .....	46
4.2.1 Displacements .....	46
4.2.2 Stresses .....	48
4.3 Comparison of the Two FE Models .....	48
4.3.1 Differences in the Bridge Model .....	48
4.3.2 Differences in Material Properties .....	50
4.3.3 Differences in Soil Model.....	50
4.3.4 Differences in Loads.....	51
4.4 Validation and Verification of the Model .....	52
4.5 Results and Discussion .....	54
4.5.1 Longitudinal Displacement at Centerline of the Bridge.....	57
4.5.1.1 Trends Due to Change in the Thermal Load for the Particular Soil Properties ..	57
4.5.1.2 Trends Due to Change in Soil Properties for the Particular Thermal Load .....	58
4.5.1.3 Discussion .....	59
4.5.2 Central Pile Bending Moment.....	65
4.5.2.1 Trends Due to Change in Thermal Load for the Particular Soil Properties .....	65
4.5.2.2 Trends Due to Change in Soil Properties for the Particular Thermal Load .....	66
4.5.2.3 Discussion .....	67
4.5.3 Central Pile Bending Stress .....	69
4.5.3.1 Trends Due to Change in Thermal Load for the Particular Soil Properties .....	69
4.5.3.2 Trends Due to Change in Soil Properties for the Particular Thermal Load .....	70
4.5.3.3 Discussion .....	71
4.5.4 Soil pressure on abutment .....	72
4.5.4.1 Trends Due to Change in Thermal Load for the Particular Soil Properties .....	72
4.5.4.2 Trends Due To Change in Soil Properties for the Particular Thermal Load.....	73
4.5.4.3 Discussion .....	74
4.5.5 Comparisons between the Central Pile and End Pile .....	75

4.5.5.1 Longitudinal displacement.....	75
4.5.5.2 Pile Bending Moment.....	76
4.5.5.3 Pile Bending Stress.....	77
4.5.5.4 Discussion.....	78
4.5.6 Axial Compressive Stress in Girders.....	78
4.5.7 Convergence of Iterations.....	79
4.6 Results for the Bridge with Approach Slab.....	88
4.6.1 Longitudinal Displacement at Centerline of the Bridge.....	89
4.6.1.1 Trends Due to Change in Soil Properties for the Particular Thermal Load.....	89
4.6.1.2 Discussion.....	90
4.6.2 Central Pile Bending Moment.....	94
4.6.2.1 Trends Due to Change in Soil Properties for the Particular Thermal Load.....	94
4.6.2.2 Discussion.....	95
4.6.3 Central Pile Bending Stress.....	96
4.6.3.1 Trends Due to Change in Soil Properties for the Particular Thermal Load.....	96
4.6.3.2 Discussion.....	97
4.6.4 Soil pressure on Abutment.....	99
4.6.4.1 Trends Due To Change in Soil Properties for the Particular Thermal Load.....	99
4.6.4.2 Discussion.....	99
4.6.5 Comparisons between the Central Pile and End Pile.....	100
4.6.5.1 Pile Bending Moment.....	100
4.6.5.2 Discussion.....	101
4.6.6 Axial Compressive Stress in Girders.....	101
4.6.7 Bending Stress in Approach Slab.....	101
4.6.8 Convergence of Iterations.....	102
4.6.9 Soil Pressure on Approach Slab.....	105
Chapter 5 - Conclusions and Recommendations.....	107
5.1 Conclusions.....	109
5.2 Recommendations.....	112
References.....	115
Appendix A - Tabular data of results.....	119

## LIST OF FIGURES

Figure 1.1: Simplified Geometry of an Integral Bridge (Arsoy, 2000) .....	2
Figure 2.2: GT-STRUDL Finite Element Model of the Bridge (Faraji et al., 2001).....	10
Figure 2.3: Finite Element Model Details for North Abutment Wall and HP Piles (Faraji et al., 2001) .....	11
Figure 2.4: Elevation View of the Scotch Road, I-95 IB (Khodair & Hassiotis, 2005) ....	13
Figure 2.5: Instrumentation of Experimental Devices on the Substructure of the Scotch Road, I-95 IB (Khodair & Hassiotis, 2005) .....	14
Figure 2.6: Evansville Bridge (a) Elevation (b) Side View (c) Plan (Shoukry et al., 2006) .....	18
Figure 2.7: Finite Element Model of Evansville Bridge (a) Full Model (b) Non-Linear Springs Modeling the Soil-Abutment Interaction (c) Non-Linear Springs Modeling the Soil-Pile Interaction (Shoukry et al., 2006).....	20
Figure 3.1: Schematics of the Bridge (Faraji et al., 2001) .....	23
Figure 3.2: Schematics of FE Model of the Bridge .....	24
Figure 3.3: Finite Element Model of the Bridge (Including the Soil Substituting Springs)	26
Figure 3.4: Nodal Temperatures for $\Delta T = 80^{\circ}F$ .....	27
Figure 3.5: Abutment Motion .....	30
Figure 3.6: Design Curves Recommended by NCHRP (1991).....	31
Figure 3.7: Design Curves Recommended by CGS (1992).....	33
Figure 3.8: Vertical Zones of the Abutment and the Corresponding Nodes .....	34
Figure 3.9: Arrangement of Springs Behind a Pile .....	37
Figure 3.10: Finite Element Model of the Bridge with Approach Slab (Including the Soil Substituting Springs) .....	40
Figure 3.11: Nodal Temperatures .....	41
Figure 3.12: Vertical Zones of the Abutment and the Corresponding Nodes .....	42
Figure 4.1: DD $100^{\circ}F$ - Longitudinal Displacement U1 (in) of the Bridge (Deformation Scale Factor=130).....	46
Figure 4.2: DD $100^{\circ}F$ - Vertical Displacement U2 (in) of the Bridge (Deformation Scale Factor=130).....	47

Figure 4.3: DD 100°F - Lateral Displacement U3 (in) of the Bridge (Deformation Scale Factor=130).....	47
Figure 4.4: DD 100°F - Axial Stress S22 (psi) in the Piles (Deformation Scale Factor=130).....	48
Figure 4.5: DD 100°F - Axial Stress S11 (psi) in the Girders (Deformation Scale Factor=130).....	49
Figure 4.6: Nodal Temperatures ( ° F) with the Abutment Detail .....	52
Figure 4.7: Comparison of Longitudinal Displacements, U1 (in) .....	53
Figure 4.8: Converged Values of K for DcD 100°F case .....	55
Figure 4.9: Converged Values of K for DD 100°F and LD 100°F cases .....	56
Figure 4.10: Trends in Longitudinal Displacement Due to Changes in Thermal Load...	57
Figure 4.11: Trends in Longitudinal Displacement Due to Changes in Soil Properties .	58
Figure 4.12: Displacement (in) at the Abutment Top vs. $\Delta T$ ( ° F) .....	60
Figure 4.13: $\delta_T$ (in) and $\delta_R$ (in) vs. $\Delta T$ ( ° F) .....	61
Figure 4.14: Comparison of Deck Displacements (in) .....	63
Figure 4.15: Trends in Central Pile Bending Moment (kip-ft) Due to Changes in Thermal Load .....	65
Figure 4.16: Trends in Central Pile Bending Moment (kip-ft) Due to Changes in Soil Properties.....	66
Figure 4.17: Displacement (in) at the Pile Top in Central Pile vs. $\Delta T$ .....	67
Figure 4.18: Maximum Bending Moment (kip-ft) in Central Pile Vs. $\Delta T$ .....	68
Figure 4.19: Trends in Central Pile Bending Stress (ksi) Due to Changes in Thermal Load .....	69
Figure 4.20: Trends in Central Pile Bending Stress (ksi) Due to Changes in Soil Properties.....	70
Figure 4.21: Maximum Bending Stress (ksi) in Central Pile vs. $\Delta T$ .....	71
Figure 4.22: Trends in Soil Pressure (psi) on Abutment Due to Changes in Thermal Load .....	72
Figure 4.23: Trends in Soil Pressure (psi) on Abutment Due to Changes in Soil Properties.....	73
Figure 4.24: Comparison of Longitudinal Displacements (in) of Central and End Piles	75

Figure 4.25: Comparison of Bending Moments (kip-ft) in Central and End Piles.....	76
Figure 4.26: Comparison of Bending Stresses (ksi) in Central and End Piles.....	77
Figure 4.27: Maximum Axial Stress S11 (ksi) in the Central Girder vs. $\Delta T$ .....	79
Figure 4.28: Convergence of Translational Displacement for $\Delta T= 60^{\circ}\text{F}$ .....	82
Figure 4.29: Convergence of Rotational Displacement $\Delta T= 60^{\circ}\text{F}$ .....	83
Figure 4.30: Convergence of Translational Displacement for $\Delta T= 80^{\circ}\text{F}$ .....	84
Figure 4.31: Convergence of Rotational Displacement for $\Delta T= 80^{\circ}\text{F}$ .....	85
Figure 4.32: Convergence of Translational Displacement for $\Delta T= 100^{\circ}\text{F}$ .....	86
Figure 4.33: Convergence of Rotational Displacement for $\Delta T= 100^{\circ}\text{F}$ .....	87
Figure 4.34: Trends in Longitudinal Displacement Due to Changes in Soil Properties .	89
Figure 4.35: Displacement Comparisons – Bridge with and without Approach Slab .....	90
Figure 4.36: Trends in Central Pile Bending Moment (kip-ft) Due to Changes in Soil Properties.....	94
Figure 4.37: Comparison of Bending Moments (kip-ft) in Bridges with and without Approach Slabs.....	95
Figure 4.38: Trends in Central Pile Bending Stress (ksi) Due to Changes in Soil Properties.....	96
Figure 4.39: Comparison of Bending Stresses (ksi) in Bridges with and without Approach Slabs .....	98
Figure 4.40: Trends in Soil Pressure on Abutment Due to Changes in Soil Properties .	99
Figure 4.41: Comparison of Bending Moments (kip-ft) in Central and End Piles.....	100
Figure 4.42: Convergence of Translational Displacement.....	103
Figure 4.43: Convergence of Rotational Displacement .....	104
Figure 4.44: Soil Pressure on Approach Slab .....	105

## LIST OF TABLES

Table 3.1: Material Properties .....	28
Table 3.2: Soil Properties .....	32
Table3.3: Dry Unit Weights of Soils.....	33
Table 4.1: Soil Combination Nomenclature .....	45
Table 4.2: Nomenclature for the Cases Studied.....	46
Table 4.3: Converged Values of the Coefficient of Lateral Earth PressureK .....	54
Table 4.4: Values of the Coefficients of the Exponential Function .....	80
Table 4.5: Values of the Coefficients of the Exponential Function .....	81
Table4.6: Values of the Coefficients of the Exponential Function .....	81
Table 4.7: Converged Values of the Coefficient of Lateral Earth PressureK .....	88
Table 4.8: Comparisons of Displacements (in).....	91
Table 4.9: Comparisons of Deck and Approach Slab Displacements (in) .....	92
Table 4.10: Comparisons of Translational and Rotational Displacements (in) of the Abutment Top .....	93
Table 4.11: Maximum Bending Stresses (ksi) in Central Piles .....	97
Table 4.12: Maximum Axial Stress (ksi) in the Central Girder .....	101
Table 4.13: Maximum Axial Stresses (ksi) in the Approach Slab .....	102
Table 4.14: Values of the Coefficients of Exponential Function .....	102
Table A.1: Comparison of Longitudinal Displacements – Shah vs. Ting & Faraji (1998) (Refer Figure 4.7).....	120
Table A.2: LD - Trends in Longitudinal Displacement Due to Changes in Thermal Load (Refer Figure 4-10).....	121
Table A.3: DD - Trends in Longitudinal Displacement Due to Changes in Thermal Load (Refer Figure 4.10).....	122
Table A.4: DcD - Trends in Longitudinal Displacement Due to Changes in Thermal Load (Refer Figure 4.10).....	123
Table A.5; 60°F - Trends in Longitudinal Displacement Due to Changes in Soil Properties (Refer Figure 4.11).....	124

Table A.6: 80°F - Trends in Longitudinal Displacement Due to Changes in Soil Properties (Refer Figure 4.11).....	125
Table A.7: 100°F - Longitudinal Displacement Due to Changes in Soil Properties (Refer Figure 4.11).....	126
Table A.8: Displacement at Abutment Top vs. $\Delta T$ (Refer Figure 4.12).....	127
Table A.9: $\delta_T$ and $\delta_R$ vs. $\Delta T$ (Refer Figure 4.13).....	127
Table A.10: LD - Comparison of Deck Displacement (Refer Figure 4.14).....	127
Table A.11: DD - Comparison of Deck Displacement (Refer Figure 4.14).....	128
Table A.12: DcD - Comparison of Deck Displacement (Refer Figure 4.14).....	128
Table A.13: LD - Trends in Central Pile Bending Moment Due to Changes in Thermal Load (Refer Figure 4.15).....	129
Table A.14: DD - Trends in Central Pile Bending Moment Due to Changes in Thermal Load (Refer Figure 4.15).....	130
Table A.15: DcD - Trends in Central Pile Bending Moment Due to Changes in Thermal Load (Refer Figure 4.15).....	131
Table A.16: 60°F - Trends in Central Pile Bending Moment Due to Changes in Soil Properties (Refer Figure 4.16).....	132
Table A.17: 80°F - Trends in Central Pile Bending Moment Due to Changes in Soil Properties (Refer Figure 4.16).....	133
Table A.18: 100°F - Trends in Central Pile Bending Moment Due to Changes in Soil Properties (Refer Figure 4.16).....	134
Table A.19: Displacement at the Pile Top in Central Pile vs. $\Delta T$ (Refer Figure 4.17)..	135
Table A.20: Maximum Bending Moment in Central Pile vs. $\Delta T$ (Refer Figure 4.18)....	135
Table A.21: LD - Trends in Central Pile Bending Stress Due to Changes in Thermal Load (Refer Figure 4.19).....	136
Table A.22: DD - Trends in Central Pile Bending Stress Due to Changes in Thermal Load (Refer Figure 4.19).....	137
Table A.23: DcD - Trends in Central Pile Bending Stress Due to Changes in Thermal Load (Refer Figure 4.19).....	138
Table A.24: 60°F – Trends in Central Pile Bending Stress Due to Changes in Soil Properties (Refer Figure 4.20).....	139

Table A.25: 80°F – Trends in Central Pile Bending Stress Due to Changes in Soil Properties (Refer Figure 4.20).....	140
Table A.26: 100°F – Trends in Central Pile Bending Stress Due to Changes in Soil Properties (Refer Figure 4.20).....	141
Table A.27: Maximum Bending Stress in Central Pile vs. $\Delta T$ (Refer Figure 4.21).....	142
Table A.28: LD – Trends in Soil Pressure on Abutment Due to Changes in Thermal Load (Refer Figure 4.22).....	142
Table A.29: DD – Trends in Soil Pressure on Abutment Due to Changes in Thermal Load (Refer Figure 4.22).....	142
Table A.30: DcD – Trends in Soil Pressure on Abutment Due to Changes in Thermal Load (Refer Figure 4.22).....	143
Table A.31: 60°F – Trends in Soil Pressure on Abutment Due to Changes in Soil Properties (Refer Figure 4.23).....	143
Table A.32: 80°F – Trends in Soil Pressure on Abutment Due to Changes in Soil Properties (Refer Figure 4.23).....	144
Table A.33: 100°F – Trends in Soil Pressure on Abutment Due to Changes in Soil Properties (Refer Figure 4.23).....	144
Table A.34: LD - Longitudinal Displacement Comparison of Central Pile vs. End Pile (Refer Figure 4.24).....	145
Table A.35: DD - Longitudinal Displacement Comparison of Central Pile vs. End Pile (Refer Figure 4.24).....	146
Table A.36: DcD - Longitudinal Displacement Comparison of Central Pile vs. End Pile (Refer Figure 4.24).....	147
Table A.37: LD – Bending Moment Comparison of Central Pile vs. End Pile (Refer Figure 4.25).....	148
Table A.38: DD – Bending Moment Comparison of Central Pile vs. End Pile (Refer Figure 4.25).....	149
Table A.39: DcD – Bending Moment Comparison of Central Pile vs. End Pile (Refer Figure 4.25).....	150
Table A.40: LD – Bending Stress Comparison of Central Pile vs. End Pile (Refer Figure 4.26).....	151

Table A.41: DD – Bending Stress Comparison of Central Pile vs. End Pile (Refer Figure 4.26).....	152
Table A.42: DcD – Bending Stress Comparison of Central Pile vs. End Pile (Refer Figure 4.26).....	153
Table A.43: Maximum Axial Stress in the Central Girder vs. $\Delta T$ (Refer Figure 4.27) ..	154
Table A.44: LD 60°F - Convergence of Displacement (Refer Figure 4.28, 4.29).....	154
Table A.45: DD 60°F - Convergence of Displacement (Refer Figure 4-28, 4-29).....	154
Table A.46: DcD 60°F - Convergence of Displacement (Refer Figure 4.28, 4.29) .....	155
Table A.47: LD 80°F - Convergence of Displacement (Refer Figure 4.30, 4.31).....	155
Table A.48: DD 80°F - Convergence of Displacement (Refer Figure 4.30, 4.31) .....	155
Table A.49: DcD 80°F - Convergence of Displacement (Refer Figure 4.30, 4.31) .....	156
Table A.50: LD 100°F - Convergence of Displacement (Refer Figure 4.32, 4.33).....	156
Table A.51: DD 100°F - Convergence of Displacement (Refer Figure 4.32, 4.33) .....	156
Table A.52: DcD 100°F - Convergence of Displacement (Refer Figure 4.32, 4.33) ....	157
Table A.53: Trends in Longitudinal Displacement Due to Changes in Soil Properties – Bridge with Approach Slab (Refer Figure 4.34).....	158
Table A.54: Displacement Comparison – Bridge with and without Approach Slab (Refer Figure 4.35).....	159
Table A.55: Trends in Central Pile Bending Moment Due to Changes in Soil Properties (Refer Figure 4.36).....	160
Table A.56: Pile Bending Moment Comparison – Bridge with and without Approach Slab (Refer Figure 4.37).....	161
Table A.57: Trends in Central Pile Bending Stress Due to Changes in Soil Properties – Bridge with Approach Slab (Refer Figure 4.38).....	162
Table A.58: Pile Bending Stress Comparison – Bridge with and without Approach Slab (Refer Figure 4.39).....	163
Table A.59: LD 80°F – Soil Pressure on Abutment Comparison – Bridge with and without Approach Slab (Refer Figure 4.40) .....	164
Table A.60: DD 80°F – Soil Pressure on Abutment Comparison – Bridge with and without Approach Slab (Refer Figure 4.40) .....	164

Table A.61: Pile Bending Moment Comparison – Central Pile vs. End (Refer Figure 4.41).....	165
Table A.62: LD 80°F - Convergence of Displacement (Refer Figure 4.42, 4.43).....	166
Table A.63: DD 80°F - Convergence of Displacement (Refer Figure 4.42, 4.43) .....	166
Table A.64: Soil Pressure on Approach (Refer Figure 4.44) .....	167

## **ACKNOWLEDGEMENTS**

This work would not have been possible without the generous support and funding from the Kansas Department of Transportation (KDOT).

The authors would like to acknowledge Mr. John Jones and Mr. Kenneth F. Hurst for their help during this project.

# CHAPTER 1 - INTRODUCTION

## 1.1 Background

Highway bridges traditionally have a system of expansion joints, roller supports, abutment bearings and other structural releases to account for cyclic thermal expansion and contraction, creep and shrinkage (Arockiasamy *et al.*, 2004). Failure of proper functioning of the expansion joints and abutment bearings due to various reasons leads to highly critical and serious problems. Leakage of water laden with salt, deicing chemicals and contaminants through the joints results in the corrosion of the reinforced concrete, girder ends, bearings and pier caps underneath (Ng *et al.*, 1998). Failure to move properly due to unanticipated movements results in overstress and subsequent structural damage to the bridge elements via split and rupture of abutment bearings, abutment-rotation and abutment-overturning (Arockiasamy *et al.*, 2004; Wasserman, 2001). Expansion joints are very expensive to design, manufacture and install. The continuous maintenance and replacements costs are not meager either (Arockiasamy *et al.*, 2004). Integral Bridges (IBs) came to the forefront as a result of a need for a definite change in the design of highway bridges.

## 1.2 Integral Bridge Concept

### 1.2.1 What are Integral Bridges?

IBs are defined as bridges without expansion joints or sliding bearings, thus eliminating all the issues associated with them. They are alternatively referred to as *integral bridges*, *joint-less bridges*, *integral bent bridges* and *rigid frame bridges* (Lock, 2002). IBs are constructed continuous and monolithic with the abutment walls (Faraji *et al.*, 2001, Jayaram *et al.*, 2001), thus enabling the superstructure and the abutment to

act as a single structural unit and assuring a full moment transfer (Khodair *et al.*, 2005) through a moment-resisting connection between them. (Faraji *et al.*, 2001; Jayaram *et al.*, 2001). Figure 1.1 shows a simplified geometry of an IB (Arsoy, 2000).

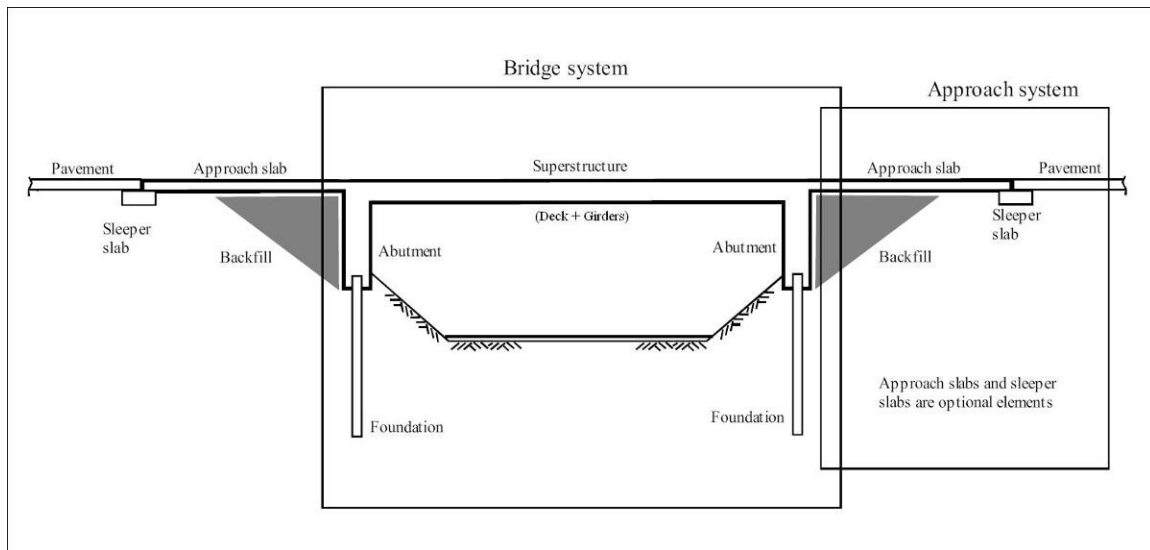


**Figure 1.1: Simplified Geometry of an Integral Bridge (Arsoy, 2000)**

Single or multiple span IBs are generally supported by a single row of flexible H-piles driven into pre-augered holes beneath the abutment wall, and aligned such that the weaker axis of bending is along the transversal direction, thus allowing a higher flexibility. According to Arockiasamy *et al.* (2004), the substructure should be flexible enough to absorb the movements induced in the superstructure due to secondary loads like thermal variations, concrete creep and shrinkage. While the flexibility can be attained by a stub abutment supported by single row of piles (Arockiasamy *et al.*, 2004), in order to maximize the flexibility, rotational as well as translational, loose sand is usually placed around each pile in the pre-augered holes to a depth of about 10 ft (Ting & Faraji, 1998). The connections between abutment and piles are constructed as rigid connections, thus allowing full moment transfer from the abutment wall to the piles.

### **1.2.2 History of Integral Bridges**

The earliest examples of IBs are masonry arch bridges. According to Bakeer *et al.* (2004), the first IB in the USA was constructed in the state of Massachusetts in 1930, while Kansas was the second state to do so in 1935. Today there are more than 1000 IBs in the state of Kansas alone (Bakeer *et al.*, 2004). The longest IB constructed till date is 1175 ft long bridge carrying Route 50 over the Happy Hollow Creek constructed in the state of Tennessee (Bakeer *et al.*, 2004). The construction of IBs has been pursued in other countries including Canada, U.K., Sweden, Poland, Germany and Japan (Ng *et al.*, 1998)

### **1.2.3 Advantages of Integral Bridges**

IBs are rapidly gaining popularity among bridge owners due to their durability, safety and cost effectiveness. Principal advantages of integral bridges, which are derived from the absence of expansion joints, are:

1. Simpler, rapid and more affordable construction
2. Reduced material and construction costs due to the absence of expansion joints (Yang *et al.*, 1985; Greimann *et al.*, 1987; Soltani & Kukreti, 1992)
3. Prevention of corrosion resulting in longevity and reduced maintenance costs (Yang *et al.*, 1985; Soltani & Kukreti, 1992, Hoppe & Gomez, 1996)
4. Smooth, uninterrupted aesthetically pleasing deck giving improved vehicular riding quality (Loveall, 1996; Soltani & Kukreti, 1996) and significantly reducing hazards and hence liability

5. Inherently increased degree of redundancy, hence an enhanced load capacity and distribution, resulting in a higher resistance to overloads, catastrophic or extreme events and earthquakes (Hoppe & Gomez, 1996; Wasserman, 2001)
6. Ease in future widening or replacement of bridge – simpler design lends itself to simpler structural modifications (Roman, *et al.* 2002).

#### **1.2.4 Critical Design Issue – Soil-Structure Interaction**

IB is a classical example of soil-structure interaction (Ting & Faraji, 1998; Wood, 2004). The continuity achieved by this type of construction results in the transfer of thermally induced deformations in the bridge deck to the abutment walls, piles and surrounding soil. A significant and complex non-linear soil-structure interaction that takes place behind the abutment walls and piles has remained largely unknown. Secondary stresses due to thermal and moisture changes of the whole structure and settlements of substructure add to the intricacies of the entire problem. The magnitude and mode of deformation, the overall soil response and the overall structural response are decidedly dominated by the level of compaction in the granular fill behind the abutment walls and adjacent to the piles along with the relative flexural stiffness of the bridge deck, abutment wall, foundation piles, lateral pressure of soil behind the wall and confining stress level in the soil (Jayaram *et al.*, 2001).

These unresolved issues create grave uncertainties in the design of IBs. Consequently, the current design guidelines are experientially based rather than scientifically based (Bakeer *et al.*, 2004). Arockiasamy *et al.* (2004) state that the limited design and construction guidelines by AASHTO and a lack of a unified procedure has led to wide variations in analysis, design and construction procedures from one state to

another. According to Bakeer *et al.* (2004) the length limits vary from 150 ft in Maine to 1000 ft in Louisiana while Tennessee specifies a maximum movement of 2 inches as the criteria instead of maximum length. The length limit for the state of Kansas is 450ft (Bakeer *et al.*, 2004). Also, Bakeer *et al.* (2004) list the variations in skew angle limits from 0° (zero) in Louisiana and Oklahoma to 45° in California and no limit in Tennessee. Bakeer *et al.* (2004) have reported the experiences with the performances of IBs in different states. While Kansas and Tennessee rate having very good experience; expensive repairs of the approaches have led to withdrawal of use of IBs in Arizona (Bakeer *et al.*, 2004).

Lack of design specifications to account for the secondary stresses and the non-linear soil behavior (Shoukry *et al.*, 2006) has called for extensive research comprising:

1. collection of field data from instrumented bridges
2. geotechnical centrifuge experiments, and
3. numerical modeling efforts

It is not a surprise that sixteen states throughout the U.S. have indicated a definite need for future research on IBs (Bakeer *et al.*, 2004).

### **1.3 Objectives and Scope of Research**

The diurnal and seasonal temperature changes induce critical secondary thermal stresses in the IBs, whose behavior is also dependent on the type of soil behind the abutment and piles. It is highly important to explore and examine the details of the complex soil-structure interaction in order to formulate recommendations for improvements in design and construction procedures. Thus, the primary objectives of this research are:

1. Conduct a literature review to establish the current state of knowledge in the area of response of IBs to thermal loads
2. Conduct numerical simulations of the response of a typical IB to thermal loads by using the finite element software ABAQUS/CAE 6.5-1
3. Include the non-linear soil behavior behind the abutments and piles into the numerical model
4. Investigate the soil-structure interaction due to different temperature changes on IBs with different types of soil behind the abutments and piles

#### **1.4 Contents of Report**

A literature review focusing mainly on the past numerical models of IBs is presented in Chapter 2. Chapter 3 discusses the details of the numerical model of the IB-soil system used in this study. Chapter 4 presents and discusses the results of the series of finite element analyses that were performed to investigate the soil-structure interaction of IBs subjected to different thermal loads and various soil conditions. Chapter 5 comprises the conclusions drawn from this research and recommendations for future studies.

## CHAPTER 2 - LITERATURE REVIEW

### 2.1 Introduction

Over the years behavior of IBs has been studied by various transportation agencies and researchers to advance the knowledge base and improve upon the prevalent design procedures and guidelines. Observations of field performance of IBs and related issues reported by different researches are summarized in this literature review along with the detailed discussion of the previous finite element studies on IBs.

Mourad *et al.* (1999) compared deck slab stresses in IBs with those in simply-supported jointed bridges by applying loading of HS20-44 trucks. A finite element analysis using computer program ALGOR (1995) was carried out for this purpose. The results indicated a more uniform distribution of loads and 25-50 % lower maximum stresses in the transverse direction in IBs as compared to the corresponding simply supported bridges.

According to Roman *et al.* (2002) the secondary stresses in the bridge deck due to temperature changes and substructure settlement of the substructure can be significantly higher than those permitted by current design specifications, thus highlighting the lack of sufficient knowledge base with reference to IBs.

After inspecting and rating 30 steel IBs Alampalli *et al.* (1998) concluded that the higher the skew of the bridge deck, the lower the condition and performance ratings were for the deck, approach slab and abutment stem.

Arockiasamy, M. *et al.*, 2004, conducted a parametric study for the response of laterally loaded piles supporting integral bridges with an emphasis on predrilled holes, elevation of the water table, soil types and pile orientation by using finite-difference

program LPILE and finite-element program FB-Pier. The study concluded that horizontal displacement at the pile top, maximum shear, axial force and moments in the pile significantly depend on the type of the soil around the pile, its degree of compaction and the orientation of pile axis; while the water table elevation has very little significance.

Ng *et al.* (1998) studied the behavior of abutments of IBs and how it differed from that of simply supported bridges subjected to cyclic loading conditions. Effects of temperature variations on the soil-structure interaction were investigated by using the centrifuge modeling technique. Displacement-controlled loading was employed in the centrifuge model tests, which were conducted on a spread-base integral bridge abutment. This was done by imposing controlled cyclic displacements at the top of the abutment wall thereby simulating the thermal expansion and contraction of the bridge. According to Ng *et al.* (1998), “The three temperature ranges considered included one extreme for 120-year design period, seasonal cycles between summer and winter temperatures, and daily cycles between day and night temperatures”. Based on these temperature ranges, controlled displacements at the deck level for a 100 m long concrete bridge deck were measured. Results showed rigid body motions, both translational as well as rotational. Three factors affected the abutment movement: magnitude of displacements imposed at the abutment top, the number of strain cycles for which the experiments were carried out, and the density of the fill materials. A strain ratcheting effect was observed due to the densification and settlement of the fill, progressively increasing the outward movement of the abutment wall with the number of strain cycles; the effect being more significant in dense than in loose fill calling for a careful consideration of sliding resistance of spread-base abutments during design.

## **2.2 Past Finite Element Studies on IBs**

Very few detailed finite element studies with focus on thermal loading have been carried out on IBs. This section of the literature review discusses those in details.

### **2.2.1 “Nonlinear Analysis of Integral Bridges: Finite-Element Model”**

#### **by Faraji et al. (2001)**

One of the most complete finite element studies of IBs was performed by Faraji *et al.* (2001) with the aim to design and construct longer span bridges and to evaluate their performance during seismic loads. A 3D finite element model of “Bemis Road Bridge: F-4-20” in Fitchburg, Massachusetts was analyzed using the finite element code GT-STRUDL. Non-linear soil behavior, modeled using non-linear springs, was incorporated in the model. The nonlinear force-deflection relations for the soil adjacent to the abutment walls were based on the recommendations by the National Cooperative Highways Research Program (NCHRP, 1991) design manual. The “*p-y*” design curves recommended by American Petroleum Institute (API) (1993) were used for nonlinear force-deflection relations for the soil adjacent to the piles. Figure 2.1 shows the GT-STRUDL finite element model of the bridge.

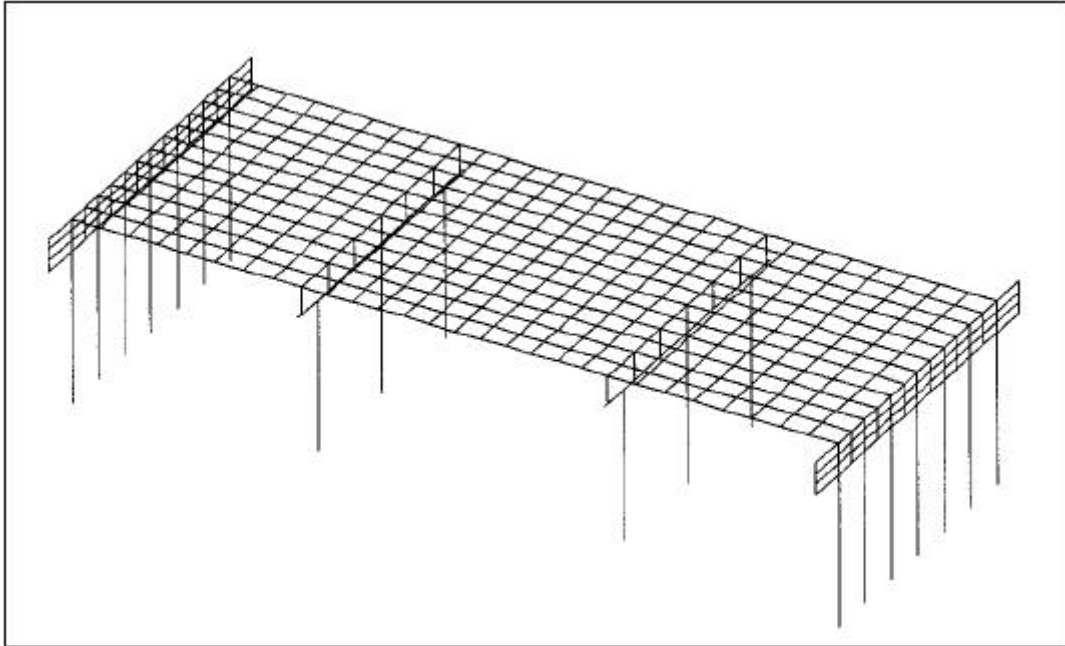


**Figure 2.1: GT-STRUDL Finite Element Model of the Bridge (Faraji et al., 2001)**

Bending and stretching plate elements were used to model the deck of 150 ft long 3-span IB with two 45 ft long end spans. The deck is 54 ft wide and 8.5 in thick concrete slab. On the other hand, beam elements were employed to model the W36x135 steel stringers and diaphragms. Beam elements modeled the 3 ft high, 3.5 ft wide and 56.5 ft long pier caps, and 3 ft diameter concrete piers as well. Rigid links were used to model the connection between deck slab and girders ensuring “strain compatibility and shear transfer between the deck slab and girder elements. The 8 ft high, 2.5 ft wide and 69 ft long abutment wall was modeled by using plate elements with an overall effective height of 6 ft, connected to the girder ends by a fixed connection. Uncoupled nonlinear Winkler springs were used to model the soil response behind the abutment. Each of the seven HP12x74 piles was modeled using beam elements, which were fixed into the abutment wall. The fixity allows a full moment transfer from the

superstructure to the piles. The  $p$ - $y$  curves modeled the soil response by using a series of nonlinear springs. Figure 2.1 shows the GT-STRUDL finite element model of the bridge.

In all, more than 1000 beam, beam-column, and slab members and elements for the deck, wall, pier, and pile systems; and over 350 nonlinear soil substituting springs were used in the finite element model. Figure 2.2 shows finite element details of north abutment wall and HP piles.

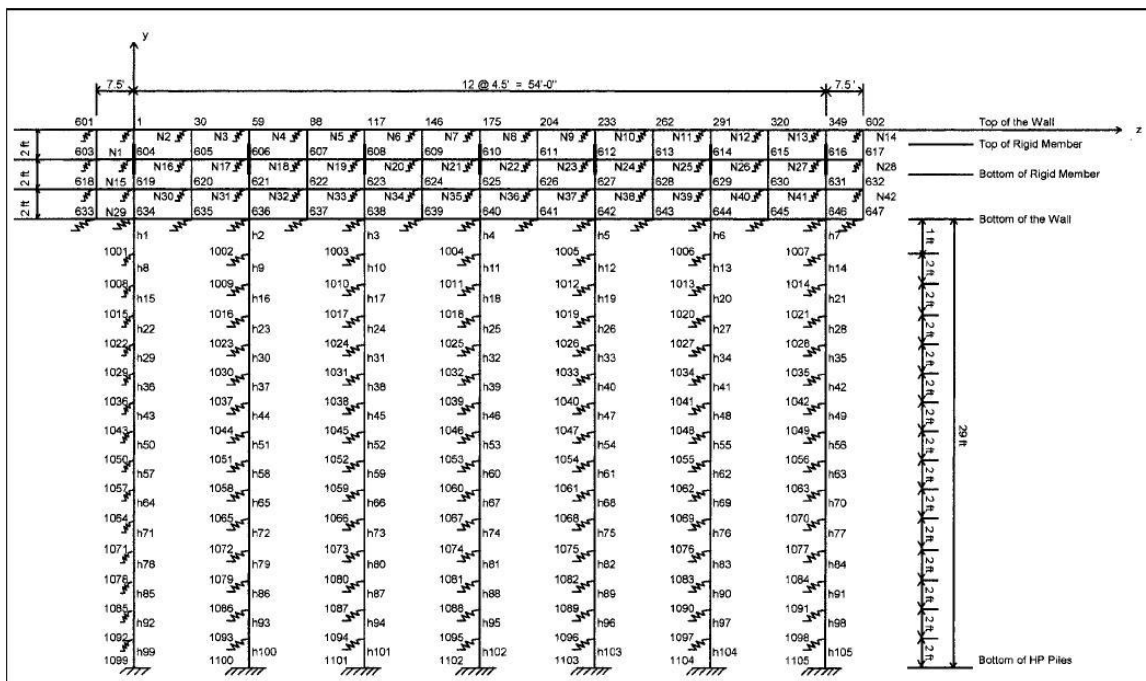


**Figure 2.2: Finite Element Model Details for North Abutment Wall and HP Piles (Faraji et al., 2001)**

The bridge was subjected to a temperature increase of 80° F for different combinations of soil properties behind the abutment and adjacent to the piles based on the compaction levels. The results of the analysis called for proper care to be taken while modeling the composite action of the superstructure. The level of soil compaction behind the abutment wall played a vital role in affecting the overall bridge behavior in

terms of axial forces and moments in the deck increasing both by more than twice in peak value when varied from loose to dense compaction range. Though the level of soil compaction adjacent to the HP piles had an impact on the moments in the piles, it was not significant in affecting the behavior of the abutment wall and the superstructure. The results also indicated that soil pressures behind the abutment wall could reach the full passive state and be considerably nonlinear for longer bridges. Faraji *et al.* (2001) recommended a more refined and full 3D modeling of the sample bridge as well as modeling of longer bridges for a more advanced understanding of the behavior of IBs.

The research carried out at Kansas State University is aligned with the direction of this recommendation by Faraji *et al.* (2001) by using a full, detailed and refined 3D model of the same bridge along with different temperature ranges, thus modeling the response of longer bridges.

### **2.2.2 “Analysis of Soil-Pile Interaction in Integral Abutment” by Khodair & Hassiotis, (2005)**

Khodair & Hassiotis (2005) studied the soil-structure interaction of the soil-pile system of the Scotch Road IB in Trenton, New Jersey built over I-95. Khodair & Hassiotis (2005) listed two objectives of the research. First, determine the thermal stresses in the piles due to temperature changes; and second, determine “lateral load transfer from the piles to the MSE (Mechanically Stabilized Earth) wall supporting the bridge foundation” (Khodair & Hassiotis, 2005). To go about achieving the objectives, they performed three tasks. First, instrumentation of abutment and piles; second, development of a 3D FE model of the substructure; and third, updating the FE model using the data obtained from monitoring the instrumented bridge.

Scotch Road, I-95 IB, located in Ewing/ Hopewell Township, is a composite concrete slab IB with 10 non-standard steel girders, of depth 5.51 ft, connected by shear studs. Nineteen HP 360x152 piles supported the 2.95 ft wide and 9.45 ft deep reinforced concrete abutment through an embedded connection ensuring the full moment transfer (Figure 2.3). A sleeper slab supported the approach slab at the far end, which was rigidly connected to the abutment on the near end. “The soil behind the abutment and under the approach slab consisted of a well-compacted porous fill” (Khodair & Hassiotis, 2005).

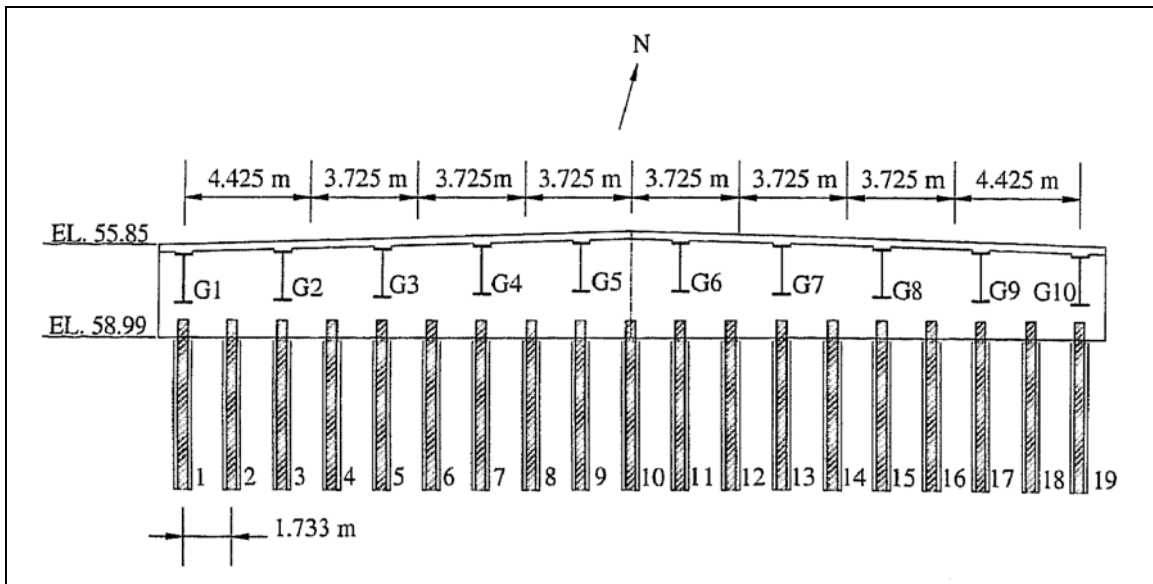


**Figure 2.3: Elevation View of the Scotch Road, I-95 IB (Khodair & Hassiotis, 2005)**

Instrumentation included four types of measuring devices: strain gages, soil pressure cells, inclinometers having temperature sensors and tilt-meters. Figure 2.4 shows the instrumentation details. Data was collected for a period of one year at the interval of every 2 hours.

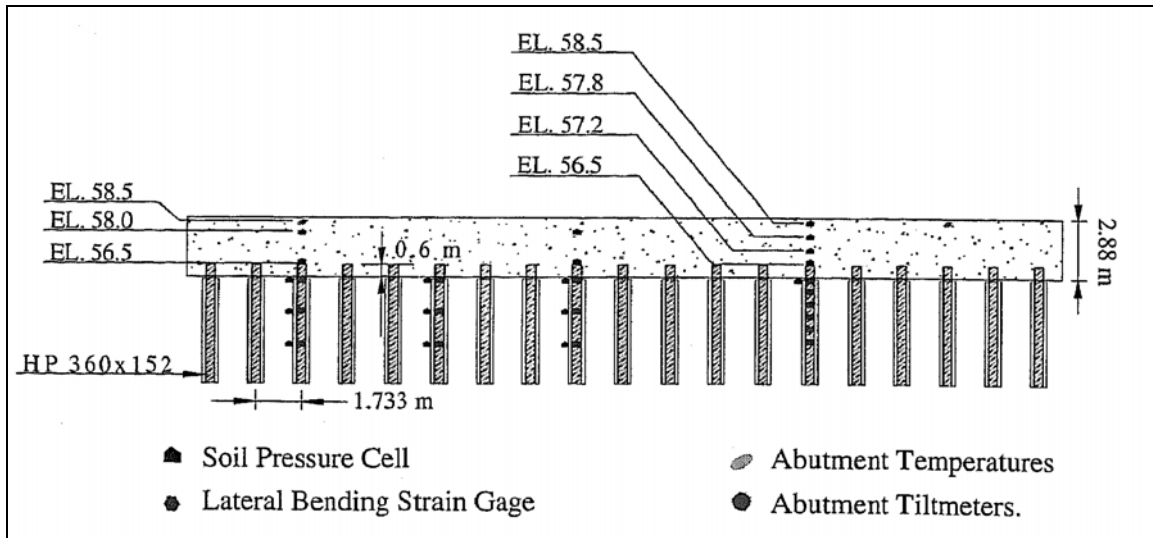


**Figure 2.4: Instrumentation of Experimental Devices on the Substructure of the Scotch Road, I-95 IB (Khodair & Hassiotis, 2005)**

According to Khodair & Hassiotis (2005) ABAQUS/Standard 6.3.1 was used to develop a 3D FE model of the HP piles embedded into a 1.97 ft diameter sand filled galvanized steel sleeve. Both, pile and soil were modeled using eight-node solid continuum elements with a non-linear response. While an elastic-plastic response was adopted for the pile elements, Mohr-Coulomb model with strain hardening idealized the non-linear soil response. Surface-to-surface contact algorithm was employed to model the sand-pile interaction. To model the tangential contact, friction coefficient for the interaction between pile and soil materials was calculated.

Two load cases were analyzed by the FE model. In the first load case, a displacement and rotation boundary condition was imposed by applying a displacement of 0.0755 ft. In words of Khodair & Hassiotis (2005) “the displacement was applied at a location corresponding to the neutral axis of the attached girder in a pattern that simulates rigid body motion”. This displacement corresponds to a temperature increase on 107.6°F calculated according to the following equation:

$$d = \alpha \delta T_{EB} L \quad \text{Equation 2.1}$$

where,

$d$  = maximum horizontal displacement

$L$  = span of the bridge

$\alpha$  = coefficient of thermal expansion

$\delta T_{EB}$  = change in EBT (Effective Bridge Temperature)

The concept of EBT, defined as the assumed uniform temperature state for the observed thermal expansion, was introduced in UK in compliance with the material of the bridge deck and the geographical location of the bridge. A parametric study for the first load case was also carried out by incrementally increasing the steel sleeve diameter from 1.97 ft to 6.56 ft.

In the second load case, the displacements and rotations measured from the field experiment were applied to the abutment in the FE model.

In order to verify the FE model, the results of the first load case of the FE model were compared with the results obtained from the Finite Difference (FD) analysis software LPILE. The results were not similar and had discrepancy which was attributed to the difference in the size of the diameter of the sand surrounding the piles in FE

analysis and FD analysis. It was also observed from the parametric study that there was a substantial decrease in the discrepancy when the size of the diameter was increased up to a value defined by LPILE as an extended single layer of sand.

The axial strains calculated from the analyses in the second loading case when compared to the measured values from the strain gages matched very favorably for piles #3 and #9, although they did not match for pile #6. This discrepancy is due to the fact that “the loading considered in the FE model was formulated to account for the effect of the girders #2 and #5” which were placed directly above piles #3 and #9 and the axes of the piles coincided with the girders. On the other hand, pile #6 was not affected directly by any of the 10 girders in the superstructure.

One interesting observation that Khodair & Hassiotis (2005) made was that irrespective of the change in the diameter of the galvanized steel sleeves, the calculated values of the crushed stone pressure at the perimeter of the galvanized steel sleeves remained approximately zero. The experimentally measured values by the soil pressure cells substantiated these calculations.

Khodair & Hassiotis (2005) made two conclusions from this research:

1. The diameter of 1.97 ft of the galvanized steel sleeve filled with sand is sufficient to accommodate the pressure developing due to the thermal loads, equivalent to 0.0755 ft displacement corresponding to 107.6°F temperature increase.
2. Increase in the size of the diameter of the steel sleeve results in higher lateral load capacity of piles.

### **2.2.3 “Field Monitoring and 3D FE Modeling of an Integral Bridge in West Virginia” by Shoukry et al. (2006)**

Shoukry *et al.* (2006) studied the axial effect of the backfill pressure against expansion of IBs in the steel girders of a three-span IB located in Evansville, West Virginia. Stating that the effect of backfill forces is being taken into account to a certain extent in the design of piles and abutment but not that of the girders, where secondary thermal axial stresses get generated, Shoukry *et al.* (2006) evaluated the response of the IB, which had been instrumented and monitored for a period of twenty months. A better understanding of the bridge behavior was attempted by a 3-D finite element model of the three girder section of the bridge, whose construction had been completed during the first phase, using finite element software ADINA (2000).

Evansville Bridge, which carries WV Route 92 over Little Sandy Creek located in Preston County, West Virginia, is a three-span 147 ft long steel girder continuous bridge with a skew angle of 55°. The 44 ft wide Evansville Bridge had two end spans of 48.5 ft and a central span of 50 ft in length. A single row comprising eight HP 12x53 piles with an embedded length of 0.98 ft support the 5.97 ft high, 2.95 ft wide and 53.15 ft long abutment wall. The 0.66 ft minimum thickness of the deck reaches to 0.74 ft over the haunches as shown in Figure 2.5 (Shoukry *et al.*, 2006).

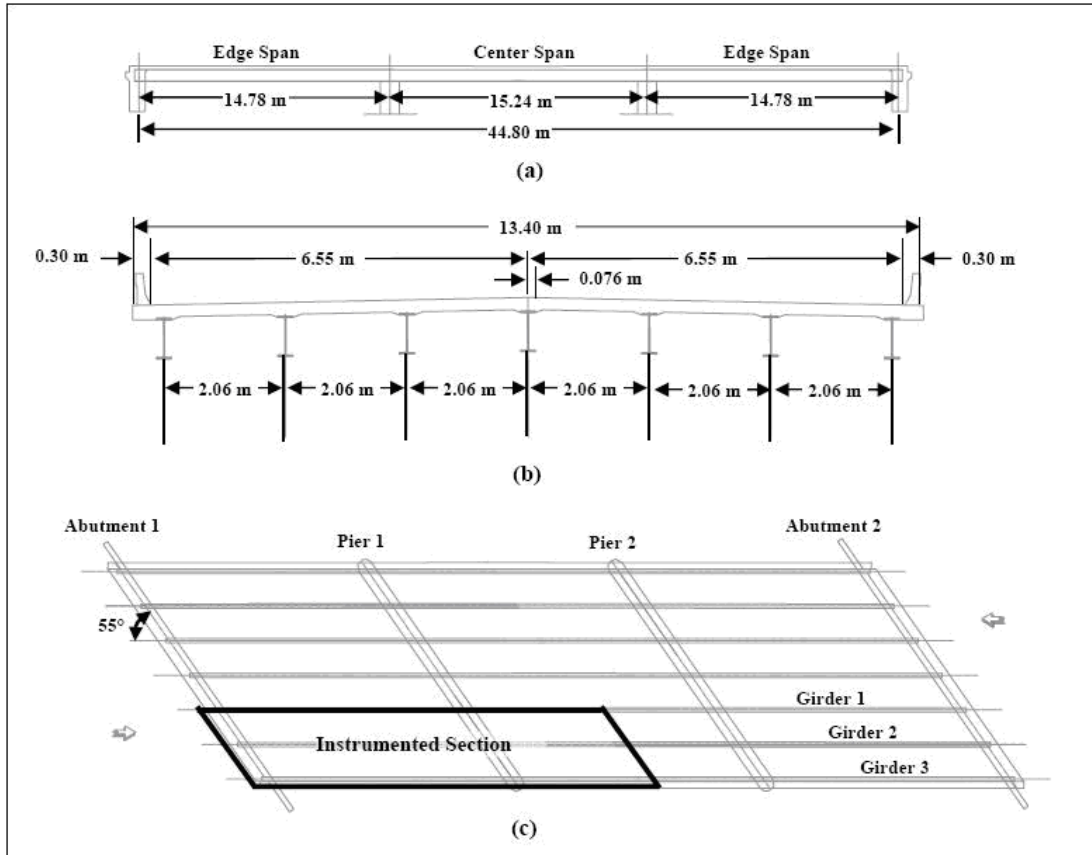


**Figure 2.5: Evansville Bridge (a) Elevation (b) Side View (c) Plan (Shoukry et al., 2006)**

While the bridge deck, abutment walls, girders and cross members at the piers were idealized using 4-node shell elements, hermitian beam elements modeled the piles and remaining cross members. Modeling of piers was taken care of by corresponding boundary conditions at the respective locations on the girders. The soil backfill and the piles, fixed at their base, supported the abutments. To allow the stiffness of the deck-girder connection to be varied, spring tied elements were employed at their interface. Nonlinear spring elements modeled the soil backfill as well as the soil around the piles.

Using the design curves by National Cooperative Highway Research Program (NCHRP, 1991), passive and active earth pressure effects behind the abutment were

modeled for the soil found to have  $18 \text{ kN/m}^3$  as the unit weight and  $\Phi=36^\circ$  as the angle of internal friction. On the other hand, the guidelines by the American Petroleum Institute (API) (1993) were utilized to develop the “ $p$ - $y$ ” curves, which represented the stiffness for the nonlinear springs substituting the soil around the piles. The “ $p$ - $y$ ” relationship is a hyperbolic tangent curve defined as follows:

$$p = Ap_u \tanh \left[ \frac{kz}{Ap_u} y \right] \quad \text{Equation 2.2}$$

where,

$p_u$  = ultimate bearing capacity,

$k$  = parameter defined by  $\Phi$  ,

$z$  = depth in soil,

$y$  = lateral displacement of pile,

$A$  = parameter that varies with soil depth in case of static loading according to the equation 2.2

$$A = 3.0 - 0.8 \frac{X}{D} \geq 0.9 \quad \text{Equation 2.3}$$

where,

$X$  = soil depth,

$D$  = average pile length.

For the FE analysis, self-weight of the structure followed by a uniform temperature change of  $\pm 20^\circ\text{C}$  with  $\pm 5^\circ\text{C}$  intervals was applied to the model. Figure 2.6 shows the finite element model of the three girder section of the bridge.

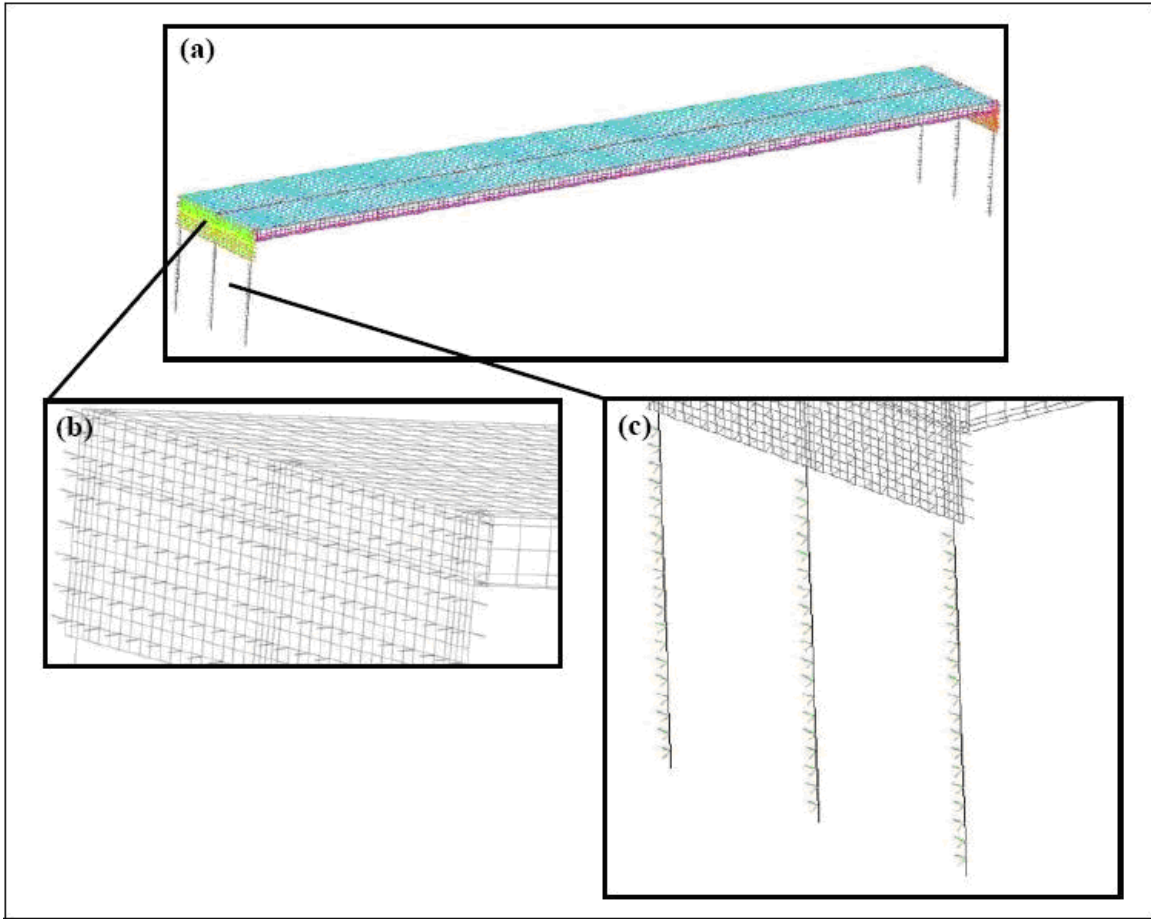


**Figure 2.6: Finite Element Model of Evansville Bridge (a) Full Model (b) Non-Linear Springs Modeling the Soil-Abutment Interaction (c) Non-Linear Springs Modeling the Soil-Pile Interaction (Shoukry et al., 2006)**

The validation of the accuracy of the finite element analysis required a comparison with the field data, whereby the field data was interpreted for self-weight and thermal loads only so as to have the consistency in the response comparison. The measured values of displacements, strains and subsequently calculated stresses matched well with the finite element results. Also, both, measurements and analysis, indicated that secondary axial thermal stresses were induced in the girders along with the piles. According to Shoukry *et al.* (2006) the secondary effects, which are taken into consideration in the design provisions for piles, have not been explicitly addressed in

the design of the superstructure. Since location of the bracing cross-members can be affected by these stresses and their ignorance may lead to the failure to meet the AASHTO Standard Specifications (2002) for stability and yield, Shoukry *et al.*, 2006, concluded that there is a definite need to address their effects while designing the components of a bridge superstructure.



## CHAPTER 3 - NUMERICAL MODELING

### 3.1 The Bridge Model

A refined and detailed 3D finite element model of the “Bemis Road Bridge: F-4-20” over the Nashua River in Fitchburg, Massachusetts (Ting and Faraji, 1998), which was subsequently modified slightly according to the requirements of KDOT, is developed using the interactive environment of finite element software ABAQUS/CAE 6.5-1.

The selection of this is bridge was based on two reasons as follows:

1. It is a typical IB within the length limit of 450ft for the state of Kansas (Bakeer *et al.*, 2004).
2. The availability of variety of results as per the report by Ting & Faraji (1998) enabled better validation and verification of the FE model.

Due to the symmetry of the bridge geometry and loading, only half of the 150 ft long 3-span steel IB is modeled. The length of central span is 60 ft while the two end spans are 45 ft each, with the width of the bridge being 54 ft. Figure 3.1 shows the elevation view schematic of the bridge.

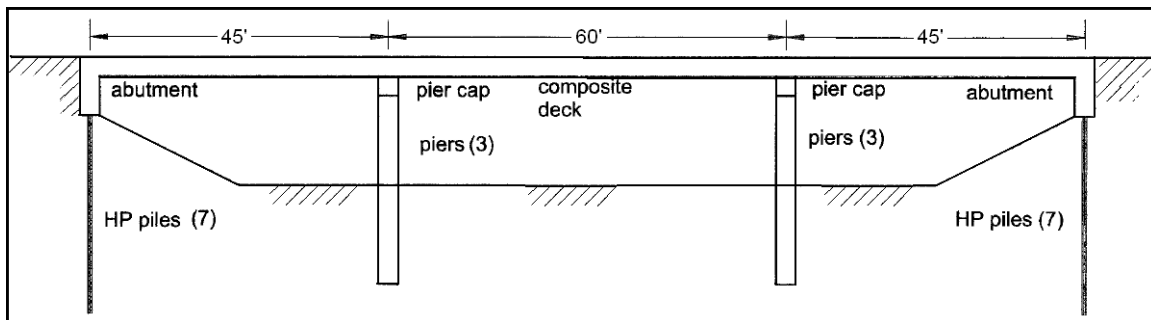
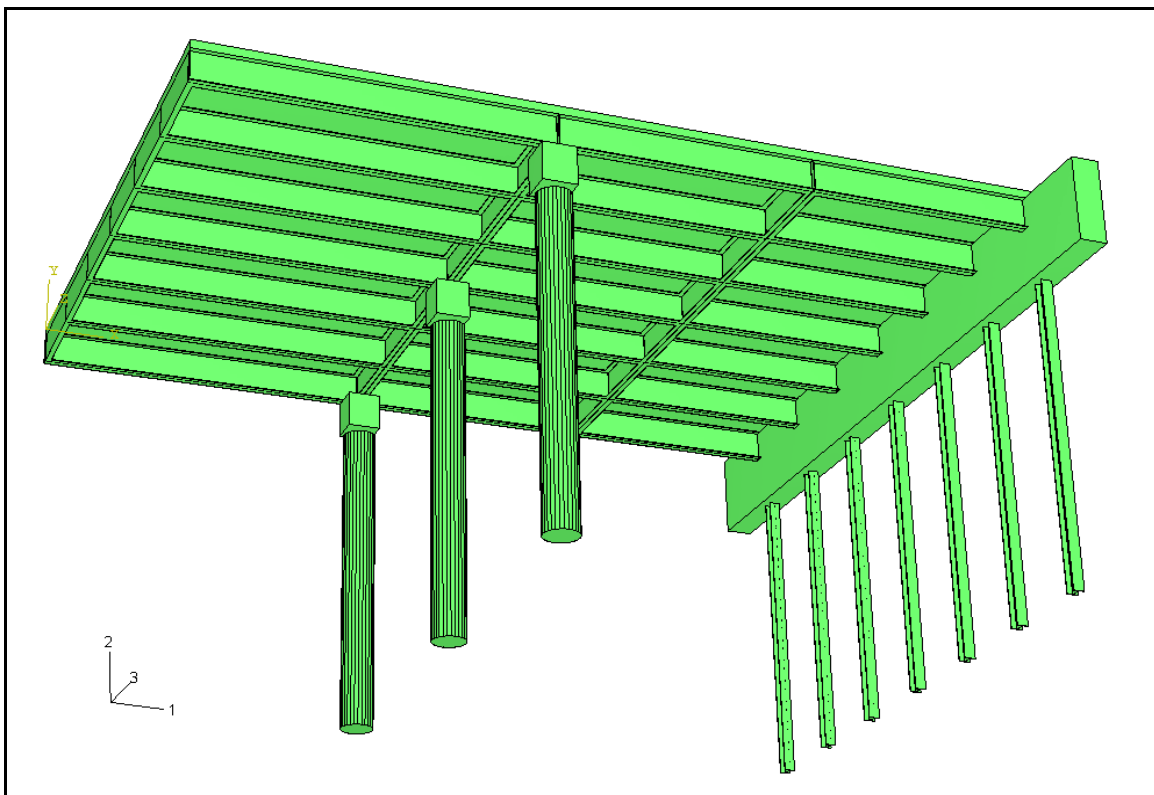


Figure 3.1: Schematics of the Bridge (Faraji et al., 2001)

The superstructure comprises the following parts:

1. 8.5 in thick, 150 ft long and 54 ft wide concrete slab,
2. Seven W36x135 steel girders spaced 9 ft apart, and
3. Seven transverse W36x135 steel beams, 54 ft long, one at the center and one at the end of each span.

Figure 3.2 shows the schematics of the FE model of bridge along with the coordinate system employed for presenting the results.



**Figure 3.2: Schematics of FE Model of the Bridge**

The superstructure rests on substructure comprising the following:

1. Two sets of 3 concrete piers, one set on each end of the central span, which are connected by hinge connections to the superstructure.
2. The piers are 3 ft in diameter and 30.2 ft long. Each is capped by a 3 ft x 3 ft x 3.5 ft pier cap.
3. Concrete abutments are 8 ft high, 2.5 ft wide and 69 ft long.
4. Each abutment is supported by seven HP12x74 piles, 29 ft long, spaced 9 ft apart allowing a full moment transfer.
5. The nonlinear force-lateral displacement relationship for the soil is modeled by linear springs and iterative equivalent linear approach. The springs are attached to the nodes located on the abutment and piles.

Finite element code ABAQUS/Standard, release 6.5-1 is used for the analyses.

The FE model of the bridge-soil system consists of total 191,894 eight-node coupled temperature-displacement elements (C3D8T), 277,530 nodes, 12 connector elements (CONN3D2) modeling hinges, and 546 linear spring elements. Figure 3.3 shows the finite element model of the bridge.

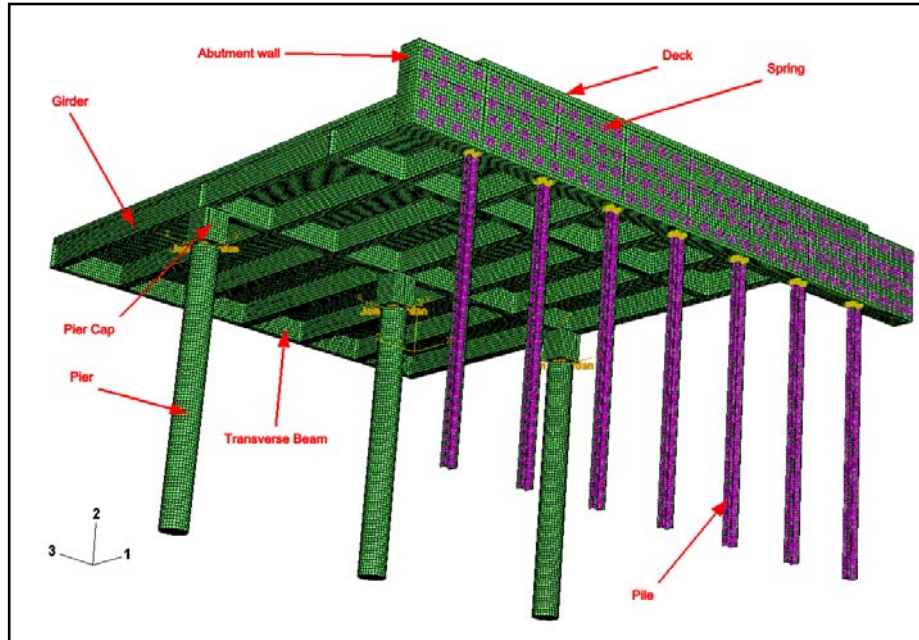


**Figure 3.3: Finite Element Model of the Bridge (Including the Soil Substituting Springs)**

### **3.2 Loads**

Thermal stresses are induced in the structure due to its continuity and presence of the soil behind the abutment and piles, which prevents a free expansion. For the finite element analyses, the temperatures of the superstructure and a partial region of the substructure exposed to the atmosphere were increased by an amount  $\Delta T$ , while the temperature of the partial region of the substructure under the ground was held constant at 50°F. Three different values for  $\Delta T$  were used herein corresponding to 60°F, 80°F and 100°F. Figure 3.4 depicts nodal temperatures for the scenario when  $\Delta T = 80^\circ\text{F}$ .

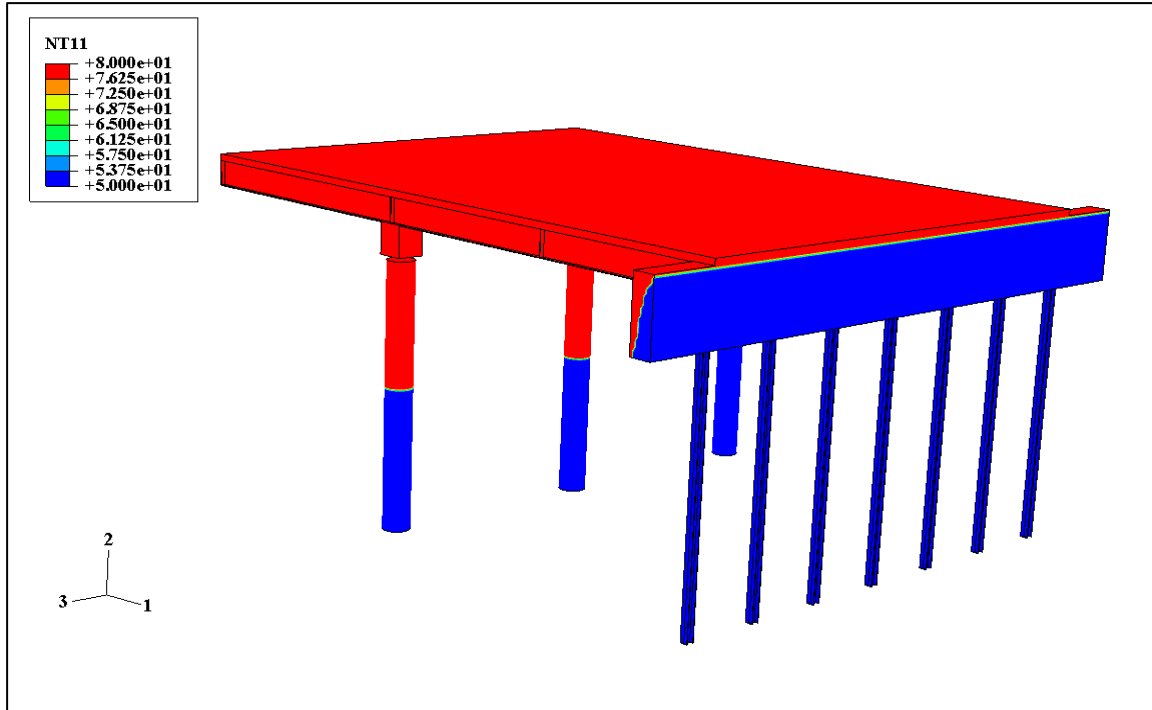


**Figure 3.4: Nodal Temperatures for  $\Delta T = 80^\circ\text{F}$**

The analysis is performed in two steps. In the first step, to account for the self-weight before any temperature changes take place, a gravity acceleration of  $32.2 \text{ ft/s}^2$  is applied to the bridge model. In the second step, a temperature increase of amount  $\Delta T$  is prescribed at each node in accordance to the Figure 3.4, while the self-weight effect from the previous step is carried forward. The analysis procedure is “coupled temperature-displacement analysis” as explained in the ABAQUS user manual.

### **3.3 Concrete and Steel properties**

The stress-strain behaviors of concrete and steel are assumed to be linear elastic. The corresponding material properties are listed in Table 3.1. They include Young’s modulus  $E$ , Poisson’s ratio  $\nu$ , coefficient of thermal expansion  $\alpha$ , mass density  $\rho$  and, thermal conductivity  $\kappa$ .

**Table 3.1: Material Properties**

<b>Property</b>	<b>Concrete</b>	<b>Steel</b>
Young's Modulus E (psi)	$4.35 \times 10^6$	$3 \times 10^7$
Poisson's ratio u	0.3	0.3
Coefficient of thermal expansion $\alpha$ (per °F)	$6 \times 10^{-6}$	$6.5 \times 10^{-6}$
Mass Density $\rho$ (slugs/ft <sup>3</sup> )	4.66	15.23
Mass Density $\rho$ (slugs/in <sup>3</sup> )	0.0027	0.0088
Thermal conductivity $\kappa$ (Btu/in*hr*°F)	0.15	2.5

### **3.4 Soil Model and its Properties**

The soil structure interaction is modeled by attaching linear springs at the selected nodes of the abutment and piles. The springs simulate the effect of the abutment fill on the bridge. The non-linear force-displacement relationship of the soil is simulated by an iterative equivalent linear approach described in the sections 3.4.1 and 3.4.2.

#### **3.4.1 Springs Behind Abutment**

Four rows of springs are attached behind the abutment such that each spring has a tributary area of

$$\Delta A = \Delta h \times \Delta b \quad \text{Equation 3.1}$$

where,

$$\Delta h = 24 \text{ in and}$$

$$\Delta b = 23.66 \text{ in.}$$

Thus, there are 35 springs in each row summing up to a total of 140 springs representing the soil behind the abutment. The stiffnesses of these springs depend on the types of soils adjacent to the abutment and piles. They are determined by an

iterative equivalent linear approach that comprises multiple iterations. The corresponding steps are described below:

1. In the first iteration, lateral displacements of the abutment top ( $\delta_0$ ) are obtained based on the bridge model without springs thus disregarding the presence of the soil.
2. Next, the initial stiffnesses of lateral springs to be attached to the abutment are determined, based on the displacements determined in step-1 and in accordance with the following equation

$$k_{1,j}(\delta_0) = \frac{F(\delta_0)}{\delta_{0,j}} = \frac{K(\delta_0)\gamma_d z \Delta A}{\delta_{0,j}} \quad j = 1 \text{ to } 4 \quad \text{Equation 3.2}$$

where,

$K(\delta_0)$  = the coefficient of lateral earth pressure, whose magnitude depends on the magnitude of the corresponding horizontal displacement  $\delta_0$  of the abutment top. The relationships between the coefficient of lateral earth pressure ( $K$ ) and lateral displacement of the top of the wall ( $\delta$ ) used herein are discussed later.

$\delta_{0,j}$  = lateral displacement at the location of the selected spring, obtained from the step above

$\gamma_d$  = dry unit weight of soil behind the abutment

$z$  = depth of the spring, from the top of the abutment

This stiffness is entered into the subsequent FE run and corresponding displacement at the top of the abutment  $\delta_1$  is obtained from the output.

3. Next, step 2 is repeated by using the displacements obtained from the updated output from the most recent iteration. The stiffnesses in each subsequent iteration are calculated according to the following equation

$$k_{i+1,j}(\delta_i) = \frac{F(\delta_i)}{\delta_{i,j}} = \frac{K(\delta_i)\gamma_d z \Delta A}{\delta_{i,j}} \quad \text{Equation 3.3}$$

where,

$\delta_{i,j}$  = output from the current iteration

$k_{i+1,j}$  = input into the subsequent iteration.

For the purpose of determining the spring stiffnesses the motion of the abutment is approximated by a rigid body motion as shown in Figure 3.5.

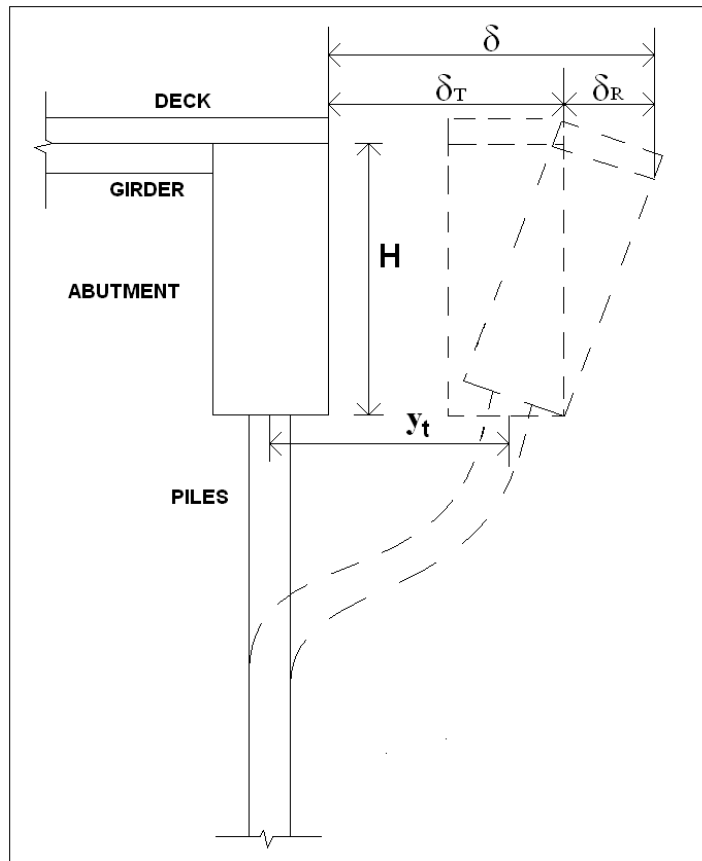


**Figure 3.5: Abutment Motion**

Thus,

$$\delta = \delta_T + \delta_R \tag{Equation 3.4}$$

where,

$\delta_T$  = abutment translation and

$\delta_R$  = displacement due to the rotation of the abutment

The relationships between the lateral displacement of the abutment top  $\delta$ , and coefficient of lateral earth pressure in soil recommended by two different agencies, National Cooperative Highways Research Program (NCHRP, 1991) design manual and Canadian Foundation Engineering Manual by Canadian Geotechnical Society (CGS, 1992) are used herein. The corresponding response curves shown in Figures 3.6 and 3.7 are used to determine the coefficient of lateral earth pressure  $K(\delta)$ . Table 3.2 lists the type of soils for which these design response curves have been recommended.

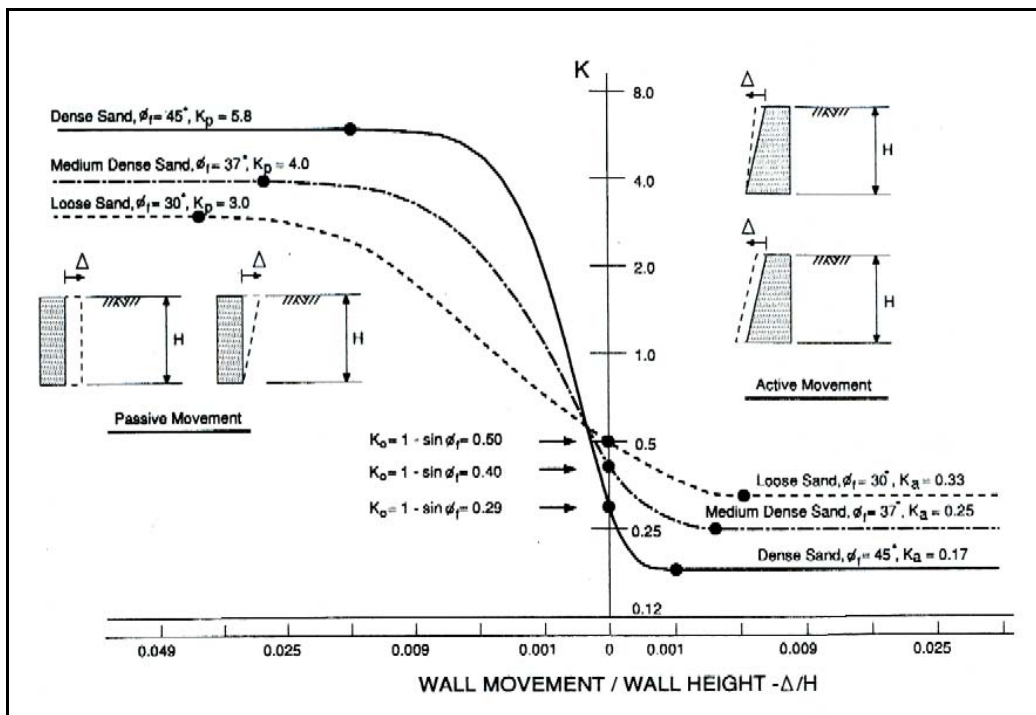


Figure 3.6: Design Curves Recommended by NCHRP (1991)

**Table 3.2: Soil Properties**

Type of sand	Angle of internal friction $\phi(^{\circ})$
Dense sand (NCHRP, 1991)	45°
Dense sand (CGS, 1992)	N/A
Loose sand (NCHRP, 1991)	30°

It is assumed that maximum dry density of sand,  $\gamma_{d,max}$  is equal to 125 lb/ft<sup>3</sup>, and the relative densities  $D_R$  of dense and loose sands are 80% and 50% respectively. It is also noted that a sand of relative density of 50% falls between a loose and medium dense sand. Herein, it is referred to as loose sand.

Based on observations of 47 granular soil samples Lee & Singh (1971) proposed the following relationship between relative density and relative compaction:

$$R = 80 + 0.2D_R \quad \text{Equation 3.5}$$

where,

$R$  = relative compaction defined as follows:

$$R = \frac{\gamma_{d,field}}{\gamma_{d,max}} \quad \text{Equation 3.6}$$

Actual dry unit weights ( $\gamma_{d,field}$ ) are calculated by using equations (3.5) and (3.6).

The corresponding values used in the analyses are reported in Table 3.3.

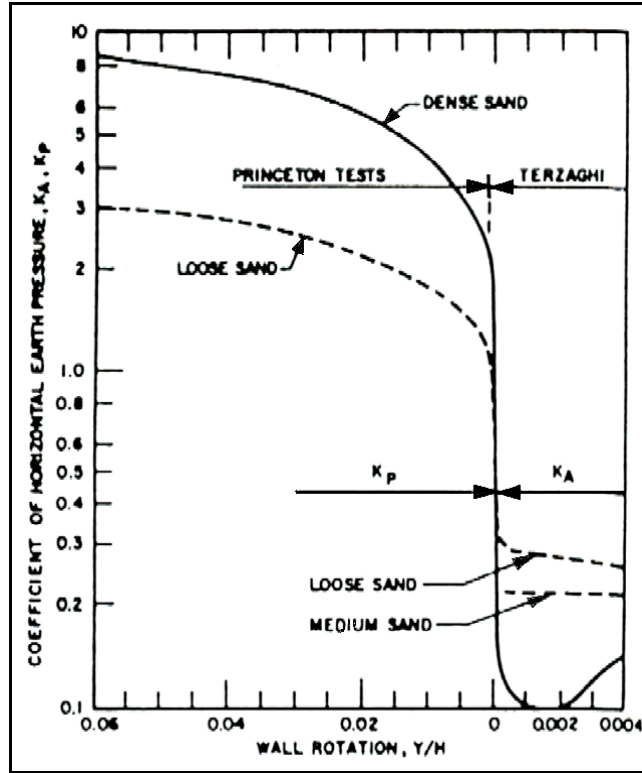
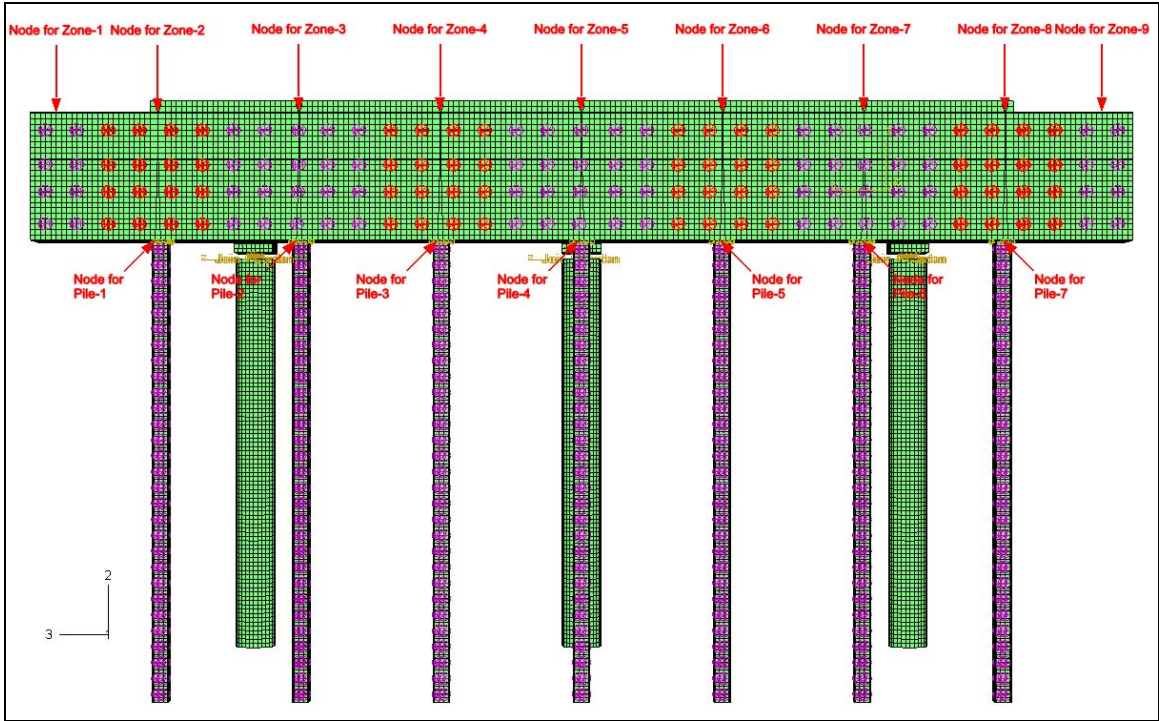


Figure 3.7: Design Curves Recommended by CGS (1992)

Table 3.1: Dry Unit Weights of Soils

Type of sand	$\gamma_{d,max}$ (lb/ft <sup>3</sup> )	$D_R$ (%)	R (%)	$\gamma_{d,field}$ (lb/ft <sup>3</sup> )
Dense sand	125 lb/ft <sup>3</sup>	80%	96%	120 lb/ft <sup>3</sup>
Loose sand	125 lb/ft <sup>3</sup>	50%	90%	112.5 lb/ft <sup>3</sup>

For the purpose of determining  $\delta$  in 3D analysis, the abutment was divided into 9 vertical zones, and longitudinal displacement at the center of each zone was used for all springs located in that zone. The abutment top central points (nodes) whose displacements were used are highlighted in Figure 3.8 along with the corresponding zones.



**Figure 3.8: Vertical Zones of the Abutment and the Corresponding Nodes**

The procedure of determination of the spring stiffness based on one set of displacement results obtained after a single iteration of the finite element analysis is as follows:

1. A normalized displacement of the abutment top  $\left(\frac{\delta}{H}\right)$ , where H is the abutment height, is determined based on the FE analysis output from the current iteration.
2. The coefficient of lateral earth pressure  $K\left(\frac{\delta}{H}\right)$  generated due to the abutment motion, is then determined from the recommended response curves for the type of soil considered.
3. A vertical effective stress  $\sigma'_z$  is calculated at each depth where the spring is attached as per the following equation.

$$\sigma'_z = \gamma_{d,field} z \quad \text{Equation 3.7}$$

where,

z = depth from the abutment top. The effective weight of soil is equal to dry weight due to a deep ground water level.

4. The horizontal effective stress  $\sigma'_y$  and the horizontal force  $F_y$  at each spring depth are then calculated as per equations (3.8) and (3.9) respectively.

$$\sigma'_y = K\left(\frac{\delta}{H}\right) \sigma'_z \quad \text{Equation 3.8}$$

$$F_y = \sigma'_y \Delta A \quad \text{Equation 3.9}$$

5. The stiffness of a spring  $k_{i+1,j}$  is then calculated as described previously by equation (3.3) and used as input into the subsequent iteration.

### **3.4.2 Springs Behind Piles**

Twenty-nine sets of two springs each, are attached behind each pile as shown in Figure 3.9, such that each spring has a tributary area of  $\Delta A_p$  given by the following equation

$$\Delta A_p = \Delta L \left( \frac{B}{2} \right) \quad \text{Equation 3.10}$$

where

$\Delta L = 12$  in and

$B = \text{depth/width of the pile section} = 12.2$  in.

Thus, a total of 406 springs represent the soil behind the seven piles. Figure 3.9 shows the arrangement of springs behind a pile.

Prakash & Kumar (1996) proposed a method alternative to “ $p$ - $y$ ” curves, which describes a load-displacement relationship for a single laterally loaded pile by considering the non-linear behavior of soil. The method is based on experimental observations collected from 14 full-scale lateral pile load tests reported by Mwindo (1992). This method describes a degradation of the spring stiffness at one meter depth below the pile head as a function of strain, according to the following equation.

$$k_h = a\gamma^{-b}k_{h\max} \quad \text{Equation 3.11}$$

where,

$k_h = \text{modulus of horizontal subgrade reaction } [FL^{-2}]$ ;

$k_{h\max} = \text{value of } k_h \text{ at shear strain of 0.002 or 0.2\% in sand}$ ;

$\gamma = \text{shear strain in sand}$ ;

$a, b = \text{empirical coefficients established by Mwindo (1992)}$

Prakash & Kumar (1996) expressed the average shear strain  $\gamma$  in terms of lateral displacement by the following equation:

$$\gamma = \frac{1+\nu}{2.5B} y_t \quad \text{Equation 3.12}$$

where,

$\nu$  = Poisson's ratio of sand;

$B$  = width of the pile;

$y_t$  = lateral displacement of the pile head for each individual pile

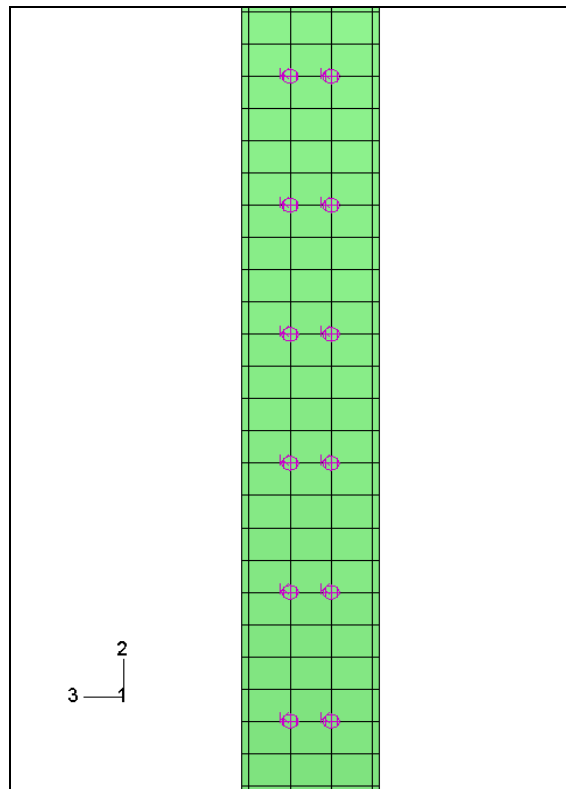


**Figure 3.9: Arrangement of Springs Behind a Pile**

It was also assumed that the variation of the lateral spring stiffness with depth  $z$  is linear according to the following equation.

$$k_h = n_h z \quad \text{Equation 3.13}$$

where,

$n_h$  = constant of horizontal subgrade reaction [ $FL^{-3}$ ]

Thus, equations (3.12) and (3.13) provide the basis for the calculation of lateral spring stiffnesses for the springs adjacent to piles.  $k_{h_{max}}$  is the input material parameter whose value is taken as 10.15 (ksi) for dense sand behind the piles and 10 ft to 15 ft deep ground water table, based on the recommendations given by Prakash & Kumar (1996).

The remaining input parameters for calculating the stiffnesses included the coefficients  $a$  and  $b$  in equation (3.10) whose values were selected to be equal to 0.05 and 0.5, respectively, as suggested by Mwindo (1992) for H steel piles.

### **3.4.3 Convergence of Iterations**

At the end of each iteration errors ( $e$ ) in  $\delta_T$ ,  $\delta_R$  and  $y_t$  are calculated according to equations (3.14) and (3.15) respectively,

$$e(\delta_T) = \left| \frac{(\delta_T)_{i+1} - (\delta_T)_i}{(\delta_T)_{i+1}} \right| \quad \text{Equation 3.14}$$

$$e(\delta_R) = \left| \frac{(\delta_R)_{i+1} - (\delta_R)_i}{(\delta_R)_{i+1}} \right| \quad \text{Equation 3.15}$$

$$e(y_t) = \left| \frac{(y_t)_{i+1} - (y_t)_i}{(y_t)_{i+1}} \right| \quad \text{Equation 3.16}$$

The convergence criterion used herein requires that the errors given by equations (3.14), (3.15) and (3.16) must be less than or equal to 0.01 or 1%. Upon meeting these criteria, iterations are completed and final solution is obtained.

### **3.5 Bridge Model Including Approach Slab**

The numerical model shown in Figure 3.3 was subsequently further modified to include an approach slab, which is monolithically connected to the abutment as shown in Figure 3.10.

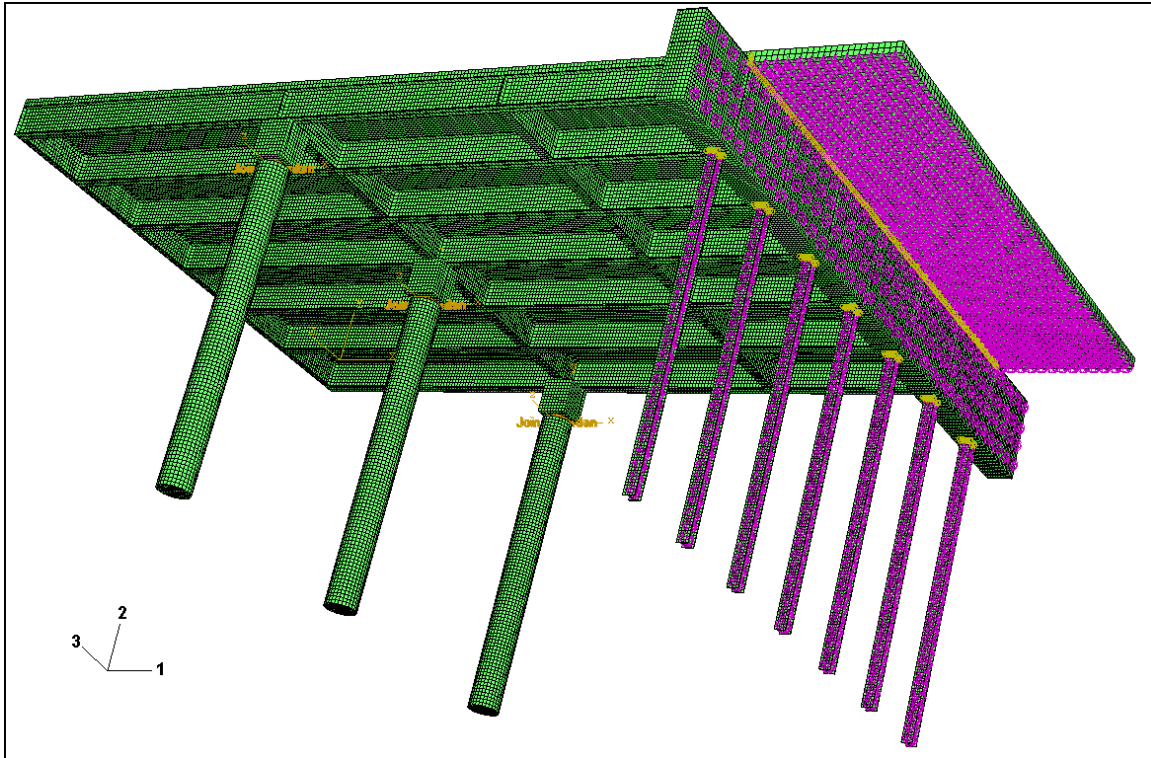


**Figure 3.10: Finite Element Model of the Bridge with Approach Slab (Including the Soil Substituting Springs)**

The concrete approach slab is 13 ft long, 54 ft wide and 1 ft thick. Presence of the soil below the slab is modeled by linear vertical springs, which are attached to the nodes located on the bottom side of the approach slab as shown in Figure 3.10. All other dimensions and properties of the numerical model of the bridge are equal to those described in Sections 3.1, 3.2 and 3.4.

### **3.5.1 Temperatures**

A response of the integral bridge with the approach slab was numerically simulated only for a single case of a thermal loading corresponding to  $\Delta T = 80^\circ\text{F}$ . A combined gravity and thermal loading was applied to the bridge, whereby the later is depicted in detail in Figure 3.11. Influence of different soil properties on the response was assessed by conducting two different analyses modeling the presences of loose

and dense sands behind the abutment (and below the approach slab). Only dense sand was assumed to be adjacent to the piles, as in the previous analyses.

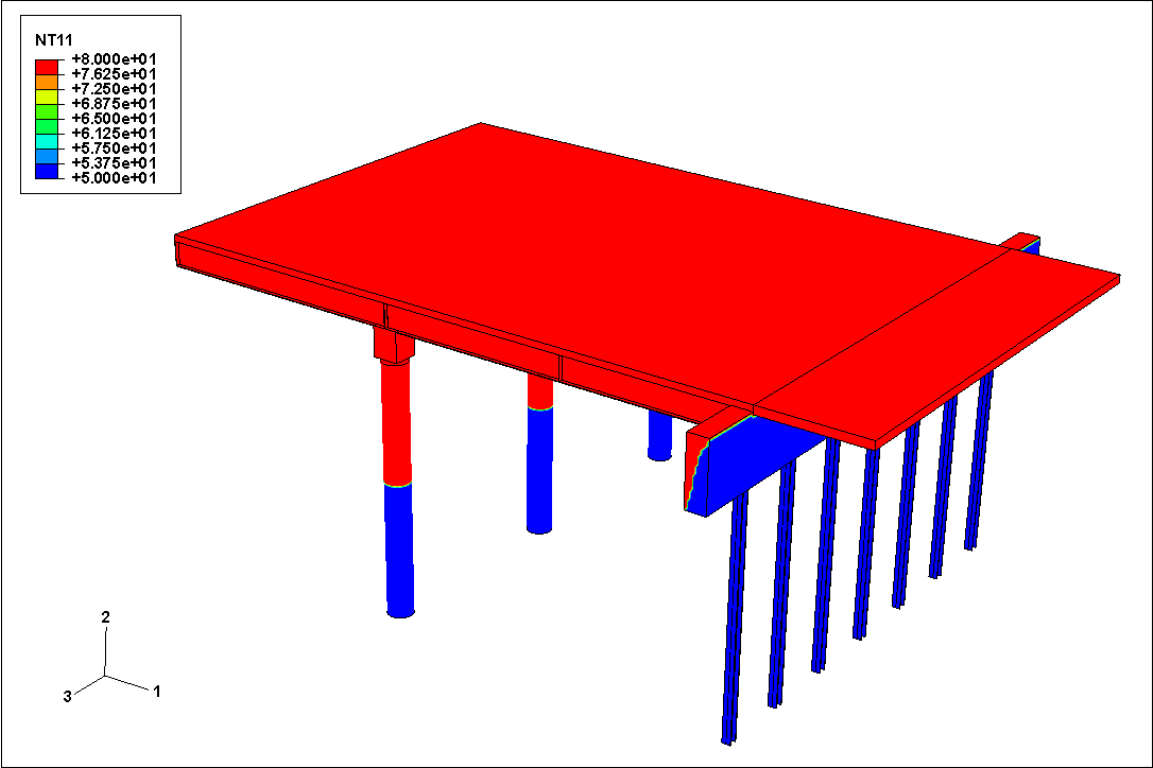


Figure 3.11: Nodal Temperatures

**3.5.2 Springs**

The stiffness of the springs attached to the approach slab is determined based on the values of coefficients of sub-grade reaction for loose and dense sands recommended by Das (1999). These values were first adjusted to reflect the size of the approach slab and subsequently multiplied by the tributary area of each spring, thus resulting in the values of 5,770 lb/in and 40,228 lb/in for loose and dense sands respectively.

Stiffness of the horizontal springs attached to the abutment and piles were determined by the equivalent iterative linear approach as described previously. The

approach slab was treated as a surface load and the increase of the vertical stresses in the soil behind the abutment due to this load was determined by using a so called 2:1 method whereby no effect was felt in front of the abutment. Equation (3.8) was used to calculate the horizontal stresses behind the abutment, which were subsequently needed for the calculation of the stiffness of springs. The vertical stresses in Equation (3.8) comprised two parts, the self weight stresses and additional stresses due to the weight of approach slab. Thus, the influence of the approach slab on the stiffness of the springs attached to the abutment decreased with the increasing depth below the approach slab.

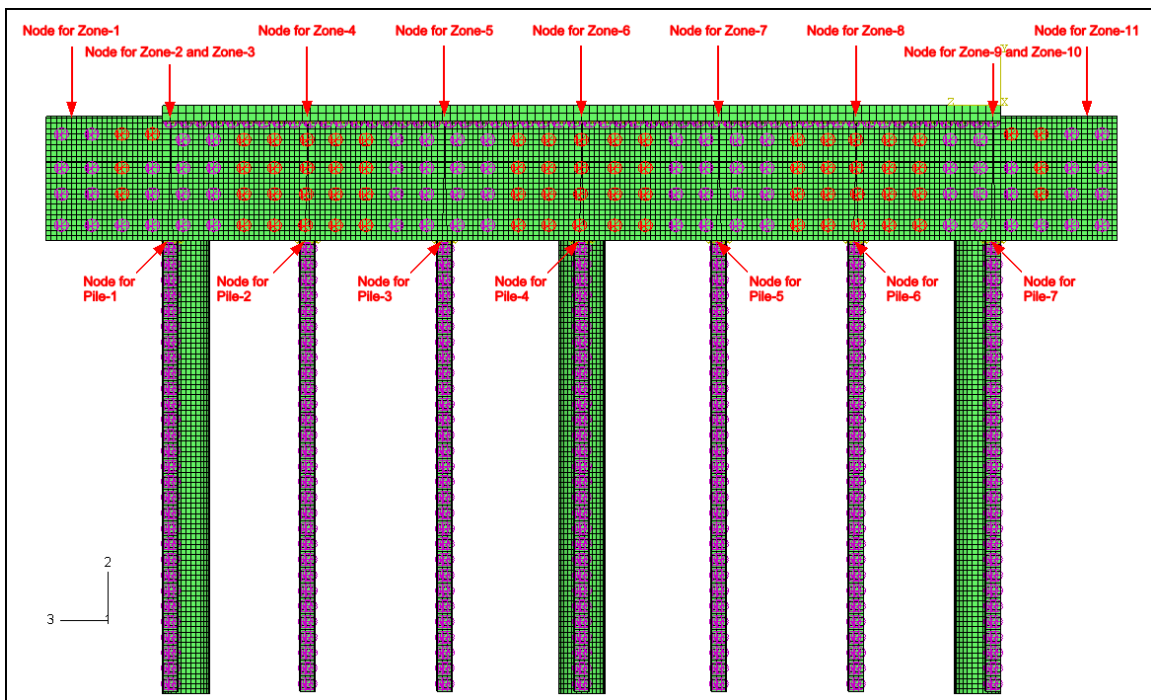


**Figure 3.12: Vertical Zones of the Abutment and the Corresponding Nodes**

Due to the influence of the approach slab on the horizontal stresses in the soil behind the abutment previously used vertical zones on the back side of the abutment shown in Figure 3.8 were changed. In the analyses of the bridge with the approach slab

the zones depicted in Figure 3.12 were used for determination of the abutment top displacements  $\delta$  in 3D analysis. A longitudinal displacement at the center of each zone was used for determination of stiffness of all springs located in that zone. The remainder of the analysis procedures was analogous to the procedures previously described in Sections 3.3 and 3.4.



## CHAPTER 4 - RESULTS AND DISCUSSION

The refined and detailed 3D finite element model of the “Bemis Road Bridge: F-4-20” over the Nashua River in Fitchburg, Massachusetts is analyzed using the finite element code ABAQUS/Standard 6.5-1. This chapter presents the results along with their verification and validation. An additional discussion is also included.

### 4.1 Nomenclature

Since the main objective of the numerical modeling was to assess the influence of temperature changes and the soil conditions on the response of the bridge, the conditions that covered a full range of soil densities and/or relative compactions for the soil adjacent to abutment were studied. The nomenclature of the cases studied is based on the soil densities recommended by the different design agencies. Table 4.1 lists the three soil combinations studied:

**Table 4.1: Soil Combination Nomenclature**

<b>Case</b>	<b>Details</b>
<b>LD</b>	Loose sand adjacent to abutment (using NCHRP, 1991 design curve) and dense sand adjacent to piles
<b>DD</b>	Dense sand adjacent to abutment (using NCHRP, 1991 design curve) and dense sand adjacent to piles
<b>DcD</b>	Dense sand adjacent to abutment (using CGS, 1992 design curve) and dense sand adjacent to piles

In addition, three different values of temperatures change ranges were investigated in this research, thereby also replicating the response of longer bridges. Table 4.2 lists the nomenclature for the 9 cases analyzed herein.

**Table 4.2: Nomenclature for the Cases Studied**

$\Delta T(^{\circ}F)$ Soil combination	60	80	100
LD	LD 60 $^{\circ}F$	LD 80 $^{\circ}F$	LD 100 $^{\circ}F$
DD	DD 60 $^{\circ}F$	DD 80 $^{\circ}F$	DD 100 $^{\circ}F$
DcD	DcD 60 $^{\circ}F$	DcD 80 $^{\circ}F$	DcD 100 $^{\circ}F$

## 4.2 Results

Displacements and stresses obtained for DD 100 $^{\circ}F$  are presented in this section.

### 4.2.1 Displacements

Figures 4.1, 4.2 and 4.3 show the longitudinal displacements U1, the vertical displacements U2 and the lateral displacements U3 of the bridge, respectively. The corresponding coordinate system is shown in the figures.

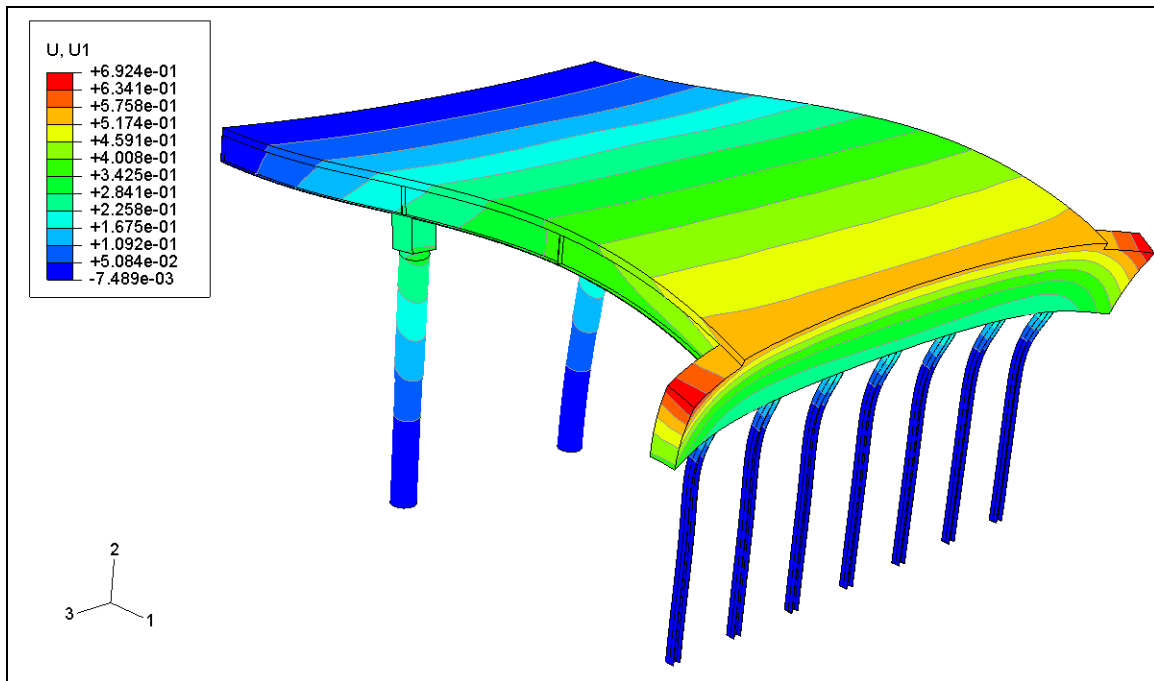


**Figure 4.1: DD 100 $^{\circ}F$  - Longitudinal Displacement U1 (in) of the Bridge (Deformation Scale Factor=130)**

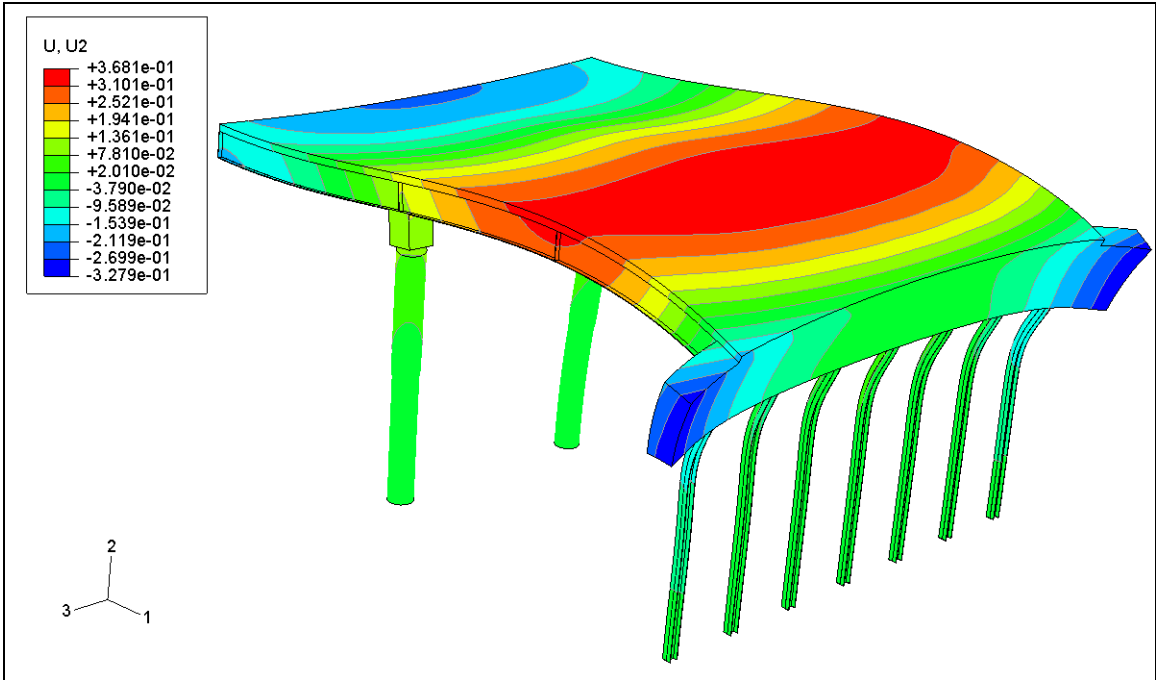


Figure 4.2: DD 100°F - Vertical Displacement U2 (in) of the Bridge (Deformation Scale Factor=130)

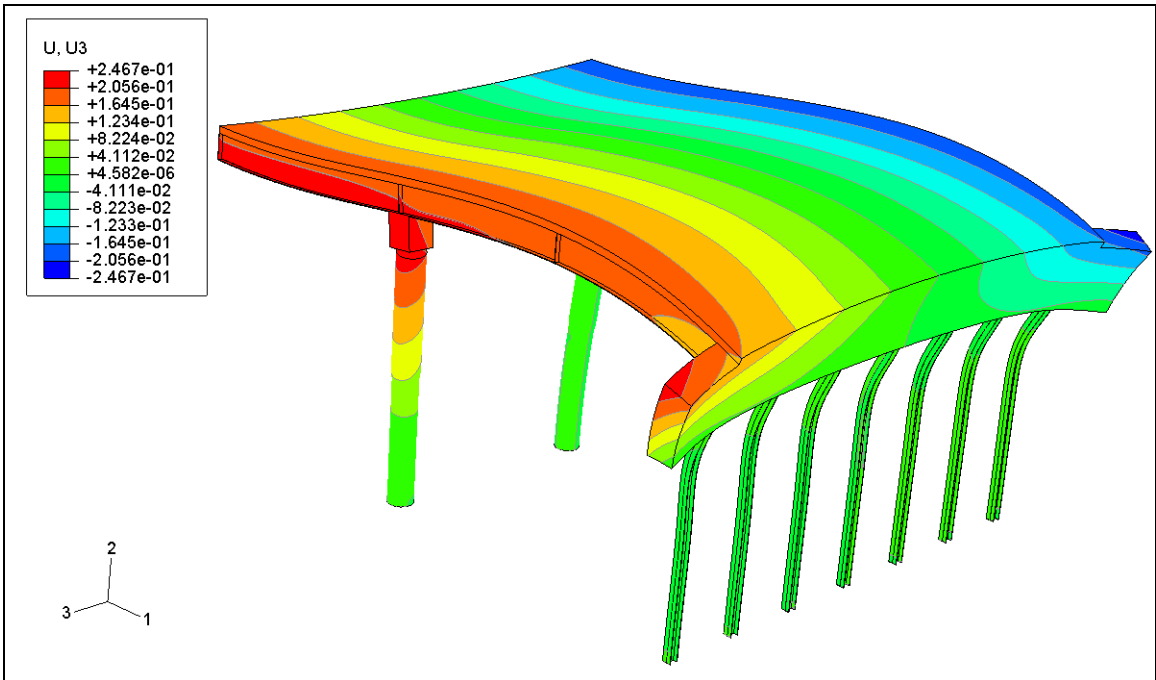
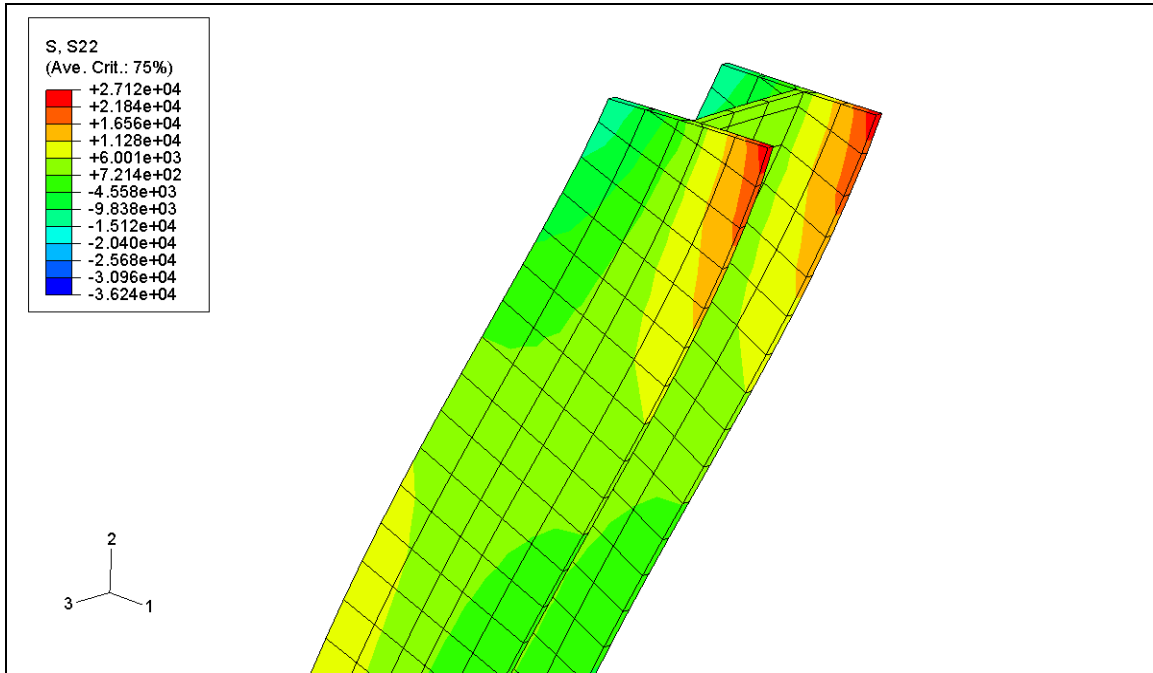


Figure 4.3: DD 100°F - Lateral Displacement U3 (in) of the Bridge (Deformation Scale Factor=130)

## **4.2.2 Stresses**

Figure 4.4 shows the axial stress S22 in the central pile.



**Figure 4.4: DD 100°F - Axial Stress S22 (psi) in the Piles (Deformation Scale Factor=130)**

Figure 4.5 shows the axial stress S11 in the girders.

## **4.3 Comparison of the Two FE Models**

In this research, the model used by Ting & Faraji (1998) has been refined. Certain modeling changes have also been incorporated as per the requirements by the KDOT. The differences are listed below:

### **4.3.1 Differences in the Bridge Model**

Complete 3D model of the selected IB: The model developed in this research does not include any simplifications. All parts of the bridge have been modeled using eight-node coupled temperature-displacement elements – C3D8T. On the other hand,

Ting & Faraji (1998) had used 1D beam elements for girders, transverse beams and piles, and bending plate and shell elements for the deck and abutment walls. Ting and Faraji (1998) had used rigid links to model the connection between the deck slab and girders, thus ensuring “strain compatibility and shear transfer between the deck slab and girder elements”. Herein, the composite action at the connection of the deck and girders is modeled by using “ABAQUS merge and tie feature, thus producing a no-slip connection.

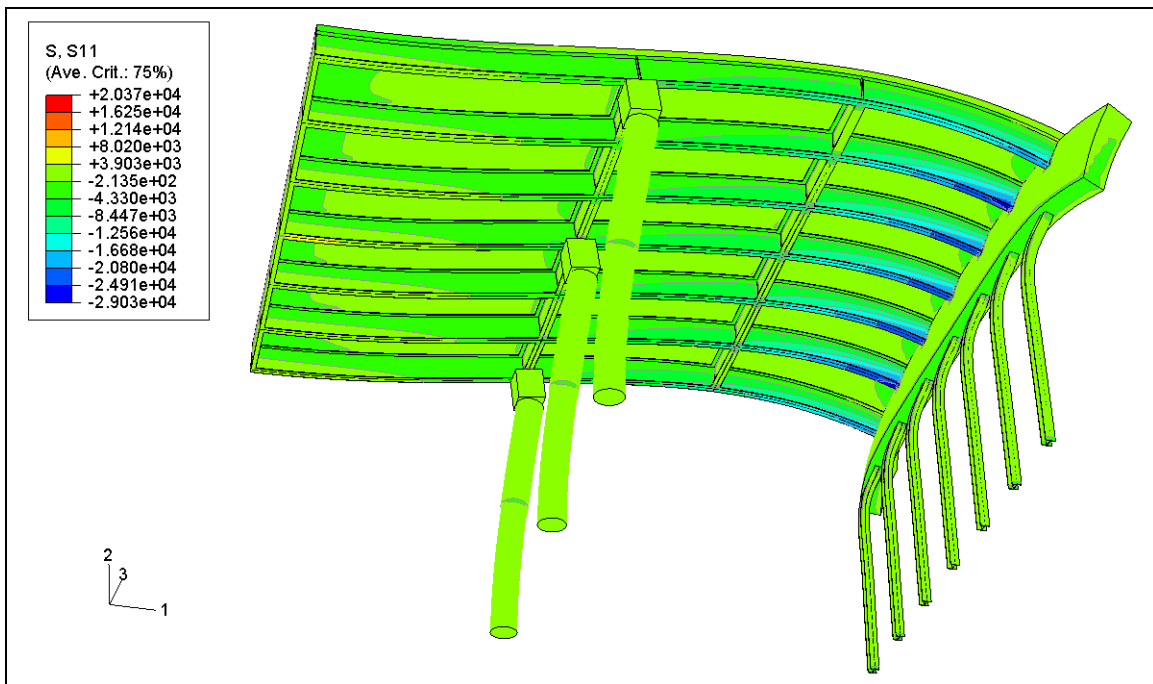


**Figure 4.5: DD 100°F - Axial Stress S11 (psi) in the Girders (Deformation Scale Factor=130)**

Hinges: To prevent any moment transfer to the piers, as required by KDOT, the connection between the bridge superstructure and the piers is modeled by a hinge using CONN3D2 connector elements. On the contrary, Ting & Faraji (1998) had modeled a fixed connection between the bridge superstructure and piers.

Pier caps: A single pier cap of dimensions 3.5 ft x 3 ft x 56.5 ft, supported by three columns, had been used by Ting & Faraji (1998). In this research, each pier was capped by an individual pier cap of dimension 3 ft x 3 ft x 3.5 ft.

Transverse beams: Ting & Faraji's FE bridge model comprised eight transverse beams, each consisting of channels and angles. In this research, the FE bridge model consisted of seven transverse steel beams of W36x135 section.

#### **4.3.2 Differences in Material Properties**

Coefficient of thermal expansion: While Ting & Faraji (1998) had used a coefficient of thermal expansion  $\alpha$  of  $6.5 \times 10^{-6}$  per °F for the composite deck, this research used two different values of coefficient of thermal expansion  $\alpha$ , one for concrete and the other for steel as listed in Table 3.1, according to the recommendations of KDOT Bridge Design Manual (2007).

#### **4.3.3 Differences in Soil Model**

Soil adjacent to abutment: The  $K - \delta$  relationships used for dense and loose soils as recommended by NCHRP (1991) had also been used by Ting & Faraji (1998). In addition, the recommendations by CGS (1992) were used in this research. While both, Ting & Faraji (1998) and this research used nonlinear soil substituting springs, the former used truly non-linear springs while the later adopted the iterative equivalent linear approach. Unit weights of the soils used for this research are listed in Table 3.3. Ting & Faraji (1998) used the unit weight of 120 lb/ft<sup>3</sup> regardless of the soil density and they did not quantify the soil density either in terms of relative density or relative compaction.

Soil adjacent to piles: Ting & Faraji (1998) had adopted the “ $p$ - $y$ ” design curves recommended by American Petroleum Institute (1993) for nonlinear force-deflection relations describing a soil-pile interaction. On the other hand, a method proposed by Prakash & Kumar (1996) as alternative to “ $p$ - $y$ ” curves was used herein. The method is based on full scale pile tests. It describes a load-displacement relationship for a single laterally loaded pile by considering the non-linear behavior of soil.

#### **4.3.4 Differences in Loads**

Self-weight: The analysis for this research includes load application in two steps as discussed in section 3.2. Ting & Faraji (1998) applied only a thermal loading without the self-weight.

Thermal gradient within the abutment: Ting & Faraji (1998) had applied the thermal loading only to the composite deck. The abutment was not subjected to any temperature changes. Herein, a thermal gradient was applied within the abutment wall (Figure 4.6) in order to better model the transition of temperatures within the bridge structure as experienced in the field. Figure 4.6 shows the thermal gradient in the abutment simulating the field conditions whereby the part of the abutment directly exposed to the atmosphere gets heated up while the part that is not exposed remains at a lower temperature.

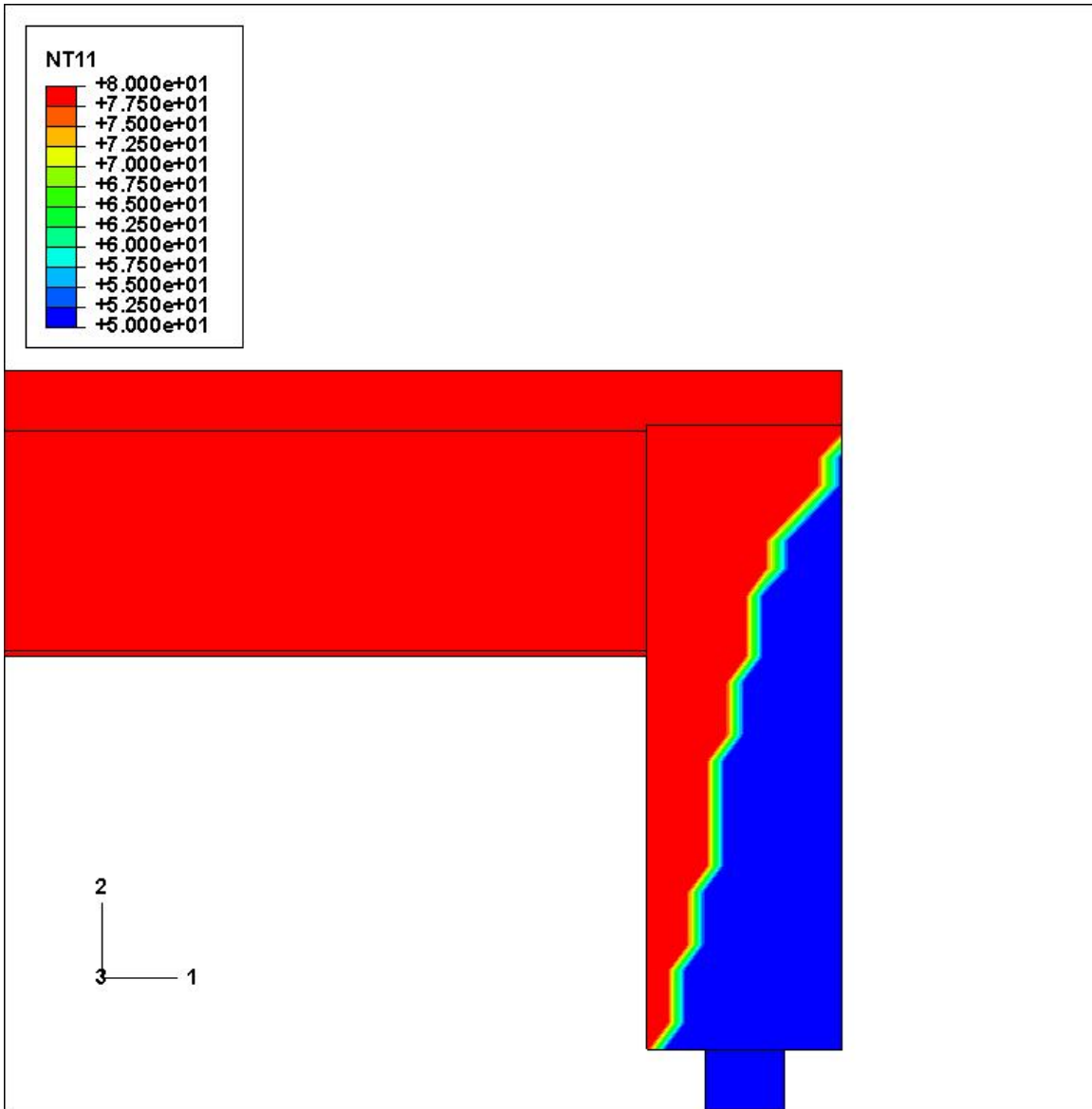


Figure 4.6: Nodal Temperatures (° F) with the Abutment Detail

#### 4.4 Validation and Verification of the Model

The method of analysis described in Chapter 3 was first validated and verified against the results reported by Ting & Faraji (1998). For that purpose, the same coefficient of thermal expansion  $\alpha$  of  $6.5 \times 10^{-6}$  (per °F) was used for both steel and concrete as had been done by Ting & Faraji, 1998 and FE analysis was conducted for the loading case DD 80°F. The unit weight on the soil was also changed in accordance

with Ting & Faraji (1988). In addition, the unit weight of the soil was changed to 120 lb/ft<sup>3</sup>, gravity load was removed and hinge connection was replaced by a fixed connection, all in accordance to the model of Ting & Faraji (1998). Moreover, in this case there was no internal temperature gradient within the abutment. All other modeling differences as explained in section 4.2 remained as they were.

The results so obtained during the validation process were close to those reported by Ting & Faraji (1998) as depicted in Figure 4.7. Small differences are attributed to the differences in the FE models as explained in section 4.3.

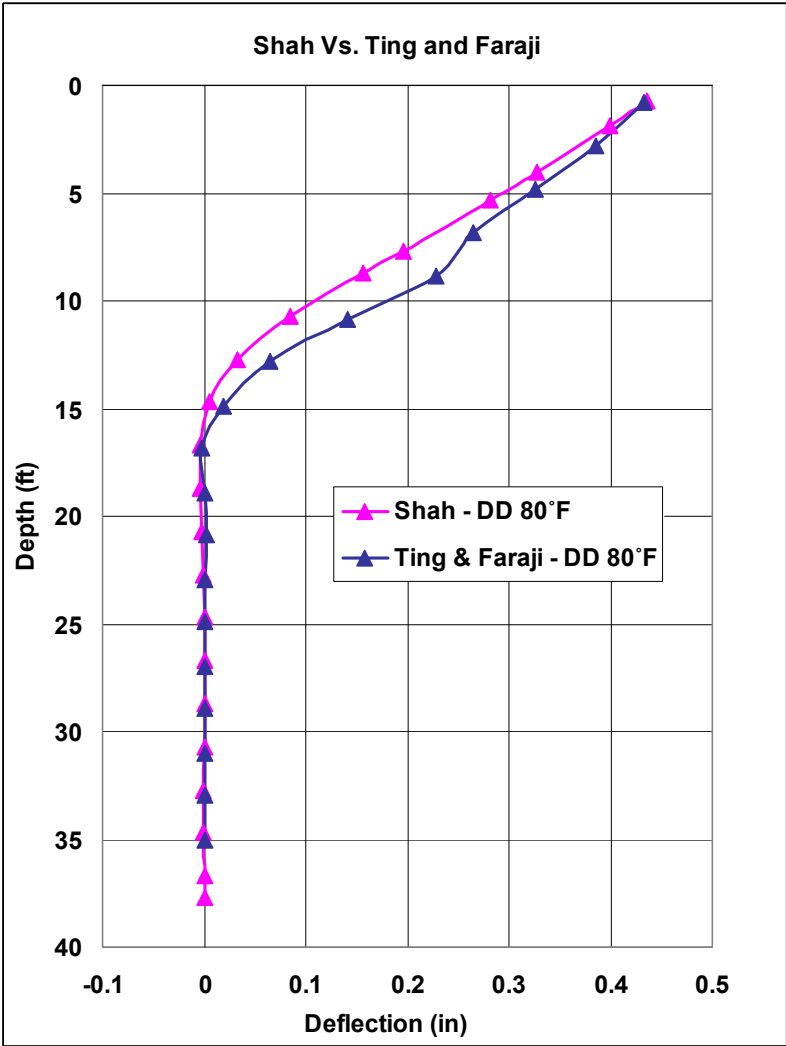


Figure 4.7: Comparison of Longitudinal Displacements, U1 (in)

Based on the comparison presented in Figure 4.7 between the results obtained herein and those obtained by Ting & Faraji (1998), it was concluded that the model used in this research is sufficiently verified and validated.

#### 4.5 Results and Discussion

Each set of results is presented in two formats. The first format shows the trends observed due to different temperature changes for the selected soil properties. The second format shows the trends observed due to different soil properties for the selected thermal load.

Table 4.3 lists the converged values of the coefficients of lateral earth pressure  $K$  for the soil behind the abutment for the nine cases analyzed. The converged values of  $K$  for 100°F are also shown in Figures 4.8 and 4.9.

**Table 4.3: Converged Values of the Coefficient of Lateral Earth Pressure  $K$**

<b>Soil combination Temperatures</b>	<b>LD</b>	<b>DD</b>	<b>DcD</b>
<b>60°F</b>	1.029	4.235	2.853
<b>80°F</b>	1.218	4.698	3.127
<b>100°F</b>	1.293	5.362	3.371

As per the design curves by NCHRP (1991) the fully passive state for loose sand is reached when the value of coefficient of lateral earth pressure  $K$  is 3.0, while for dense sand, the value is 5.8. The design curves by CGS (1992) indicate a value of 8.3 for the coefficient of lateral earth pressure  $K$  at fully passive state. As depicted in Figures 4.8 and 4.9 there is only one loading combination that results in the soil behind abutment closely approaching the fully passive failure state and that is DD 100° F. For practical purposes this loading combination leads to the passive failure in the soil

behind the abutment according to NCHRP (1991) design curves. On the other hand, use of the Canadian design curve depicted in Figure 4.8 does not result in passive failure for the loading combination DcD 100° F .

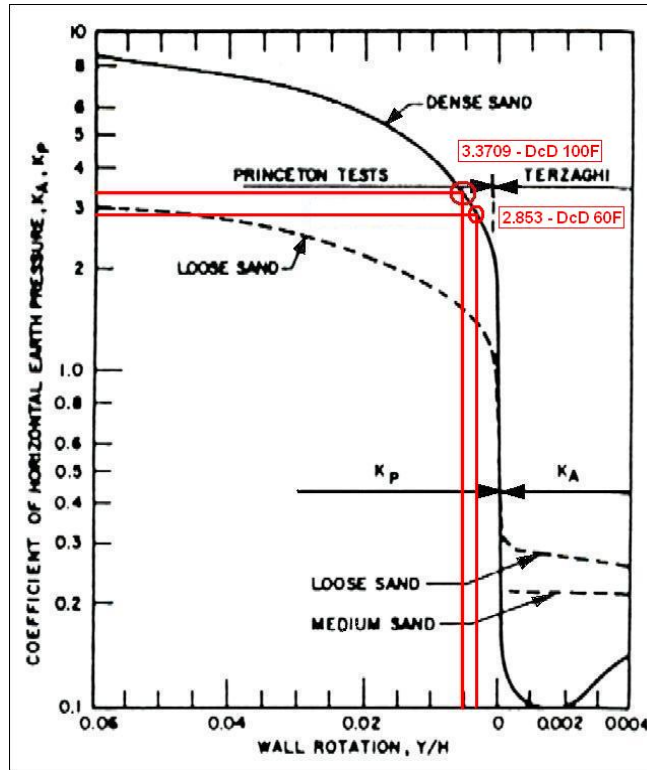


Figure 4.8: Converged Values of K for DcD 100° F case

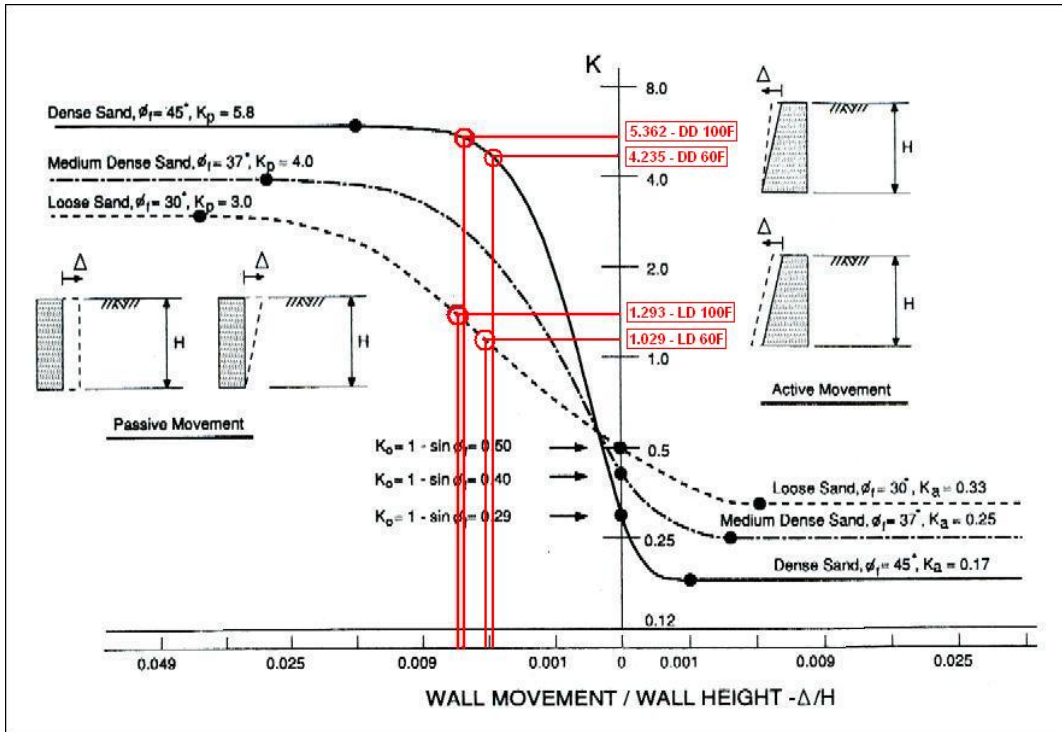


Figure 4.9: Converged Values of  $K$  for DD 100°F and LD 100°F cases

#### 4.5.1 Longitudinal Displacement at Centerline of the Bridge

##### 4.5.1.1 Trends Due to Change in the Thermal Load for the Particular Soil Properties

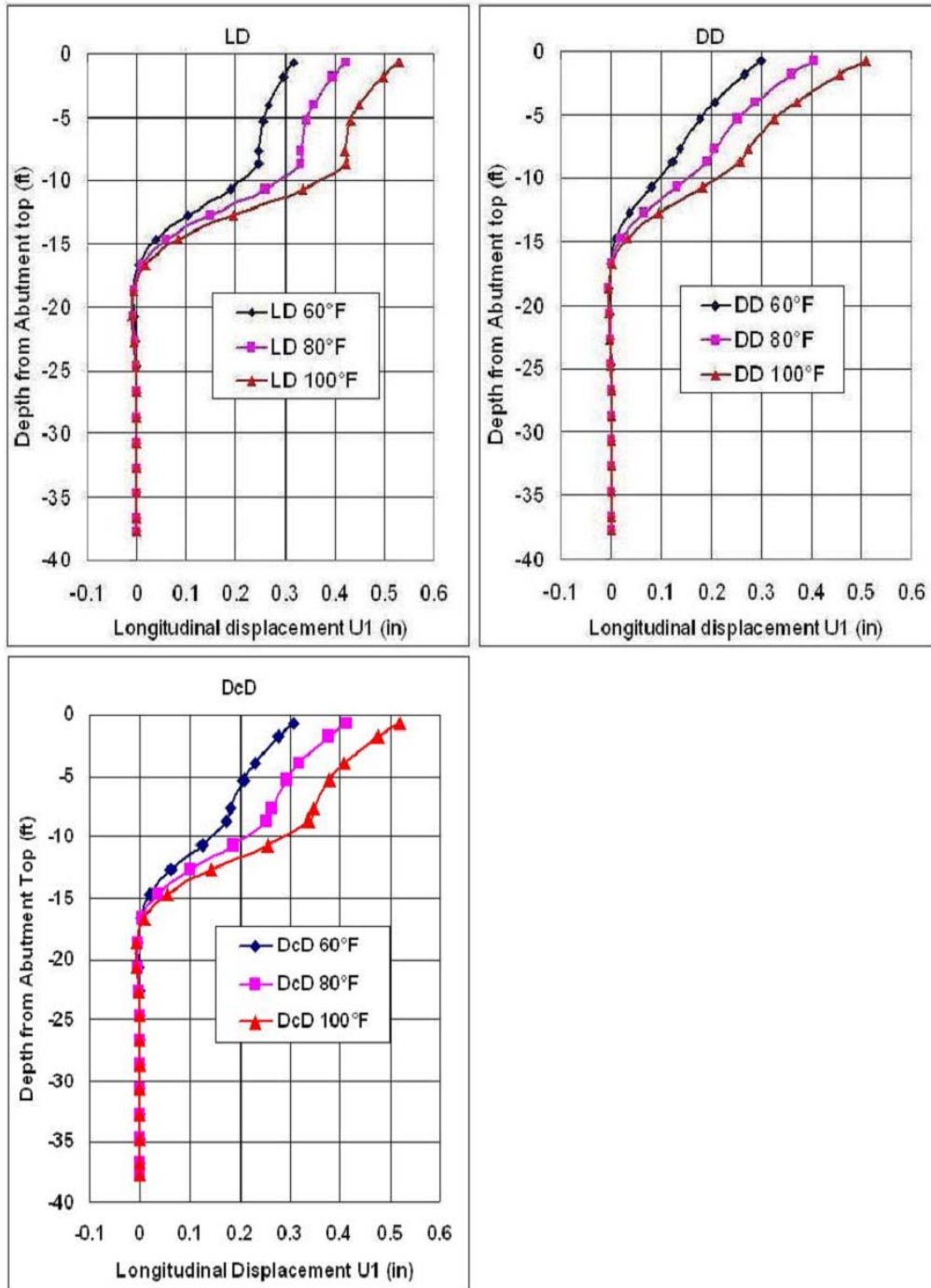
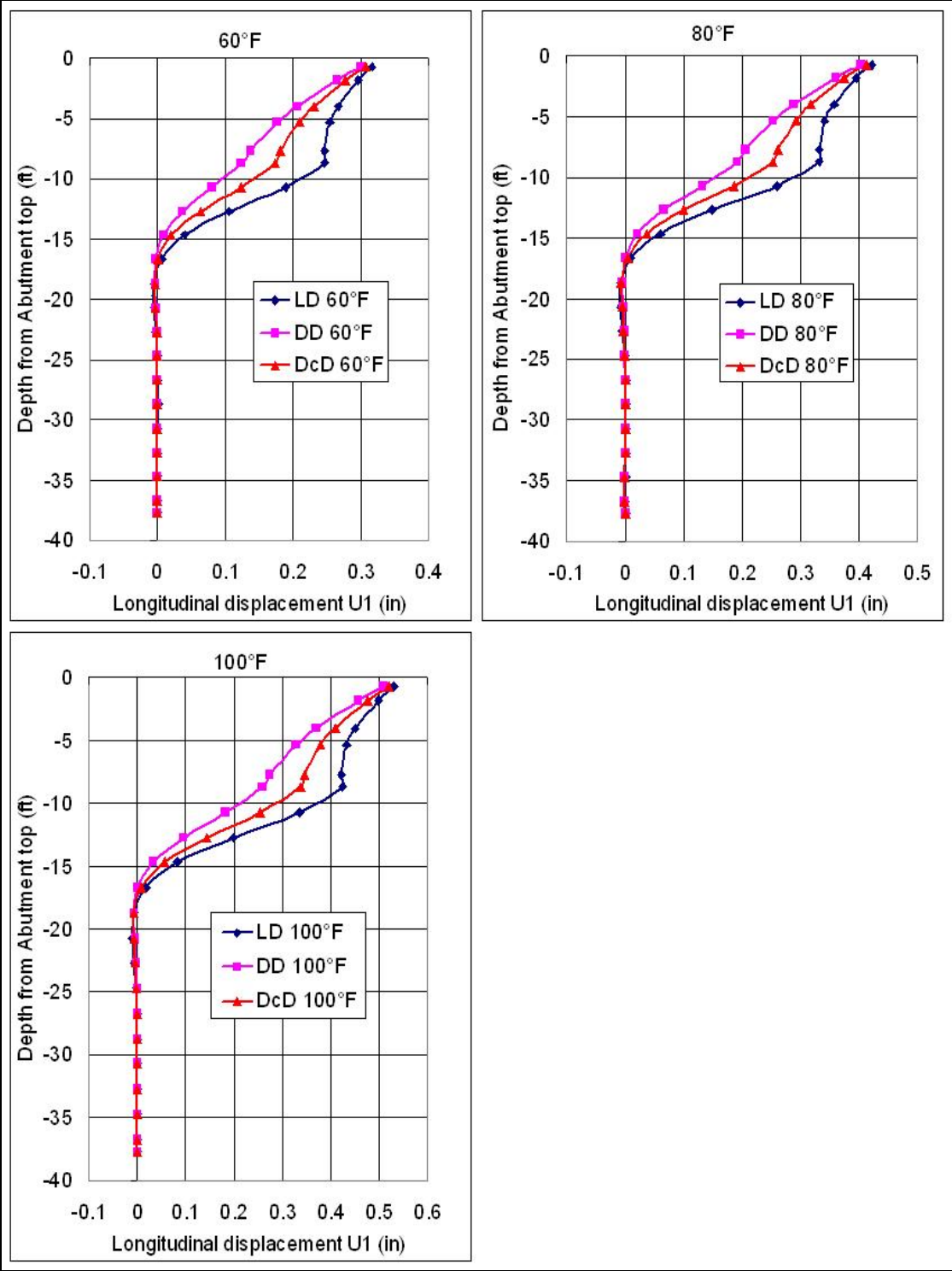


Figure 4.10: Trends in Longitudinal Displacement Due to Changes in Thermal Load

**4.5.1.2 Trends Due to Change in Soil Properties for the Particular Thermal Load**



**Figure 4.11: Trends in Longitudinal Displacement Due to Changes in Soil Properties**

#### **4.5.1.3 Discussion**

Based on the plots in Figure 4.10, it can be stated that the behavior of the bridge is qualitatively independent of the temperature change range for the selected soil properties. It is because the curves are geometrically similar that the depicted behavior is only quantitatively dependent on the temperature change. On the contrary, the plots shown in Figure 4.11 clearly indicate that the behavior of the bridge is qualitatively and quantitatively dependent on the soil properties. Figure 4.11 indicates that properties of the soil behind abutment have a significant influence on the pile head displacement. Specifically, for any given range of temperature change, the pile head displacement is reduced by 39% or more when relative compaction of the soil is increased from 90% to 96%. It is also observed from the plots in Figure 4.10 that the displacements are varying in a linear fashion with the change in temperature, for the particular soil properties. The displacements at the abutment top are extracted from these results and plotted versus temperature changes in Figure 4.12, which confirms the linearity of the results. It is also observed from this plot that soil properties have a negligible influence on the displacement of the deck.

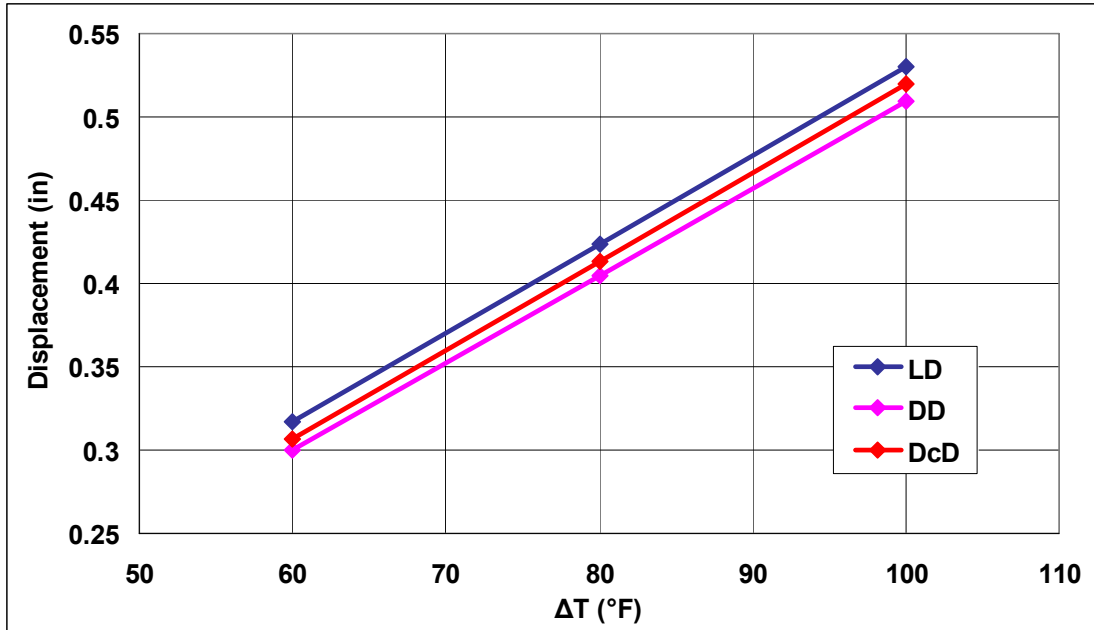


**Figure 4.12: Displacement (in) at the Abutment Top vs.  $\Delta T$  (° F)**

Another behavior observed is the bending of the abutment, which becomes less significant when the soil adjacent to the abutment gets denser. While the bending of the abutment originates from the thermal gradient applied within the abutment (Figure 4.6), the density of the soil adjacent to the abutment controls the extent of the bending. The bending behavior is prominent in the LD case, the effect gets reduced for DcD case and even more so for DD case (Figure 4.10). This is due to the fact that the soil stiffness increases at a faster rate with depth when the soil is denser. So while the translation of the abutment ( $\delta_T$ ) is significantly higher than the rotation ( $\delta_R$ ) of the abutment in LD case, the difference gets reduced as the soil behind the abutment becomes denser as demonstrated by DcD case depicted in Figure 4.13. Moreover, in DD case rotation is larger than translation, but the difference gets reduced with increase in the temperature

range resulting in the rotation being equal to the translation for temperature change of 100 ° F (Figure 4.13).

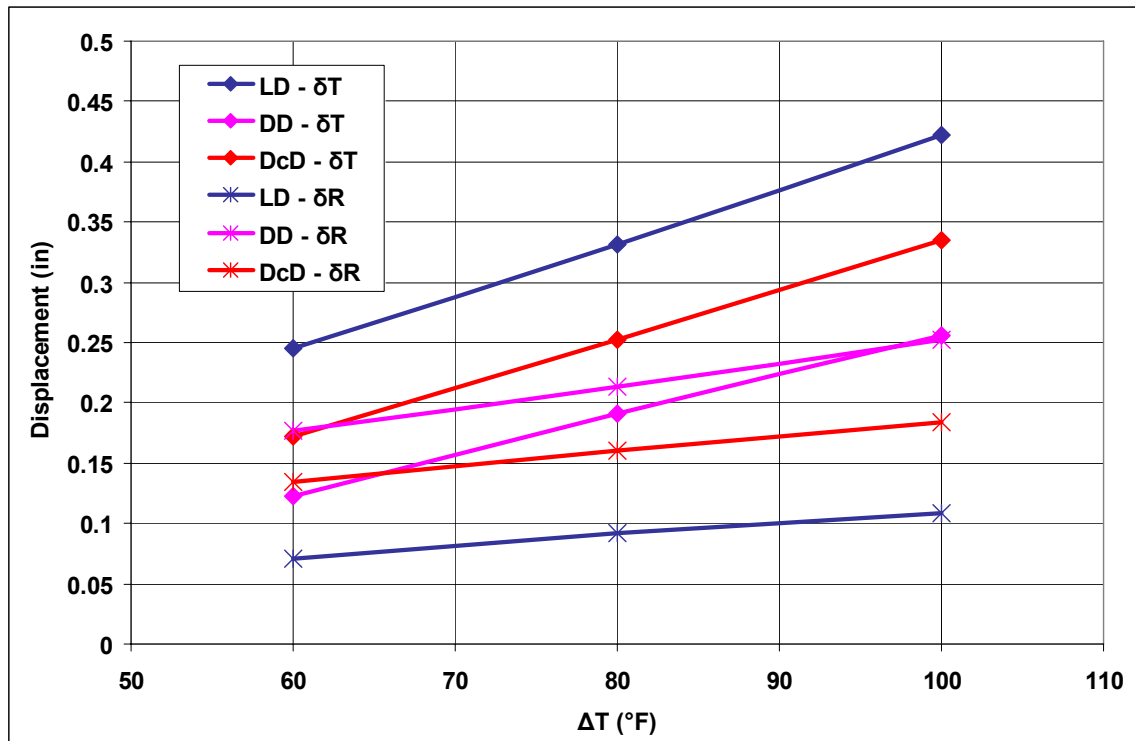


**Figure 4.13:**  $\delta_T$  (in) and  $\delta_R$  (in) vs.  $\Delta T$  (° F)

Figures 4.11 and 4.12 clearly show that while the displacement at the abutment top is very similar for a given temperature change and for all soil properties, it varies with depth (Figure 4.11), depending on the type of soil adjacent to the abutment.

It is noteworthy to mention that the displacement at the pile top is dictated mainly by the type of soil behind the abutment. The deflected shape of the pile remains the same for different soils behind the abutment. Also the depth at which the lateral pile deflection becomes negligible is slightly affected by the soil type behind the abutment; i.e. the depth is larger for LD case than for DD and DcD cases (Figure 4.11). These trends can be explained by the presence of same soil behind the piles in all cases,

showing that the influence of the type of soil adjacent to the abutment on the pile behavior diminishes with increasing depth from the pile head.

Graphs in Figure 4.14 depict displacements at various locations along the depth from the deck to the pile top, versus temperature change. These displacements are compared with the displacement calculated analytically by using the following equation:

$$\Delta l = \alpha_{\text{comp}} \Delta T \frac{L}{2} \quad \text{Equation 4.1}$$

where,

$\Delta l$  = expansion of the deck for half of the bridge

$\Delta T$  = temperature change

$\frac{L}{2}$  = Half-length of the bridge = 75ft

$\alpha_{\text{comp}}$  = composite coefficient of thermal expansion of the concrete deck and steel

girders calculated using the following equation:

$$\alpha_{\text{comp}} = \frac{\alpha_s A_s + \alpha_c A_c}{A_s + A_c} \quad \text{Equation 4.2}$$

where,

$\alpha_c, \alpha_s$  = coefficients of thermal expansion of concrete and steel, respectively, as listed in Table 3.1

$A_c, A_s$  = total area of cross-section of the concrete deck and steel girders, respectively.

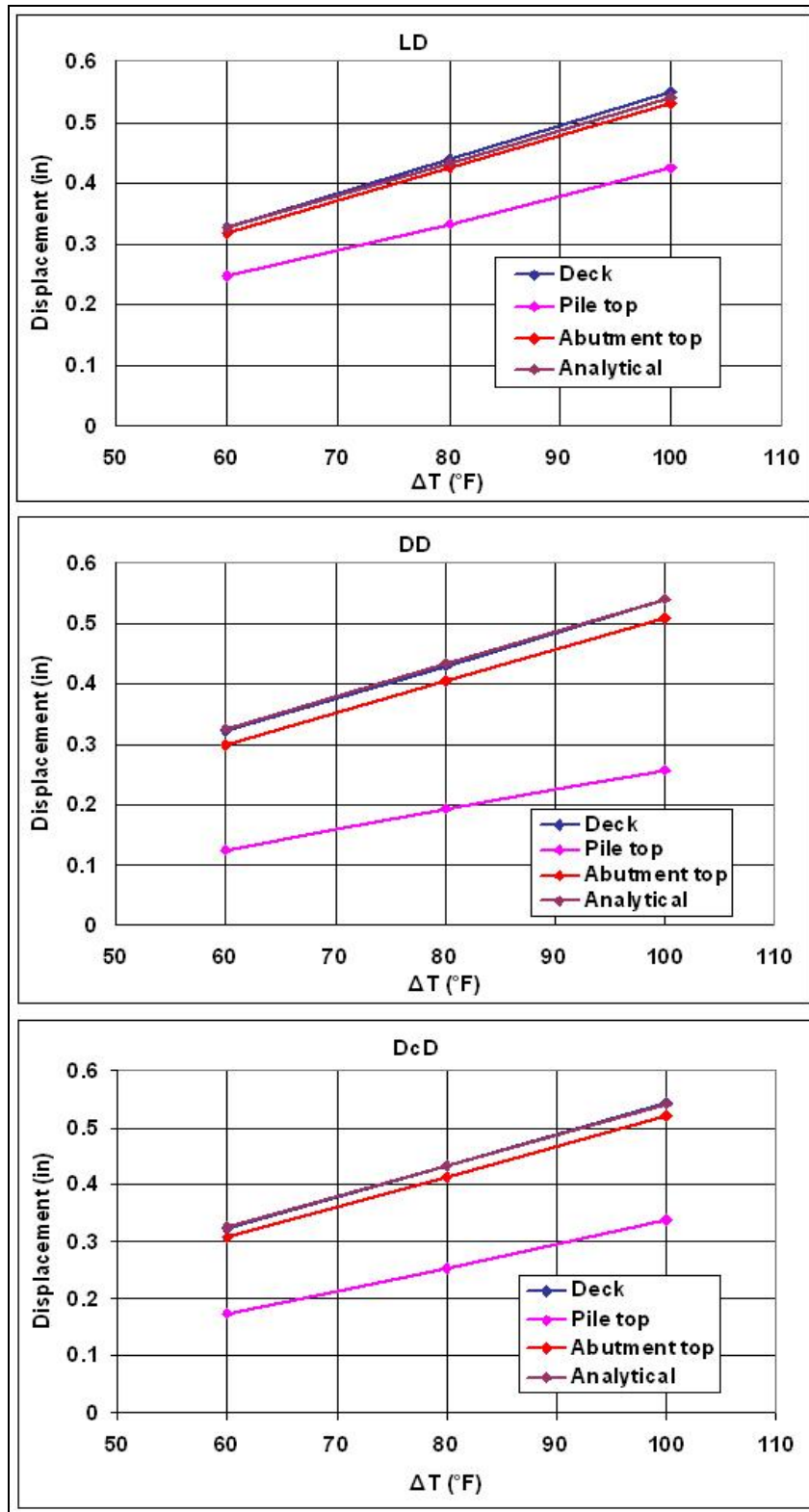


Figure 4.14: Comparison of Deck Displacements (in)

Figure 4.14 shows that presence of soil has virtually no influence on the deck displacement. This is confirmed by the fact that the deck displacement obtained from FE simulation matches very closely to the one calculated from Equation (4.1). The longitudinal displacement of the abutment top is affected by the presence of soil, more significantly in the DD case than in the DcD case. In LD case influence of soil on the abutment top displacement is negligible. However, the longitudinal displacement of the pile top is significantly affected by the presence of soil behind abutment in all cases studied. The largest difference between the longitudinal displacements of the abutment top and pile top is observed in DD case which is followed by DcD case. The difference is the smallest in the LD case.

## 4.5.2 Central Pile Bending Moment

### 4.5.2.1 Trends Due to Change in Thermal Load for the Particular Soil Properties

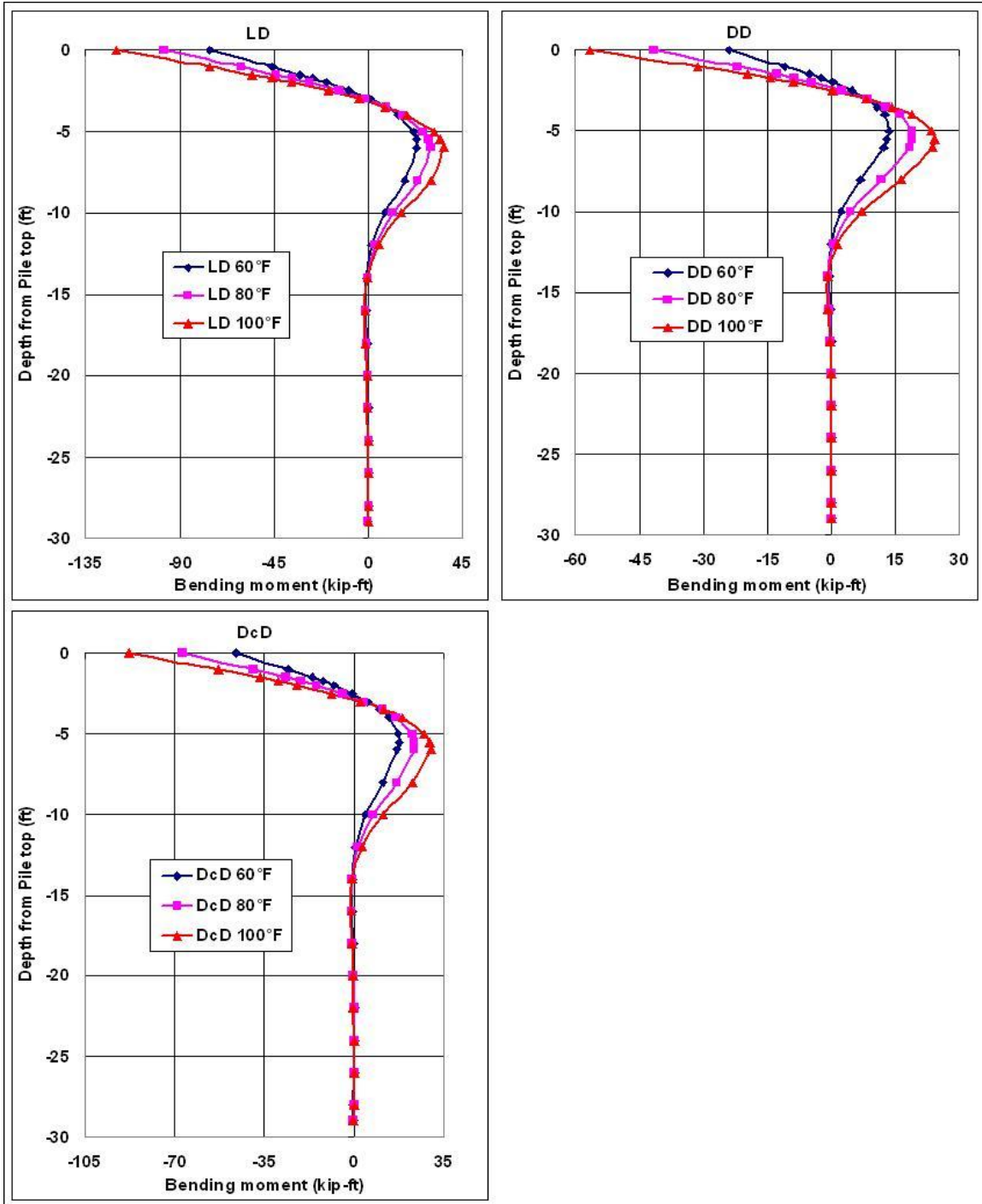
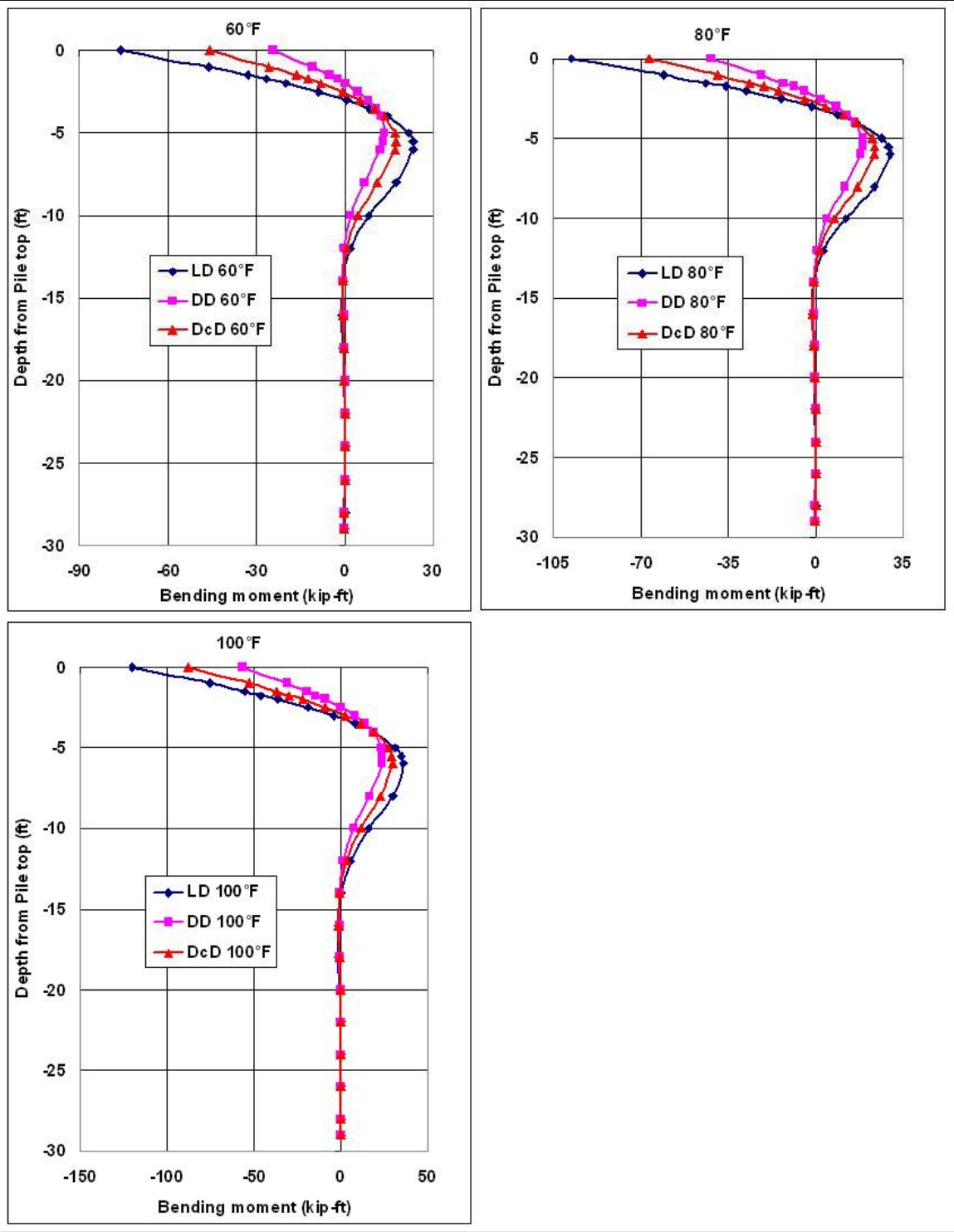


Figure 4.15: Trends in Central Pile Bending Moment (kip-ft) Due to Changes in Thermal Load

**4.5.2.2 Trends Due to Change in Soil Properties for the Particular Thermal Load**



**Figure 4.16: Trends in Central Pile Bending Moment (kip-ft) Due to Changes in Soil Properties**

### 4.5.2.3 Discussion

The displacements at the pile top are extracted from these results and plotted versus temperature changes in (Figure 4.17), which confirms the linearity of the results. It is also observed from Figure 4.17 that soil properties have a major influence on the displacement of the pile top.

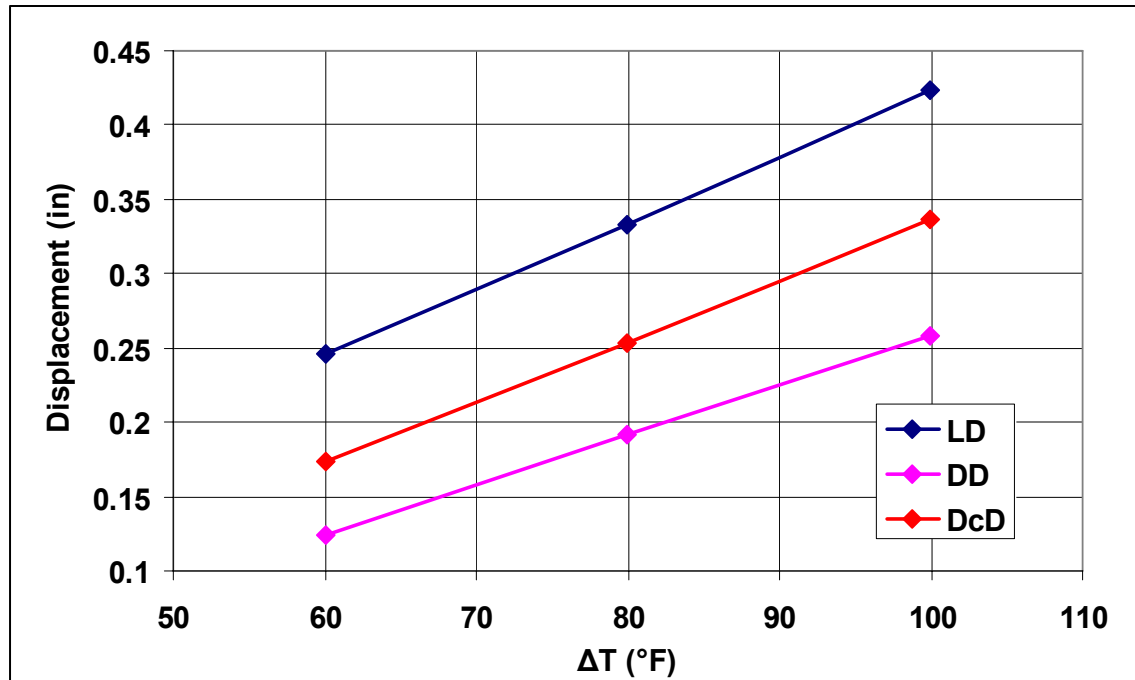
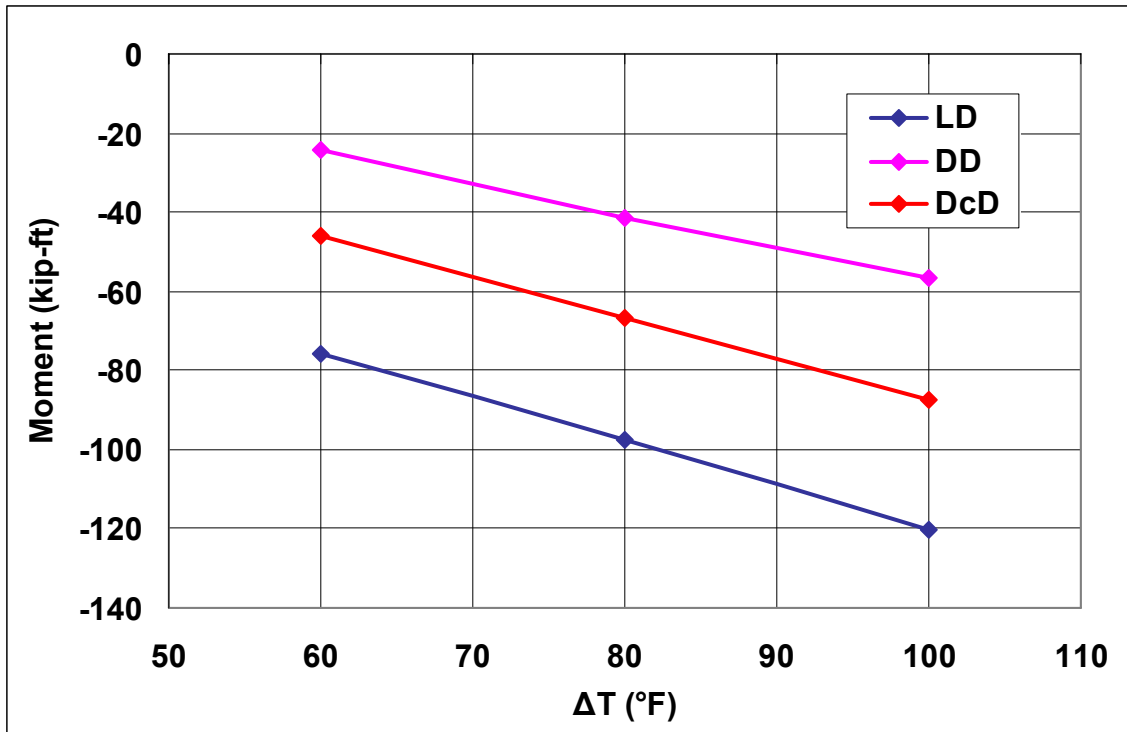


Figure 4.17: Displacement (in) at the Pile Top in Central Pile vs.  $\Delta T$

The bending moment in a pile depends mainly on the pile top displacement  $y_t$ , which is in turn dependent on the temperature change range, the stiffness of the soil adjacent to the abutment and piles, and stiffness of the pile itself. The larger the value of  $y_t$ , the larger is the maximum bending moment, which is located at the pile top. Thus, for the particular soil properties, higher temperature change produces, larger  $y_t$  resulting in larger maximum bending moments (Figure 4.15). The difference between the

maximum bending moments at  $\Delta T = 60^\circ \text{ F}$  and  $\Delta T = 100^\circ \text{ F}$  is the largest for LD case and equal to 44.46 kip-ft.



**Figure 4.18: Maximum Bending Moment (kip-ft) in Central Pile Vs.  $\Delta T$**

For a particular temperature change, having looser soil behind the abutment results in larger pile head displacement,  $y_t$  and subsequently larger maximum bending moment. As the soil gets denser,  $y_t$  decreases thereby reducing the value of the maximum bending moment. Differences between maximum bending moments for any given temperature change range, due to different soils are significant. Maximum bending moment for DD case is about 47% of the maximum bending moment for LD case. Thus, maximum bending moments, which occur at the pile head, are significantly influenced by the change in the stiffness of the soil behind the abutment. The increase in relative density from 50% to 80%, which corresponds to the increase in relative

compaction from 90% to 96% reduces the maximum bending moment by about 53% or more for any temperature change ranges considered herein. The reduction in bending moments is more significant for lower temperature change range (Figure 4.18).

### 4.5.3 Central Pile Bending Stress

#### 4.5.3.1 Trends Due to Change in Thermal Load for the Particular Soil Properties

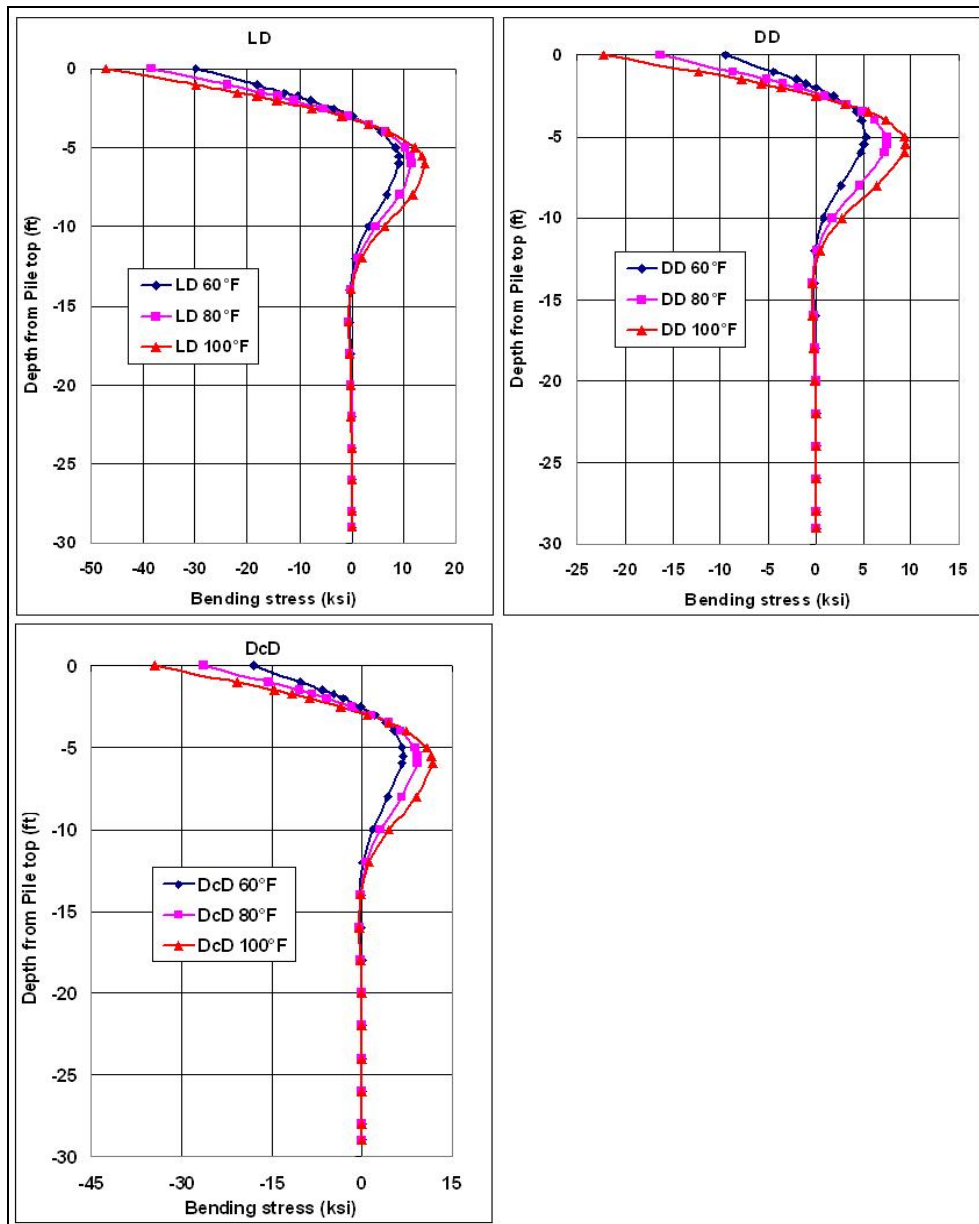


**Figure 4.19: Trends in Central Pile Bending Stress (ksi) Due to Changes in Thermal Load**

**4.5.3.2 Trends Due to Change in Soil Properties for the Particular Thermal Load**

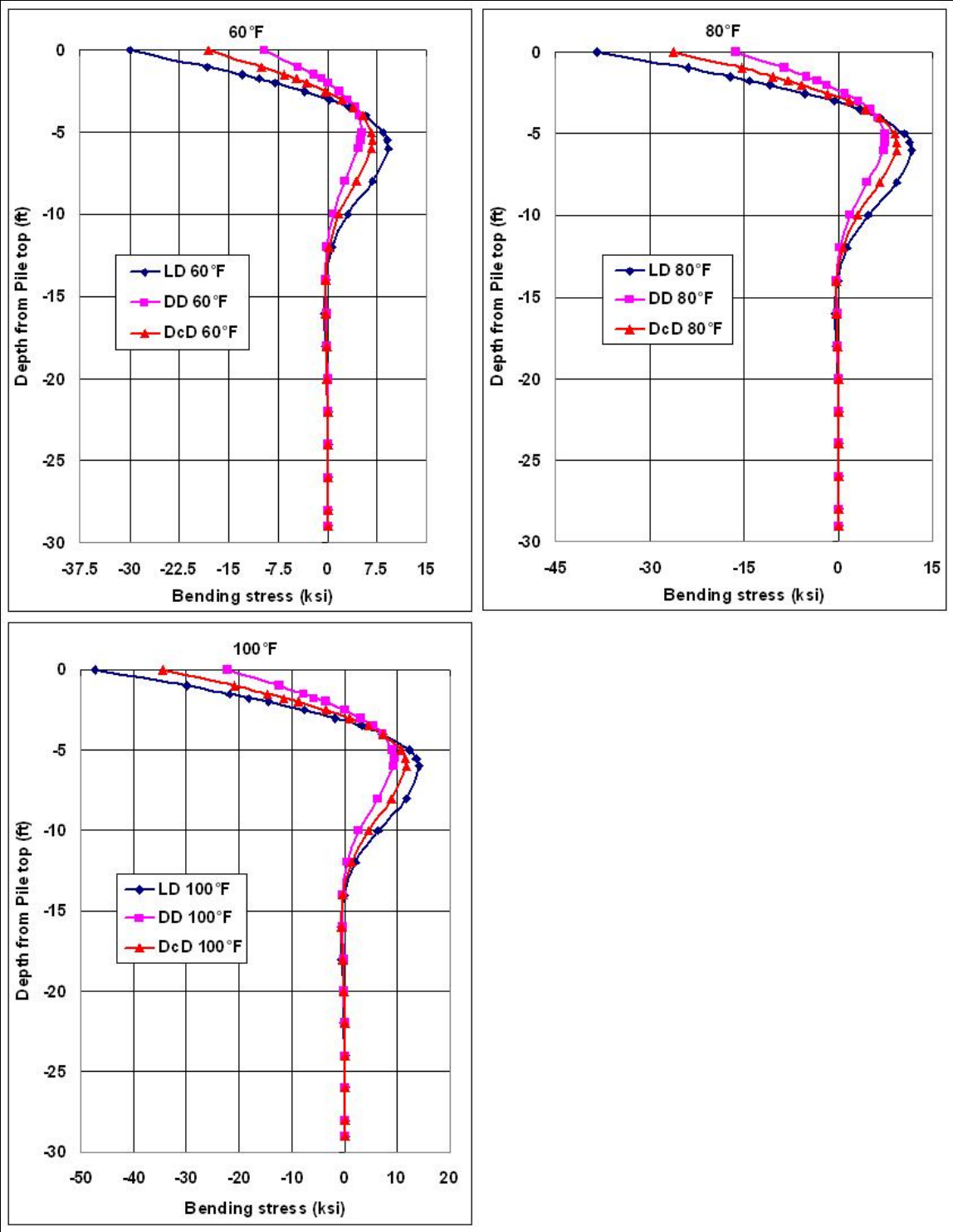


**Figure 4.20: Trends in Central Pile Bending Stress (ksi) Due to Changes in Soil Properties**

### 4.5.3.3 Discussion

The bending stresses in piles are directly dependent on the bending moment. Thus a higher bending moment results in a higher bending stress on the pile cross-section. Figures 4.19 and 4.20 clearly indicate this trend. The behavior observed in these two figures corresponds to trends in Figures 4.15 and 4.16, respectively.

Figure 4.21 confirms the observation of linearity of the results with temperature change range for the particular soil properties. It is important to note the sign convention employed for presenting the results for normal stresses: tension is positive and compression is negative. Although figure 4.21 shows compressive bending stresses only, it also implies that the tensile bending stresses have the same magnitude as the compressive bending stresses.

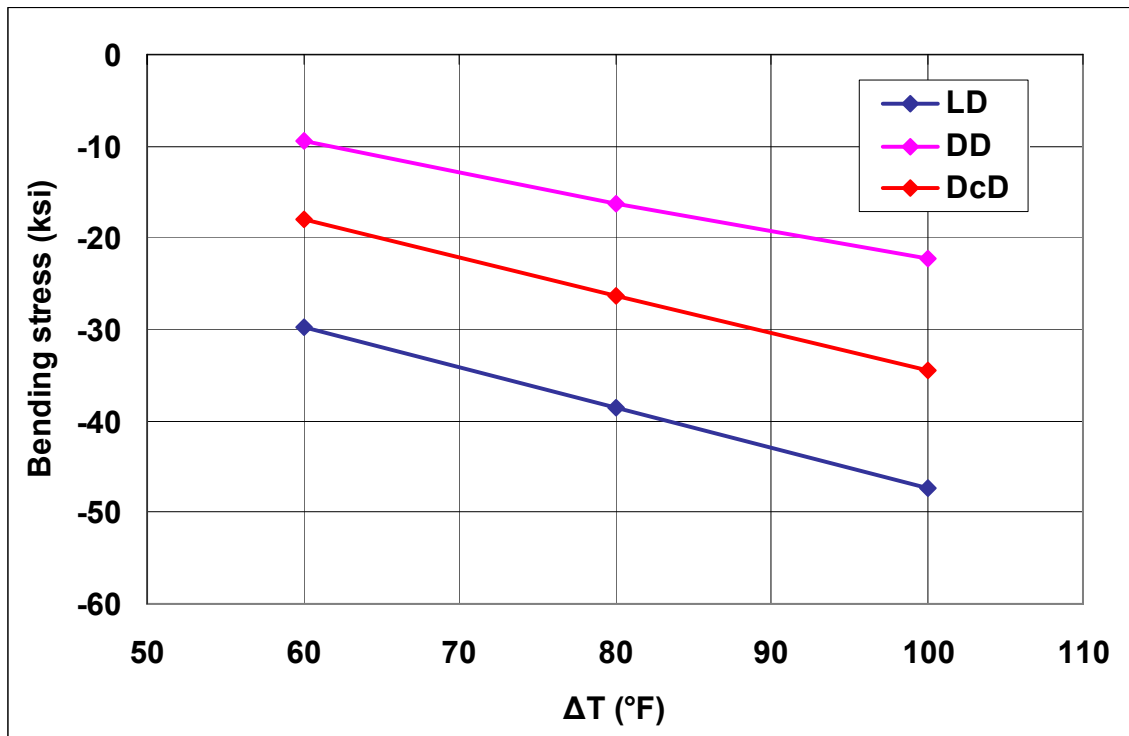


Figure 4.21: Maximum Bending Stress (ksi) in Central Pile vs.  $\Delta T$

#### 4.5.4 Soil pressure on abutment

##### 4.5.4.1 Trends Due to Change in Thermal Load for the Particular Soil Properties

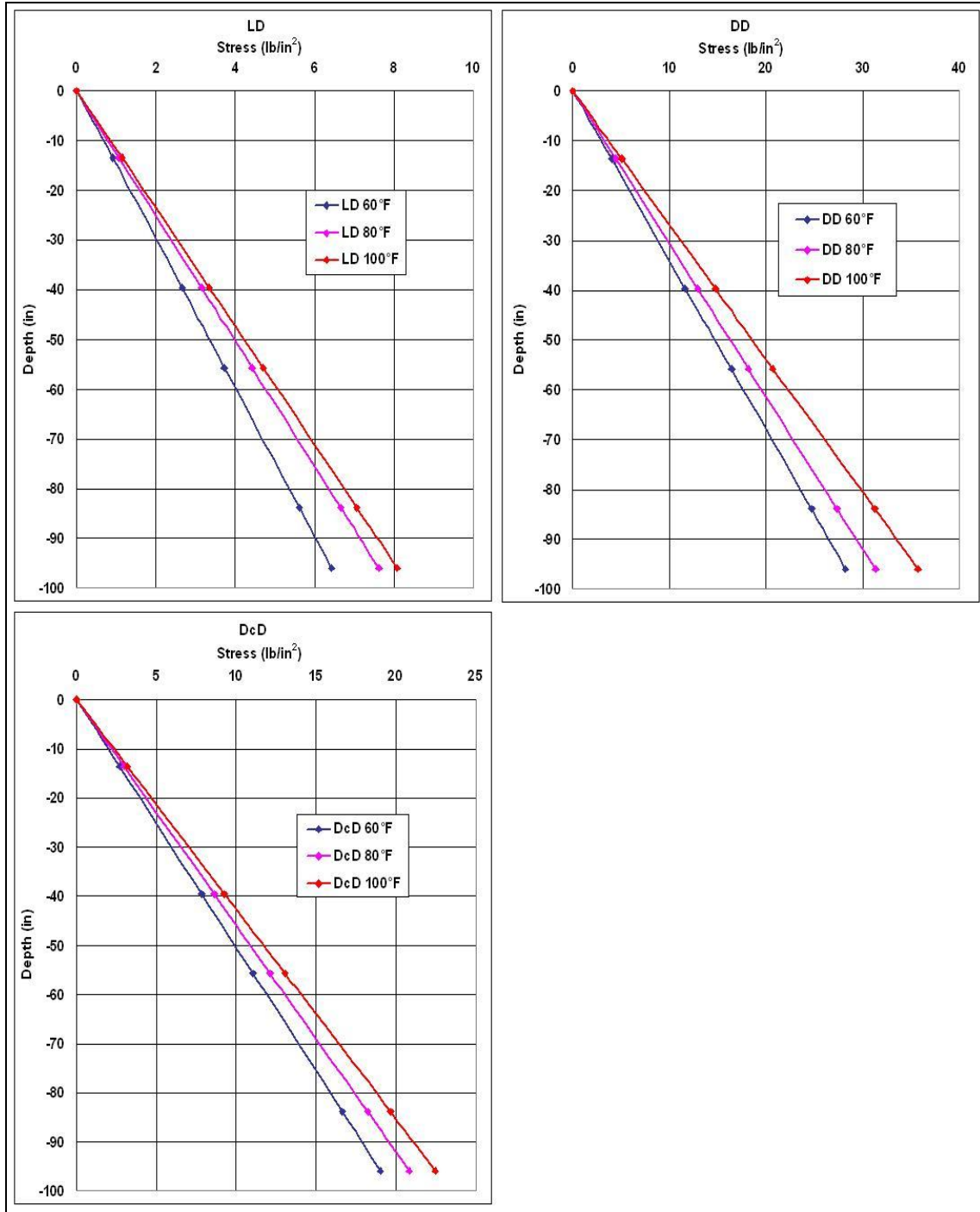
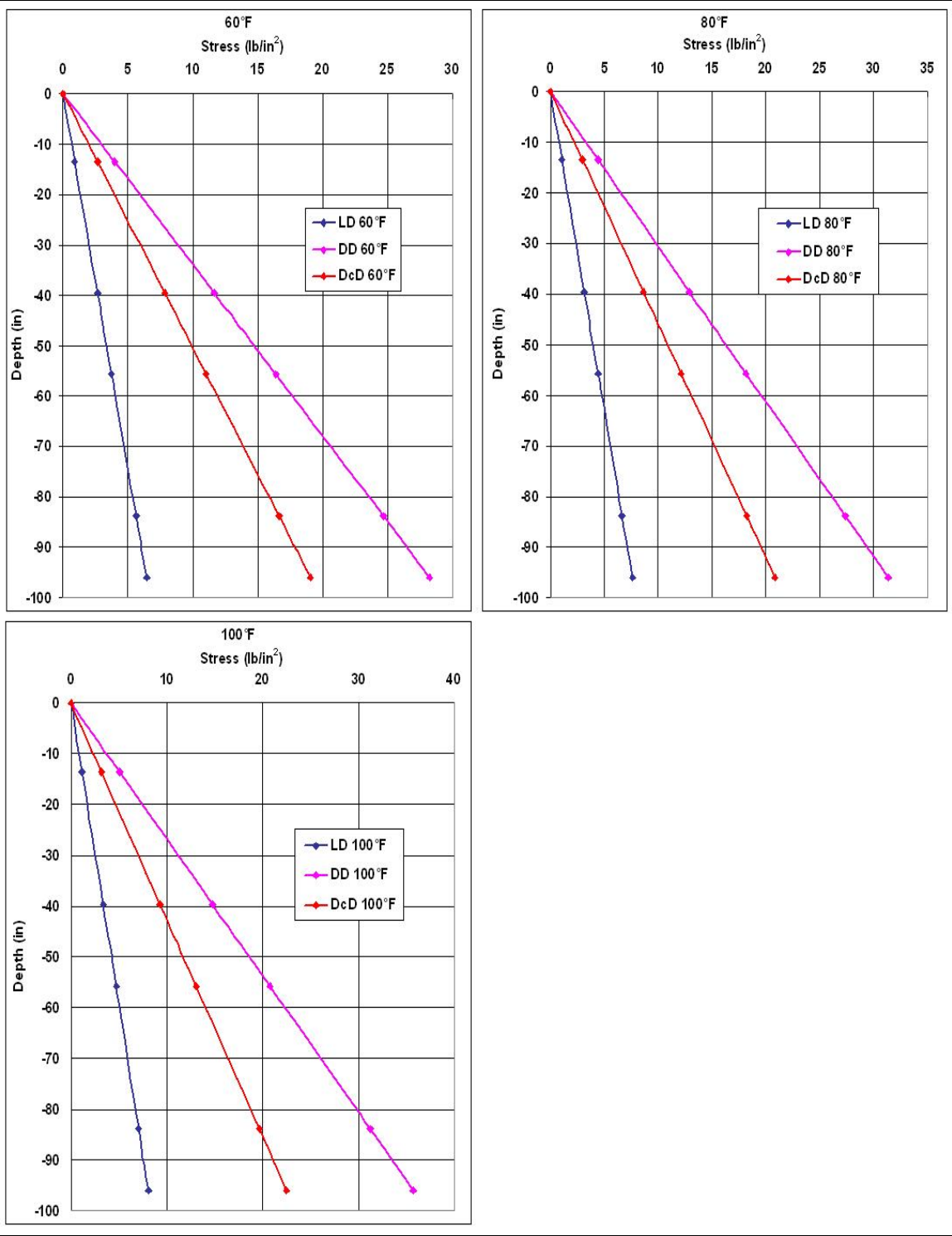


Figure 4.22: Trends in Soil Pressure (psi) on Abutment Due to Changes in Thermal Load

**4.5.4.2 Trends Due To Change in Soil Properties for the Particular Thermal Load**



**Figure 4.23: Trends in Soil Pressure (psi) on Abutment Due to Changes in Soil Properties**

#### **4.5.4.3 Discussion**

A soil pressure acting on the abutment depends on the coefficient of lateral earth pressure  $K(\delta)$  and the vertical effective stress, increase of which depends on the unit weight of the soil. The coefficient of lateral earth pressure  $K(\delta)$  is a function of the abutment top displacement, as discussed in section 3.4.1. Thus, a horizontal effective stress in soil is a linear function of depth. As expected the stress exerted by the soil on the abutment increases linearly with depth (Figures 4.22 and 4.23). In addition, the larger the temperature change range, the larger the stress. For the selected soil properties, the soil pressure exerted on abutment increases between 4 to 4.5 times as relative compaction increases from 90% to 96%.

## 4.5.5 Comparisons between the Central Pile and End Pile

### 4.5.5.1 Longitudinal displacement

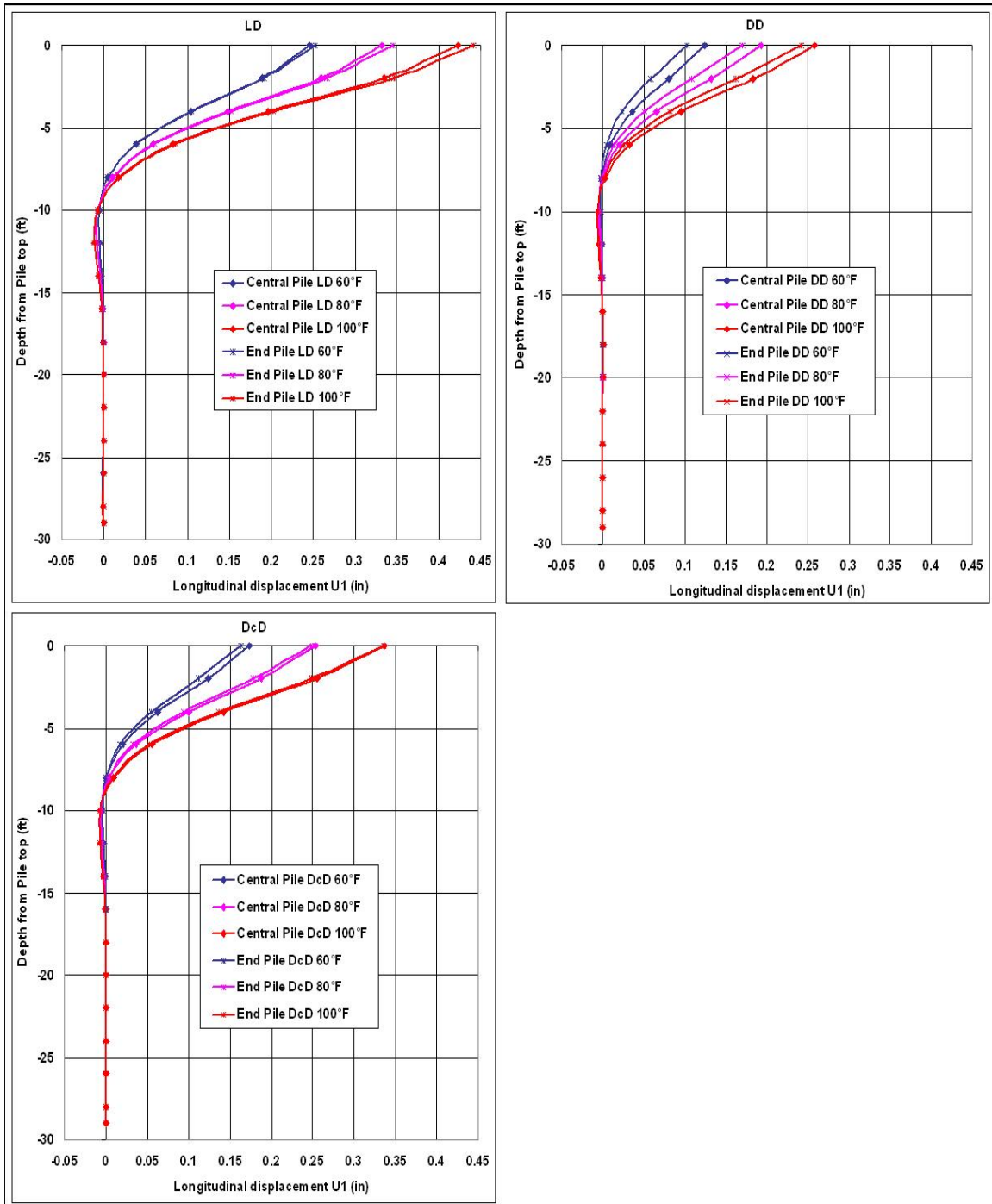


Figure 4.24: Comparison of Longitudinal Displacements (in) of Central and End Piles

### 4.5.5.2 Pile Bending Moment

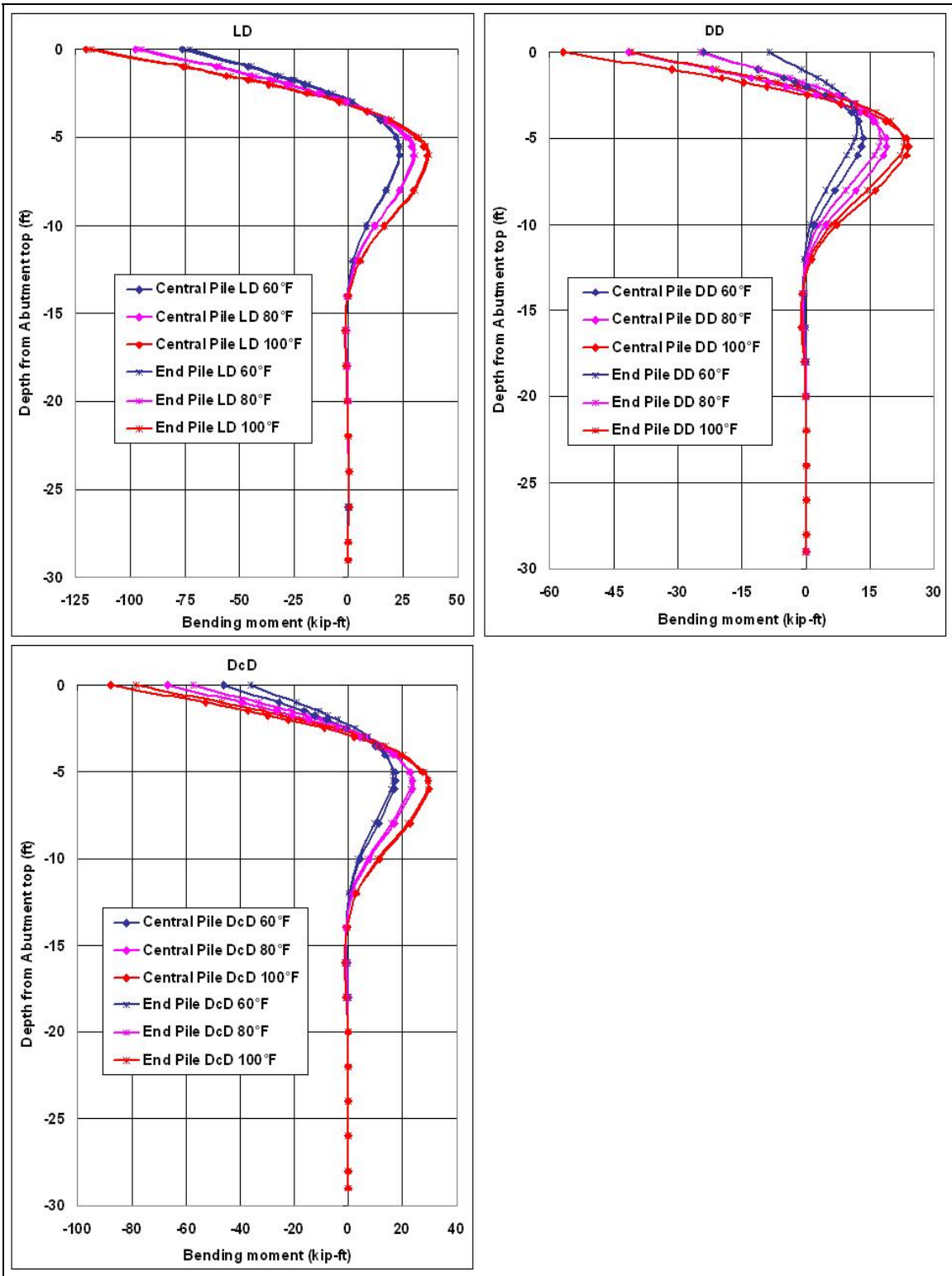


Figure 4.25: Comparison of Bending Moments (kip-ft) in Central and End Piles

### 4.5.5.3 Pile Bending Stress

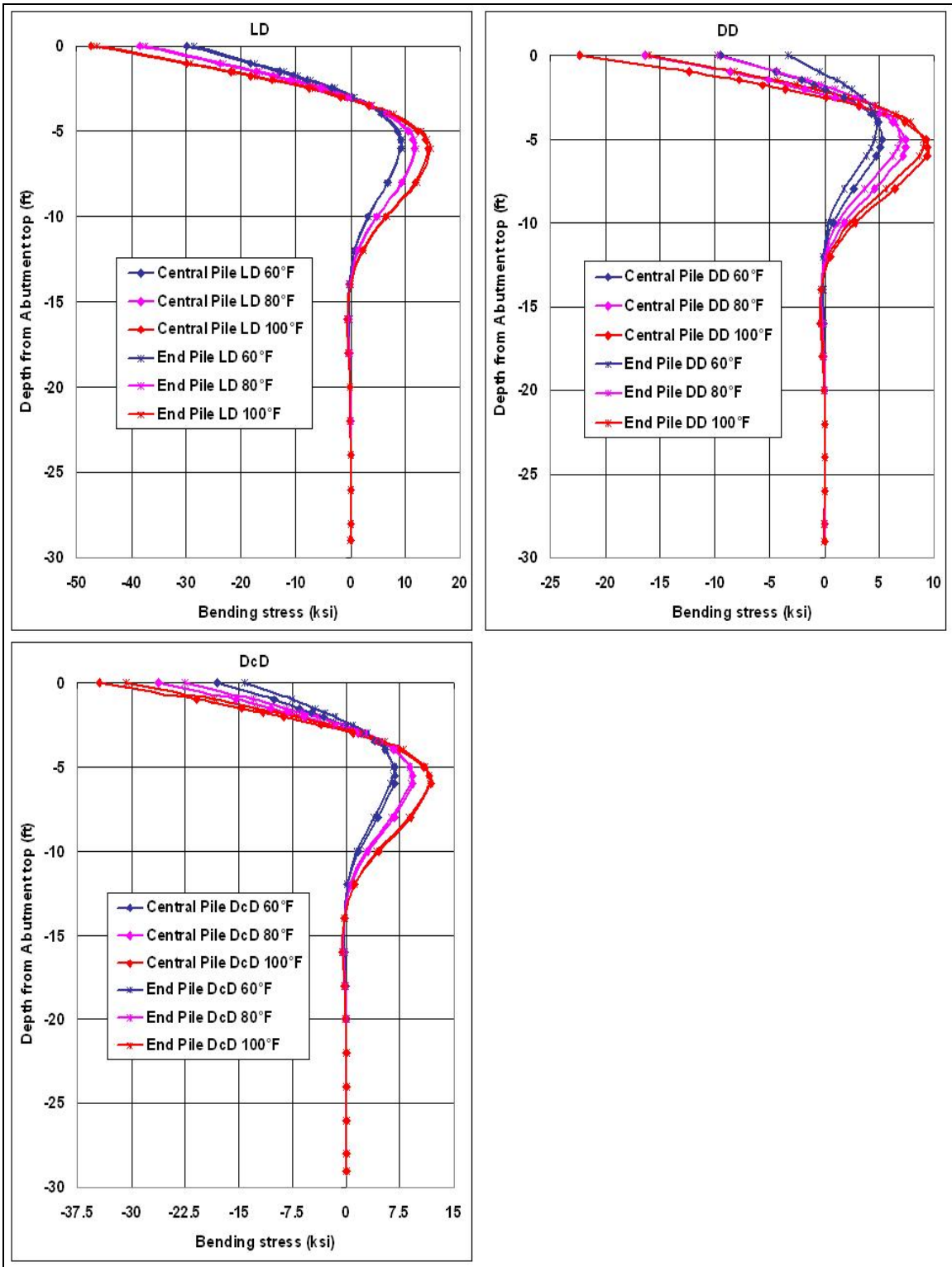


Figure 4.26: Comparison of Bending Stresses (ksi) in Central and End Piles

#### **4.5.5.4 Discussion**

Comparisons between the responses of central and end piles are shown in Figures 3.24 through 4.26. The figures show results of three-dimensional FE analysis in which the soil is assumed to be uniform and homogeneous throughout the width of the abutment. Bending moments and bending stresses follow the same trend, which can be traced to the displacements (Figure 4.24). It is interesting to observe that the end pile deflected slightly more than the central pile in the presence of loose soil. Conversely, as the soil behind the abutment got denser, the central pile deflected relatively more than the end pile. This behavior may be explained by comparing the differences between displacements of central and end piles (Figure 4.24) with the rotational and translational displacements of the abutment (Figure 4.13). Based on this comparison it appears that the dominant translational motion of the abutment, which occurs in loose soil, is responsible for larger deflections of the end pile as compared to the central pile. Conversely, a dominant rotational motion of the abutment, which occurs in dense soil, causes larger deflection of the central pile. Behavior of piles in the presence of Canadian dense sand (CGS, 1992) falls in between the above two cases.

#### **4.5.6 Axial Compressive Stress in Girders**

One of the interesting observations of the IB behavior is generation of compressive axial stresses in the girders (Figure 4.5). Though it may be premature to say that this behavior can help in increasing the load carrying capacity of the bridge structure, this finding definitely needs more attention. Figure 4.27 shows the maximum axial stresses observed in the central girder near the connection of the girder and abutment wall.

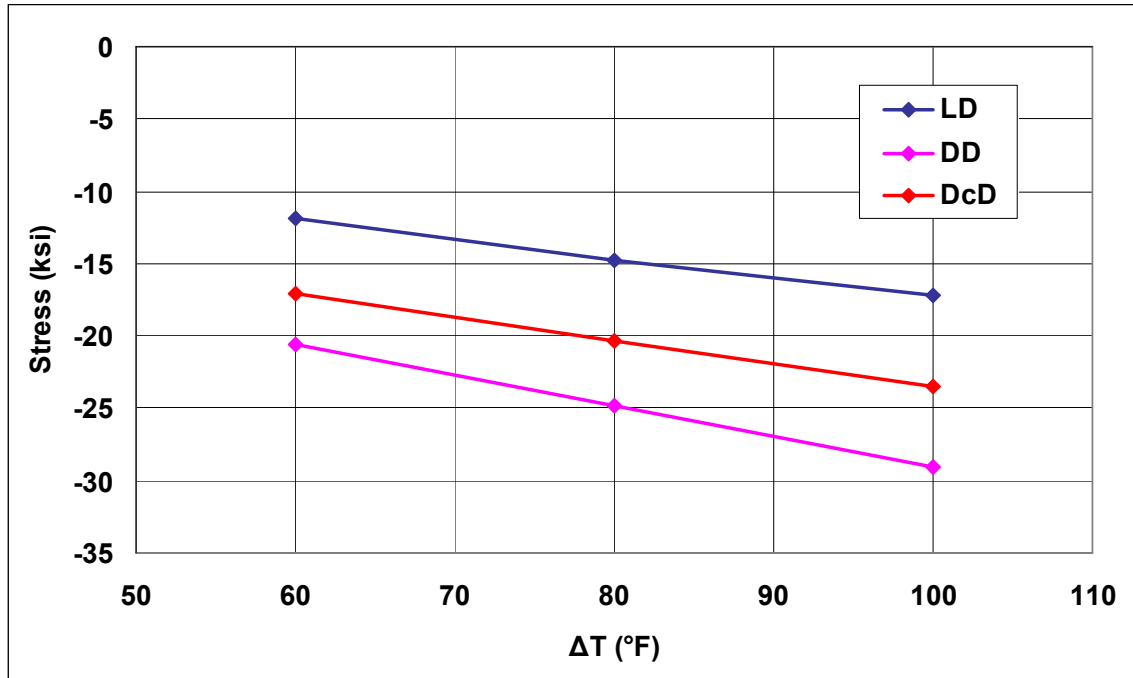


**Figure 4.27: Maximum Axial Stress S11 (ksi) in the Central Girder vs.  $\Delta T$**

For the increase in the relative compaction of soil behind abutment from 90% to 96 %, the maximum axial compressive stress in girders increases by about 67% regardless of the amount of temperature change. Thus, the maximum axial compressive stress in girders increases linearly with the temperature change increase for each type of soil.

#### **4.5.7 Convergence of Iterations**

The criterion used to establish the convergence of iterations comprising the iterative equivalent linear analysis used herein was defined in Section 3.4.3. It requires that the error in the displacements obtained from two consecutive iterations falls below 1% or 0.01. The convergence plots, which show the evolution of translational ( $\delta_T$ ), and rotational ( $\delta_R$ ), abutment top displacements with the number of iterations for all cases

analyzed are shown in Figures 4.28 through 4.33. In addition, the analytical expression tracing the evolution of iterations is established as follows:

$$y = ae^{bx} + c \quad \text{Equation 4.4}$$

where,

$$y = \delta_T \text{ or } \delta_R$$

x = iteration number

a,b,c = parameters

Parameters a,b,c are determined by fitting the expression given in Equation (4.3) to the actual iterative behavior obtained from the finite element analyses. Their values are provided in Tables 4.4 through 4.6, whereby the subscript 'r' denotes the values related to the convergence of the rotational displacement while the subscript 't' denotes the values related to the convergence of the translational displacement. Equation (4.3) is also shown graphically in Figures 4.28 through 4.33. These figures demonstrate that convergence is achieved in all cases analyzed herein. Moreover, the analytical expression given by Equation (4.3) traces the convergence effectively, thus providing the accurate converged values of the abutment top displacements.

**Table 4.4: Values of the Coefficients of the Exponential Function**

	60°F		
	LD	DD	DcD
<b>a<sub>r</sub></b>	-1.14053	-0.757875	-0.887771
<b>b<sub>r</sub></b>	-2.02764	-1.08246	-1.42522
<b>c<sub>r</sub></b>	0.0709331	0.177527	0.134258
<b>a<sub>t</sub></b>	1.21223	0.83568	0.966638
<b>b<sub>t</sub></b>	-2.01638	-1.07712	-1.41648
<b>c<sub>t</sub></b>	0.245606	0.122387	0.172525

**Table 4.5: Values of the Coefficients of the Exponential Function**

	<b>80°F</b>		
	<b>LD</b>	<b>DD</b>	<b>DcD</b>
<b>a<sub>r</sub></b>	-1.48601	-1.02017	-1.05633
<b>b<sub>r</sub></b>	-2.08768	-1.20335	-1.42882
<b>c<sub>r</sub></b>	0.0919705	0.213985	0.16083
<b>a<sub>t</sub></b>	1.57927	1.1226	1.23635
<b>b<sub>t</sub></b>	-2.07749	-1.19902	-1.49593
<b>c<sub>t</sub></b>	0.331372	0.190714	0.252176

**Table 4.6: Values of the Coefficients of the Exponential Function**

	<b>100°F</b>		
	<b>LD</b>	<b>DD</b>	<b>DcD</b>
<b>a<sub>r</sub></b>	-1.8851	-1.18725	-1.41408
<b>b<sub>r</sub></b>	-2.17444	-1.19831	-1.58395
<b>c<sub>r</sub></b>	0.108981	0.252897	0.184815
<b>a<sub>t</sub></b>	2.00086	1.30311	1.52846
<b>b<sub>t</sub></b>	-2.1646	-1.19305	-1.57363
<b>c<sub>t</sub></b>	0.421646	0.256109	0.334501

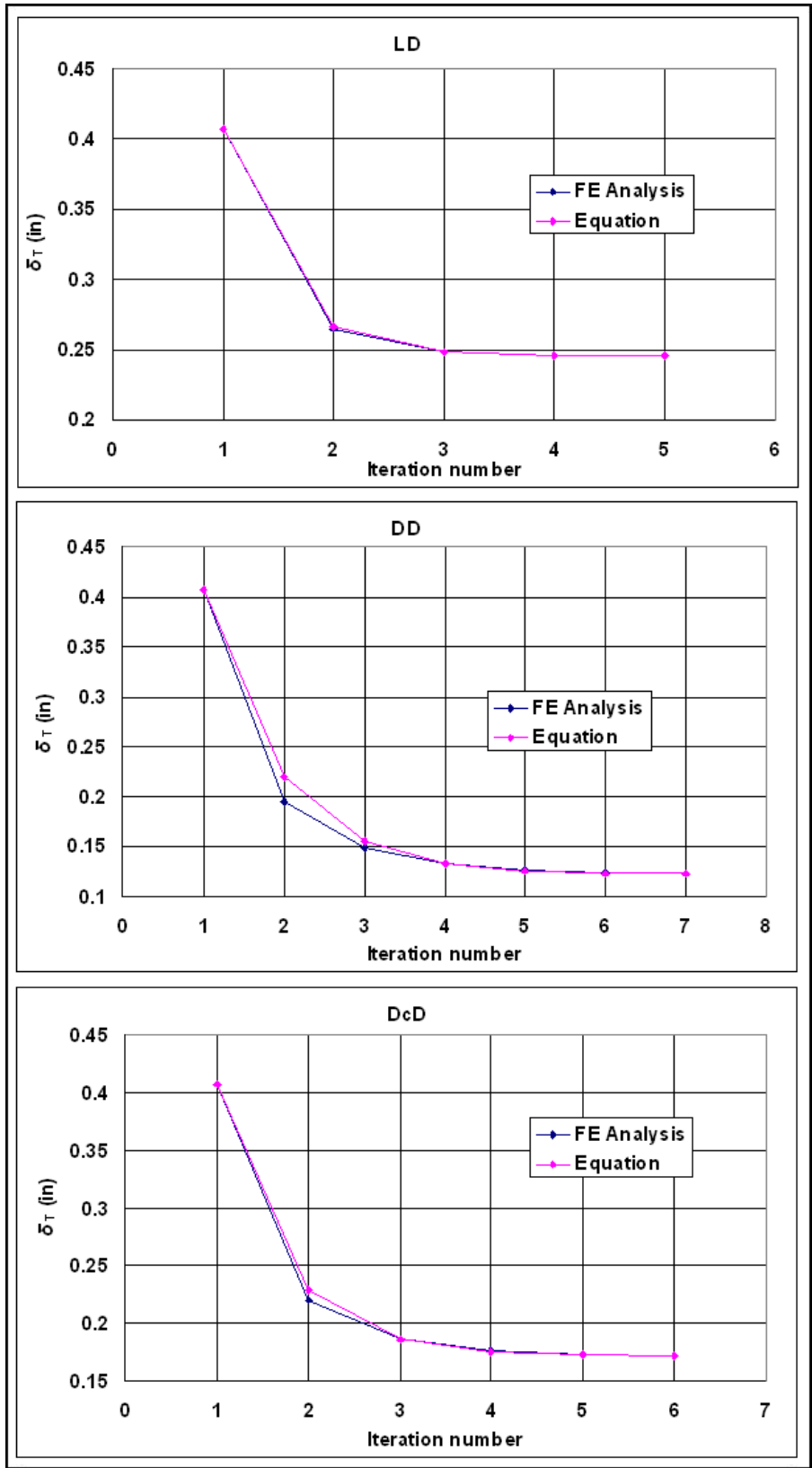


Figure 4.28: Convergence of Translational Displacement for  $\Delta T = 60^\circ\text{F}$

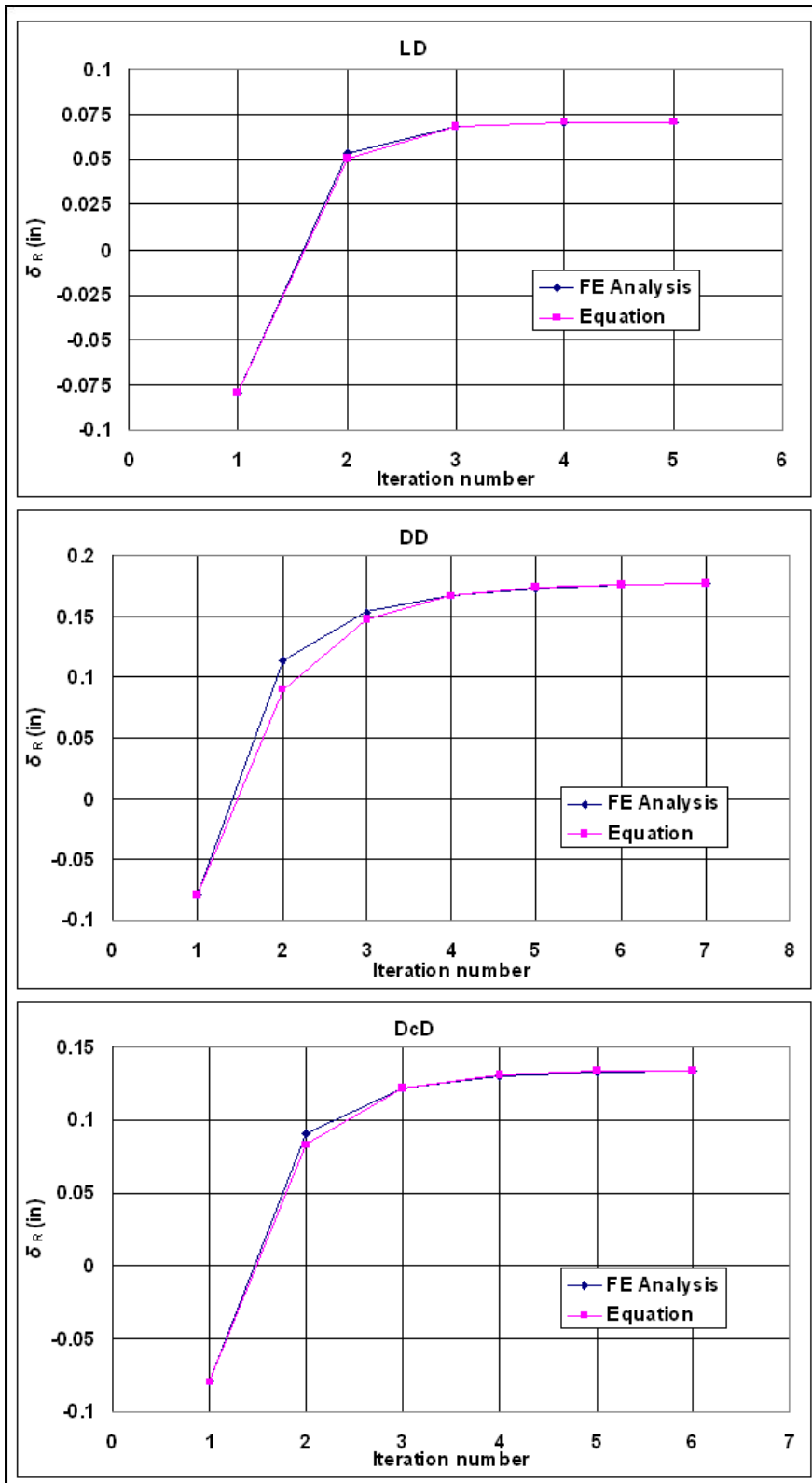


Figure 4.29: Convergence of Rotational Displacement  $\Delta T = 60^\circ\text{F}$

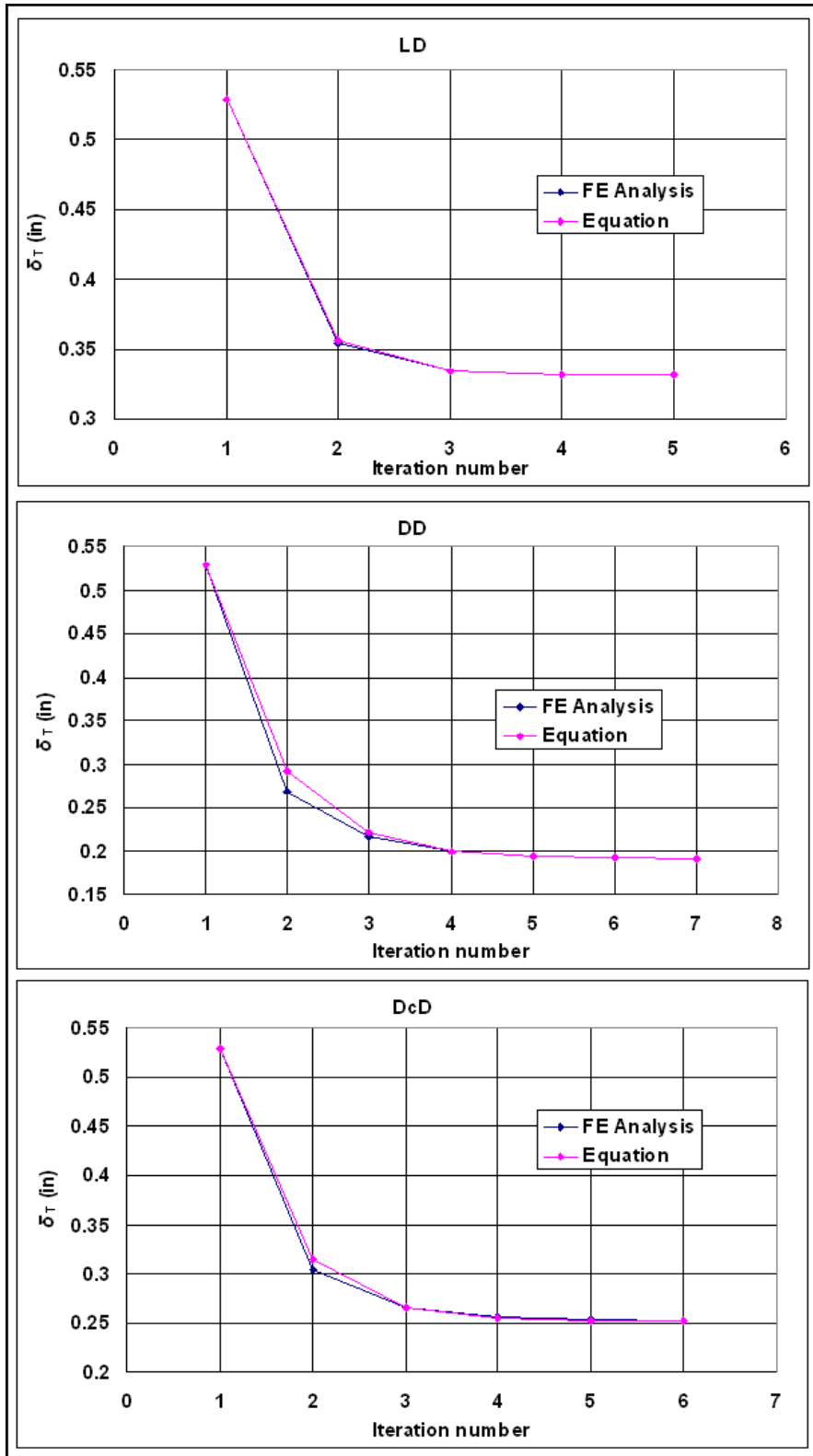


Figure 4.30: Convergence of Translational Displacement for  $\Delta T = 80^\circ\text{F}$

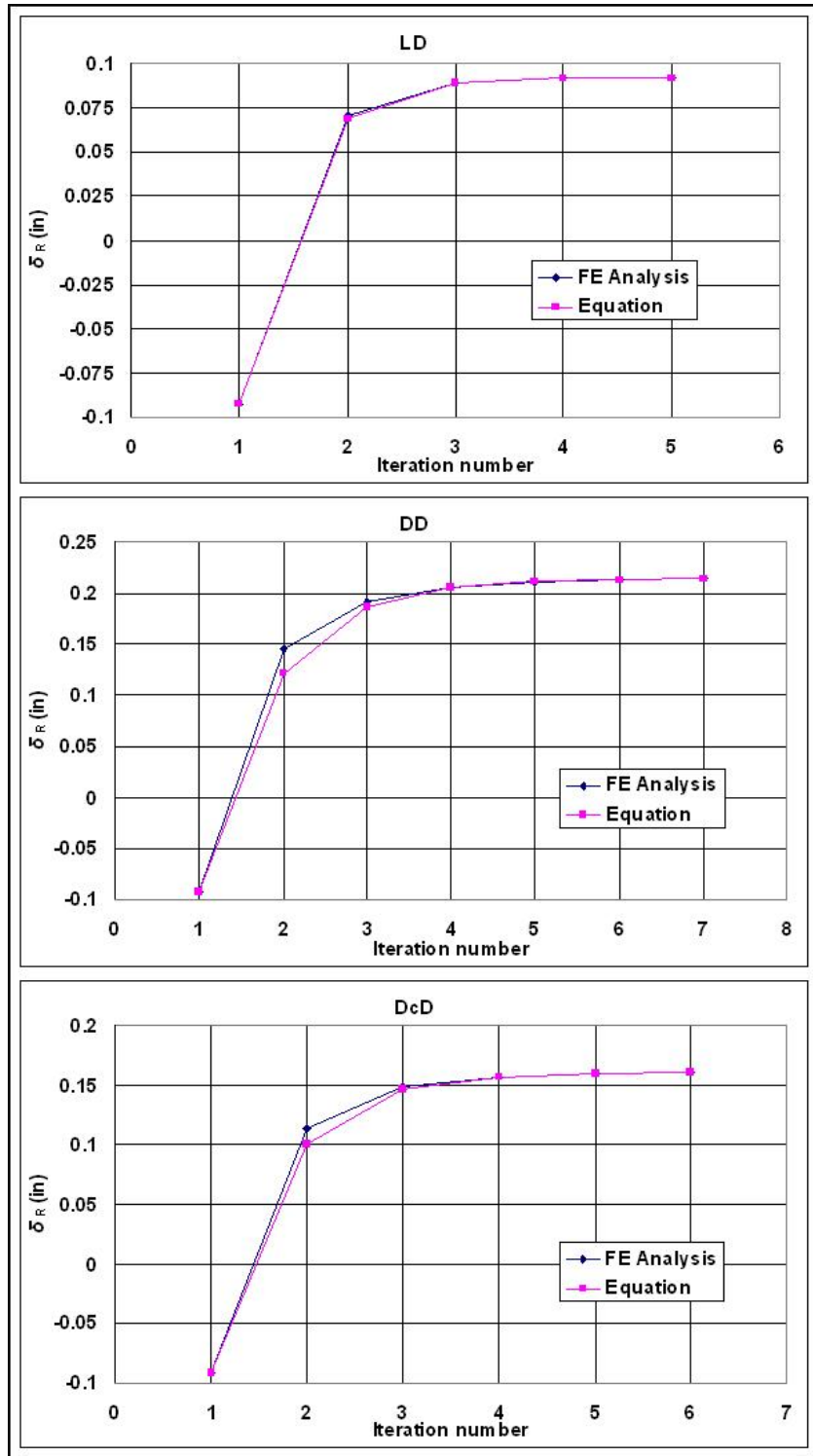


Figure 4.31: Convergence of Rotational Displacement for  $\Delta T = 80^\circ\text{F}$

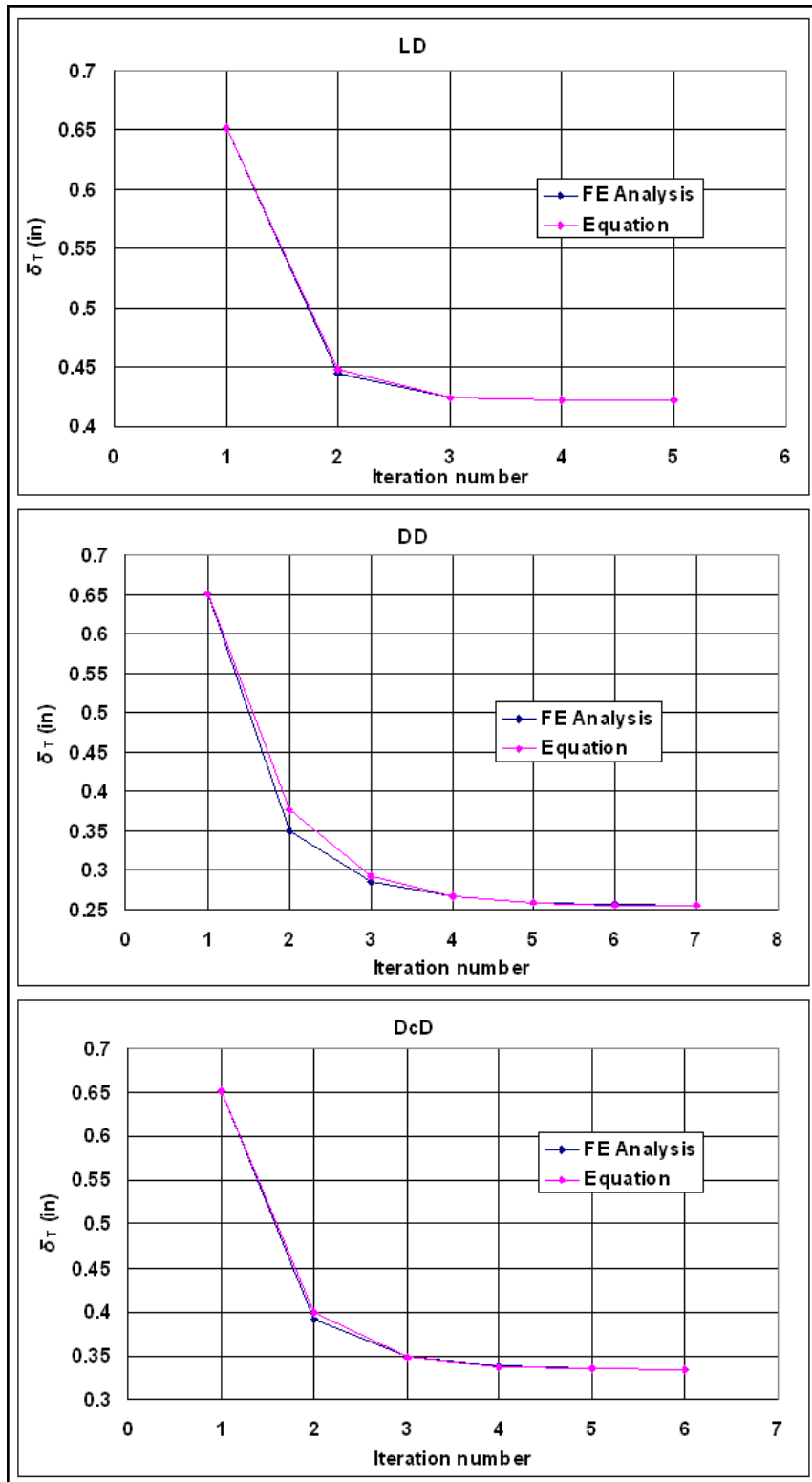


Figure 4.32: Convergence of Translational Displacement for  $\Delta T = 100^\circ\text{F}$

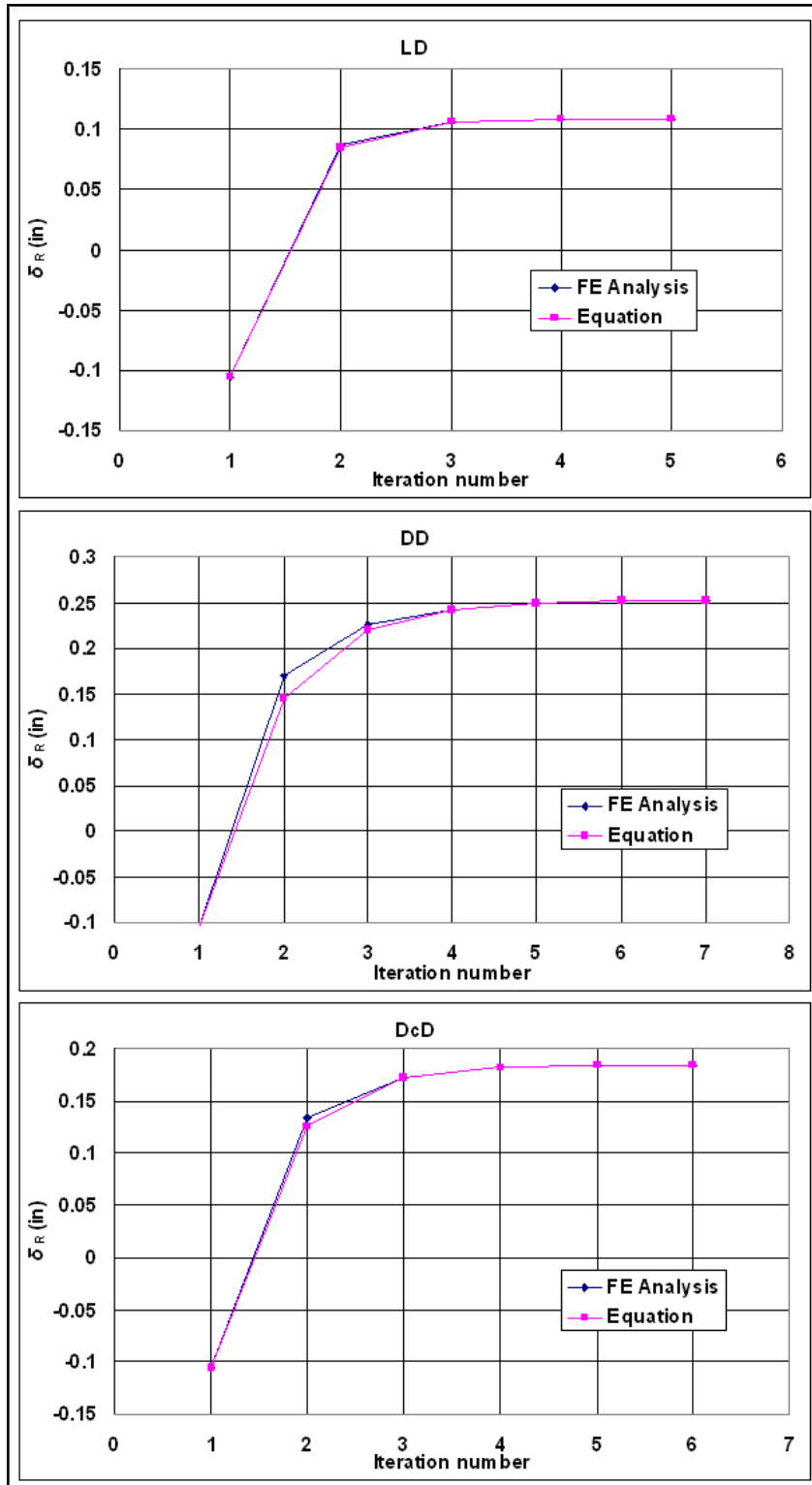


Figure 4.33: Convergence of Rotational Displacement for  $\Delta T= 100^\circ\text{F}$

#### 4.6 Results for the Bridge with Approach Slab

As stated in Section 3.5, where the finite element model of the bridge with the approach slab was described, only a single thermal loading was applied comprising the temperature change of 80°F. Two different analyses were performed, thus accounting for the presence of loose and dense sands (NCHRP, 1991) behind the abutment. Table 4.7 lists the converged values of the coefficients of lateral earth pressure  $K$  for the soil behind the abutment for the two cases analyzed.

**Table 4.7: Converged Values of the Coefficient of Lateral Earth Pressure  $K$**

<b>Soil combination Temperatures</b>	<b>LD</b>	<b>DD</b>
<b>80°F</b>	1.187	4.845

The values of the coefficients of lateral pressure reported in Table 4.7 are slightly different from those in Table 4.3, whereby the later were obtained for the bridge without the approach slab. The difference is attributed to a decreased height of the abutment that is exposed to the lateral earth pressure due to the presence of the approach slab. Thus, in the analysis of the bridge with the approach slab different referent points for the abutment top displacement were used as well as different abutment heights.

**4.6.1 Longitudinal Displacement at Centerline of the Bridge**

**4.6.1.1 Trends Due to Change in Soil Properties for the Particular Thermal Load**

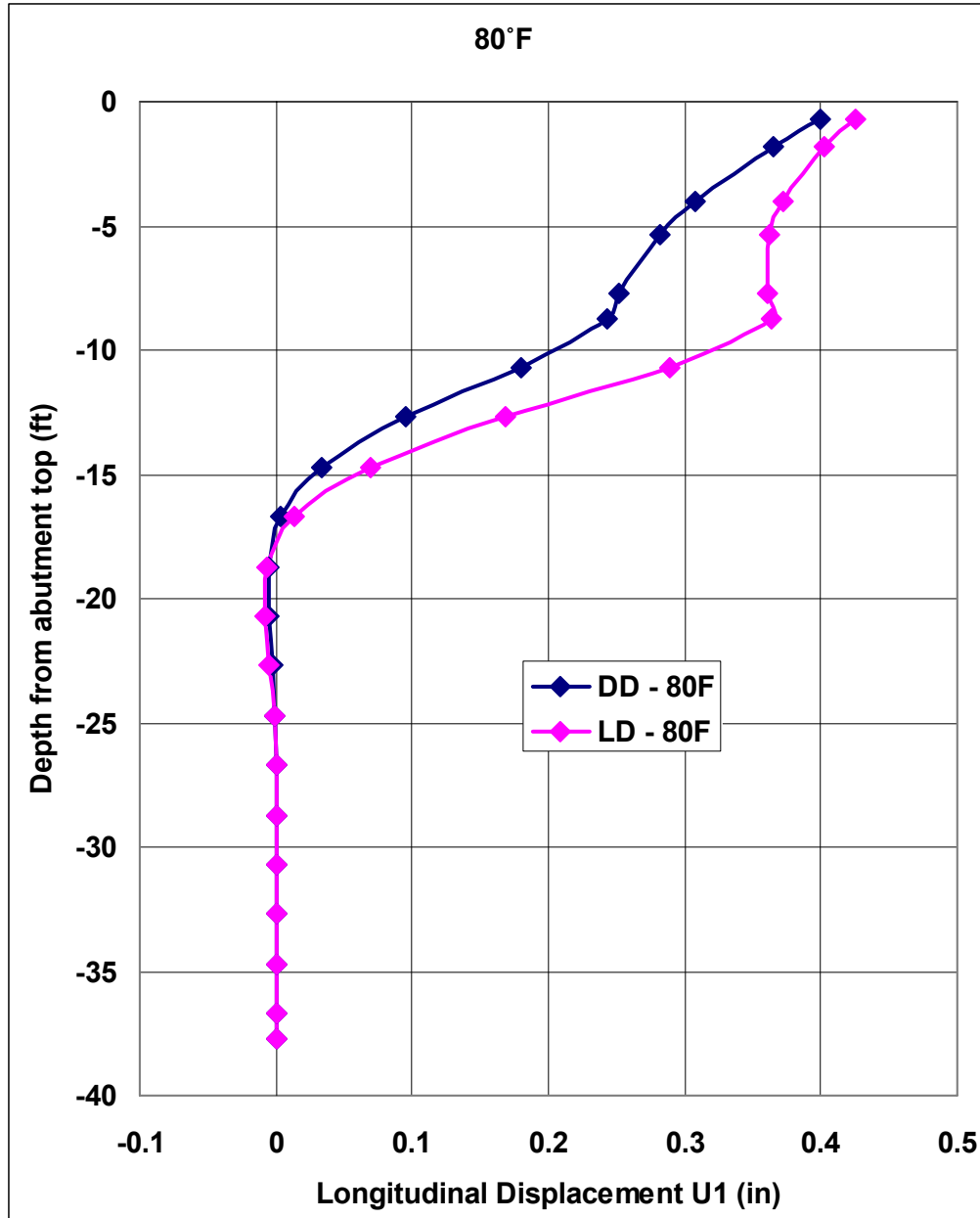


**Figure 4.34: Trends in Longitudinal Displacement Due to Changes in Soil Properties**

#### 4.6.1.2 Discussion

Figure 4.34 depicts longitudinal displacements along the centerline of the bridge, from the abutment top to the bottom of the pile. The observed trend is qualitatively very similar to the bridge without the approach slab.

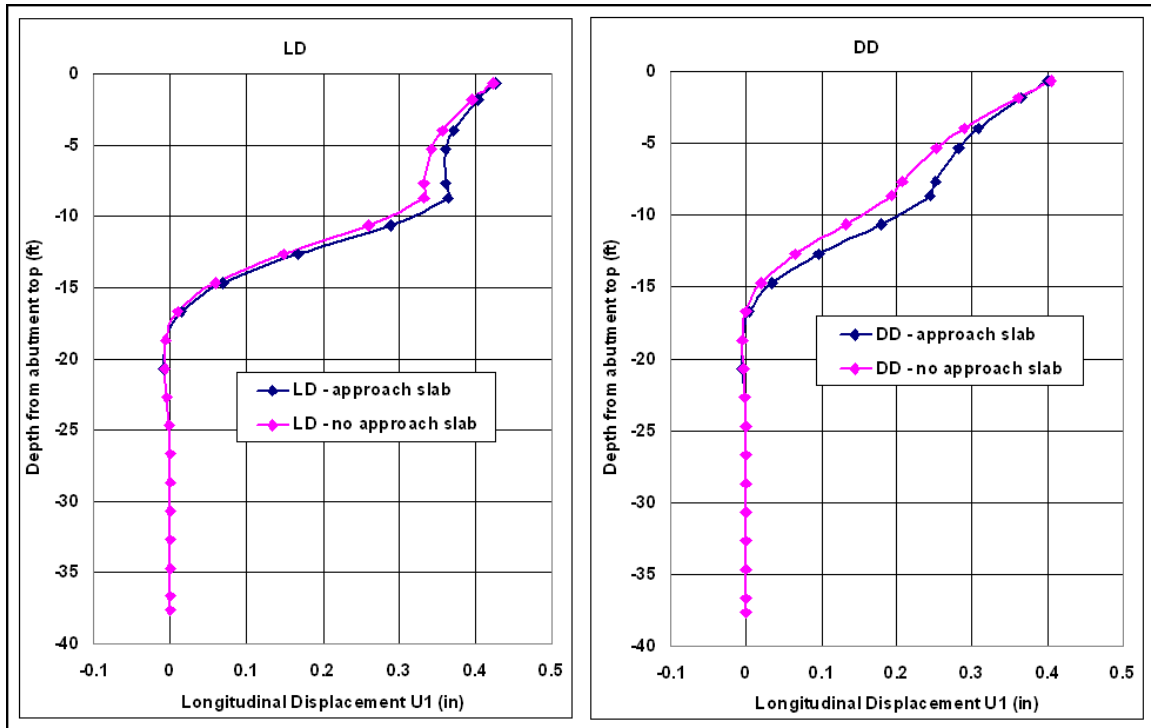


Figure 4.35: Displacement Comparisons – Bridge with and without Approach Slab

Figure 4.35 shows direct comparisons of longitudinal displacements of the bridges with and without the approach slab for the same loading scenarios. As expected, displacements at the very top of the abutment are not affected by the approach slab. On the contrary, displacements of the back side of the abutment and lateral deflections of the central pile are consistently larger in the bridge with the approach slab regardless of the soil properties. Thus, the presence of the approach slab decreases the rotation of the abutment while increasing its translation and bending. This trend is attributed to the increase in the lateral earth pressure caused by the weight of

the approach slab. The rotation of the abutment is decreased due to the more pronounced increase in the lateral earth pressure towards to the top of the abutment.

Table 4.8 compares longitudinal displacements in bridges with and without approach slabs at several different locations. It is noted that the decrease in the abutment rotation in the presence of a dense sand results in a larger increase of the pile head displacement than in the presence of the loose sand behind the abutment.

**Table 4.8: Comparisons of Displacements (in)**

<b>CASE</b>	<b>Deck top</b>	<b>Abutment top</b>	<b>Pile Head</b>	<b>Analytical Deck top</b>
	<b>(in)</b>	<b>(in)</b>	<b>(in)</b>	<b>(in)</b>
<b>LD – no approach slab</b>	0.438	0.423	0.332	0.433
<b>LD – with approach slab</b>	0.437	0.426	0.364	0.433
<b>DD – no approach slab</b>	0.430	0.405	0.192	0.433
<b>DD – with approach slab</b>	0.418	0.400	0.243	0.433

Table 4.9 provides comparisons of the abutment top and the approach slab end displacements. The abutment top displacements listed in Tables 4.8 and 4.9 are provided at the identical locations in bridges with and without approach slabs. However, in the bridges with approach slabs these abutment top displacements were not used during the equivalent iterative linear analyses simply because the corresponding location is above the abutment surface exposed to the soil.

**Table 4.9: Comparisons of Deck and Approach Slab Displacements (in)**

<b>CASE</b>	<b>No Approach Slab</b>		<b>With Approach Slab</b>	
	<b>Abutment top</b>		<b>Abutment top</b>	<b>Approach Slab end</b>
	<b>(in)</b>		<b>(in)</b>	<b>(in)</b>
<b>LD</b>	0.423		0.426	0.503
<b>DD</b>	0.405		0.400	0.480

Table 4.10 provides values of rotational and translational displacements of the abutment tops. In this table the values of displacements for the bridge with the approach slab are provided for the location along the centerline where the abutment connects to the approach slab, which is located 1 ft below the deck top. For the bridge without the approach slab the displacement values are provided at the abutment top, which is located 8.5 in below the deck top. Although there is an elevation difference of 3.5 in between these locations the listed displacement values further substantiate the main influence of the approach slab described above. The displacements provided in Table 4.10 can be normalized with respect to the corresponding heights of the abutments, which are 8 ft and 7.71 ft for bridges without and with approach slabs respectively. By doing so it can be further concluded that the approach slab decreases the rotation of the abutment and increases the translation of the abutment by about 28% in the presence of the dense sand. In the case of the loose sand, the presence of the approach slab reduces the rotation of the abutment by about 38%, while it increases the translation by about 11%.

**Table 4.10: Comparisons of Translational and Rotational Displacements (in) of the Abutment Top**

<b>CASE</b>	<b>No Approach Slab</b>		<b>With Approach Slab</b>	
	$\delta_T$ (in)	$\delta_R$ (in)	$\delta_T$ (in)	$\delta_R$ (in)
<b>LD</b>	0.331	0.092	0.350	0.055
<b>DD</b>	0.191	0.214	0.233	0.144

## 4.6.2 Central Pile Bending Moment

### 4.6.2.1 Trends Due to Change in Soil Properties for the Particular Thermal Load

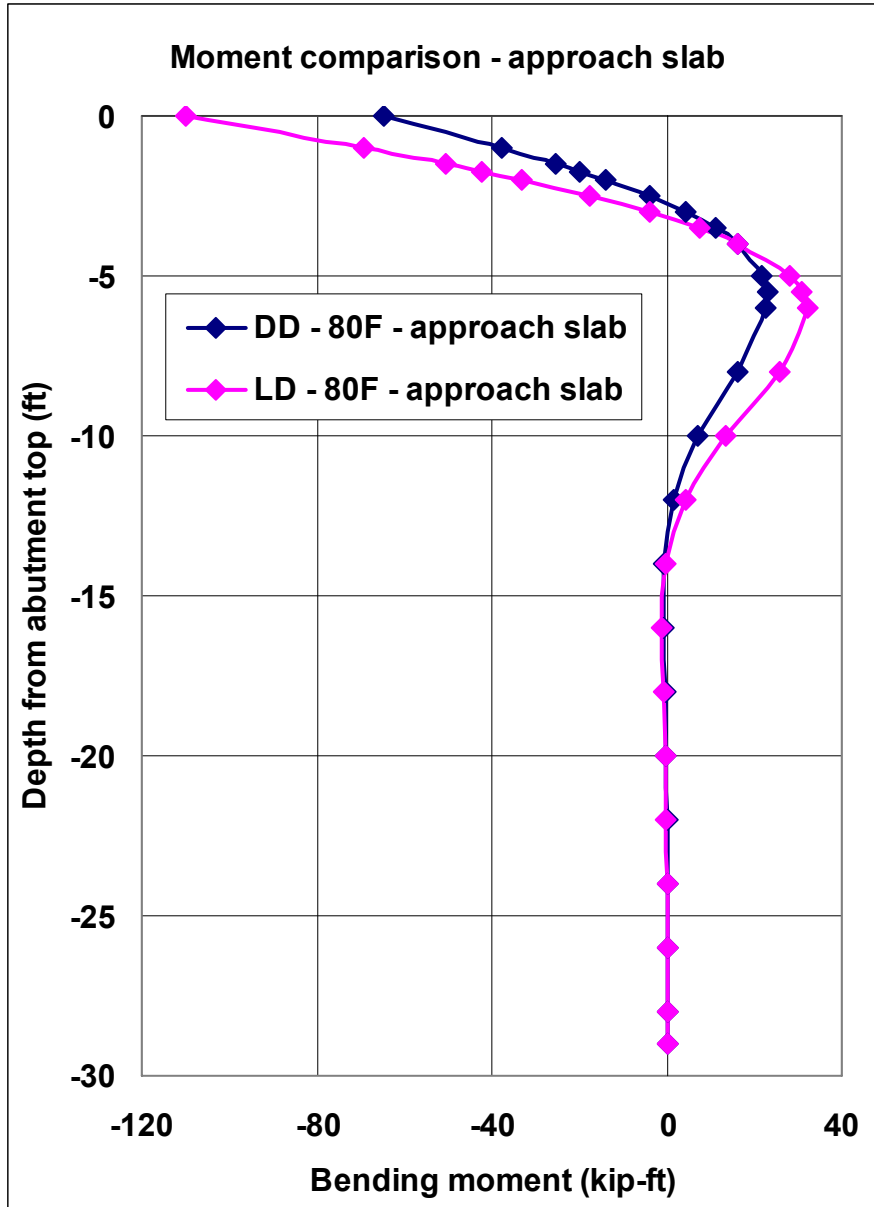
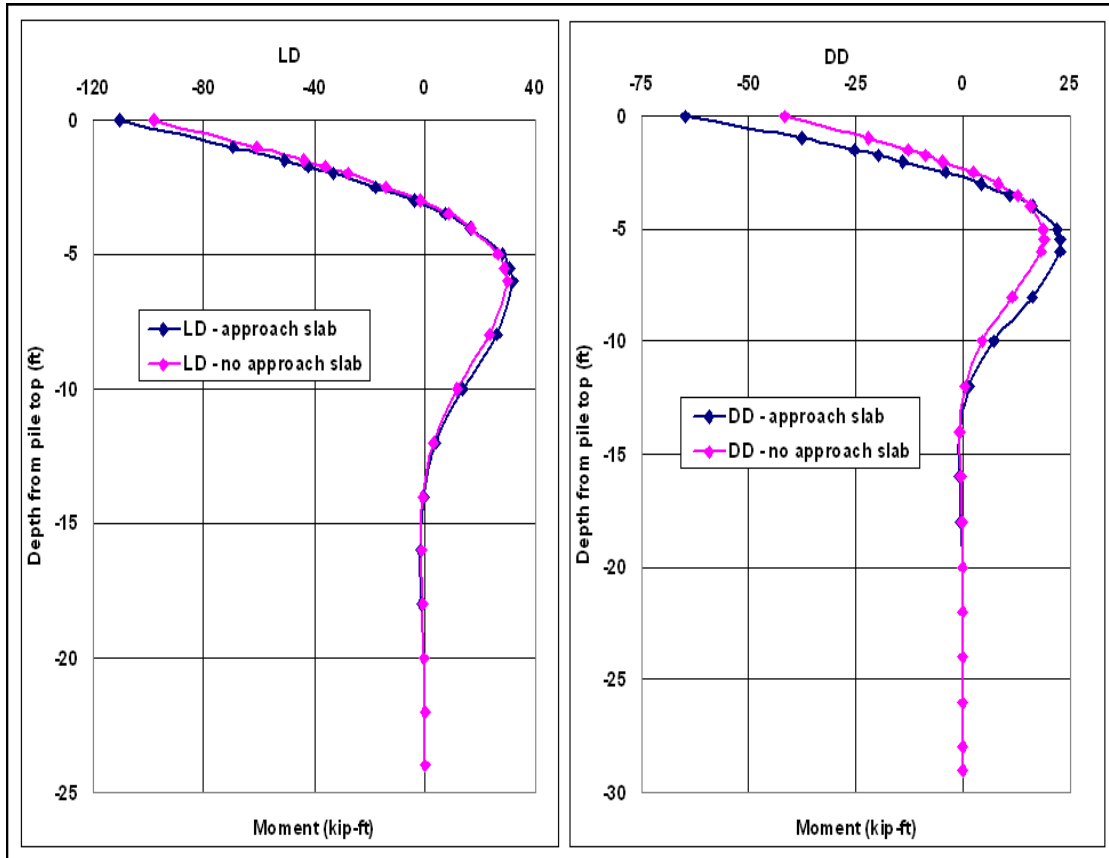


Figure 4.36: Trends in Central Pile Bending Moment (kip-ft) Due to Changes in Soil Properties

### 4.6.2.2 Discussion

Figure 4.36 shows distributions of bending moments in the central pile versus depth. As in the bridge without the approach slab the absolute values of maximum and minimum bending moments in the pile are larger in the presence of the loose sand behind the abutment.



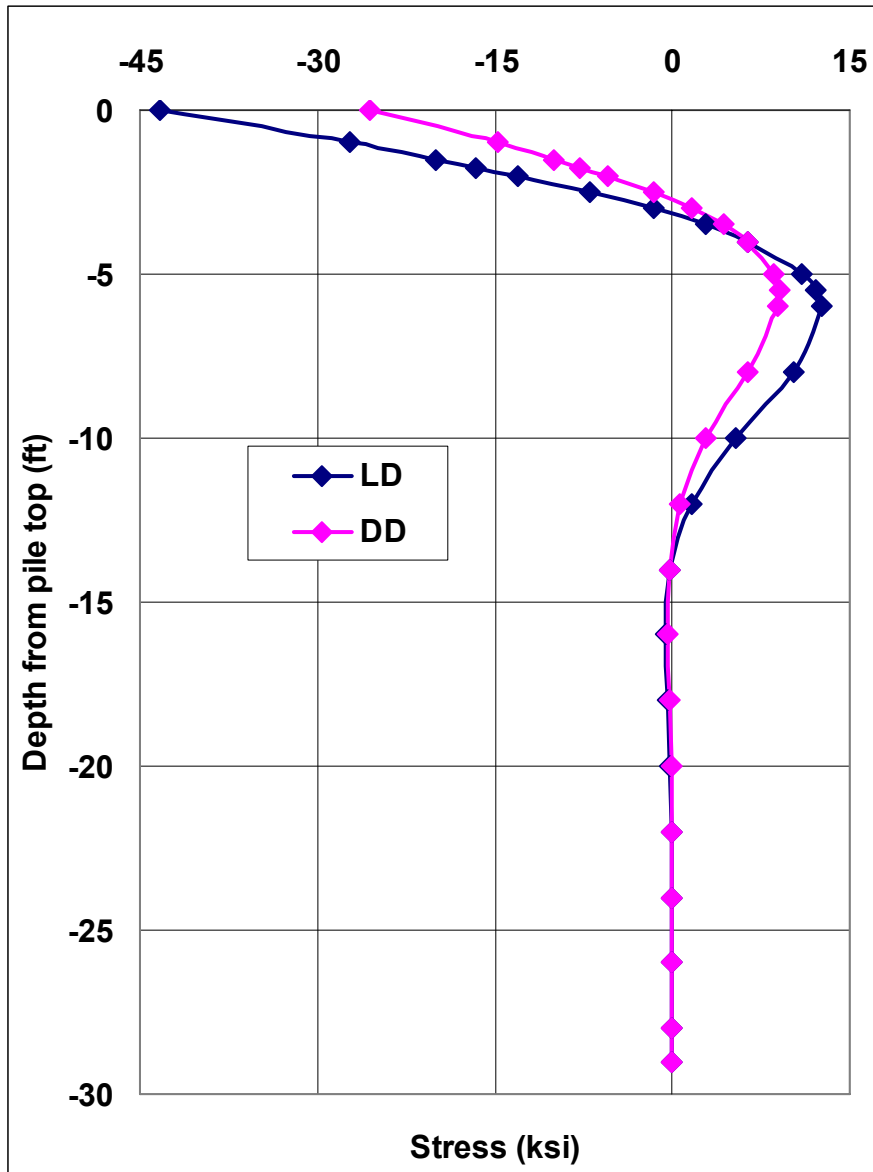
**Figure 4.37: Comparison of Bending Moments (kip-ft) in Bridges with and without Approach Slabs**

Figure 4.37 provides direct comparisons between the bending moments in the central piles in bridges with and without the approach slabs. As expected based on the previous discussion of the displacement patterns in both cases shown in Figure 4.37 pile head moments increase due to the presence of the approach slab. The increase is

larger in the case of the dense sand, which can be traced to the larger increase of the abutment translation.

**4.6.3 Central Pile Bending Stress**

**4.6.3.1 Trends Due to Change in Soil Properties for the Particular Thermal Load**



**Figure 4.38: Trends in Central Pile Bending Stress (ksi) Due to Changes in Soil Properties**

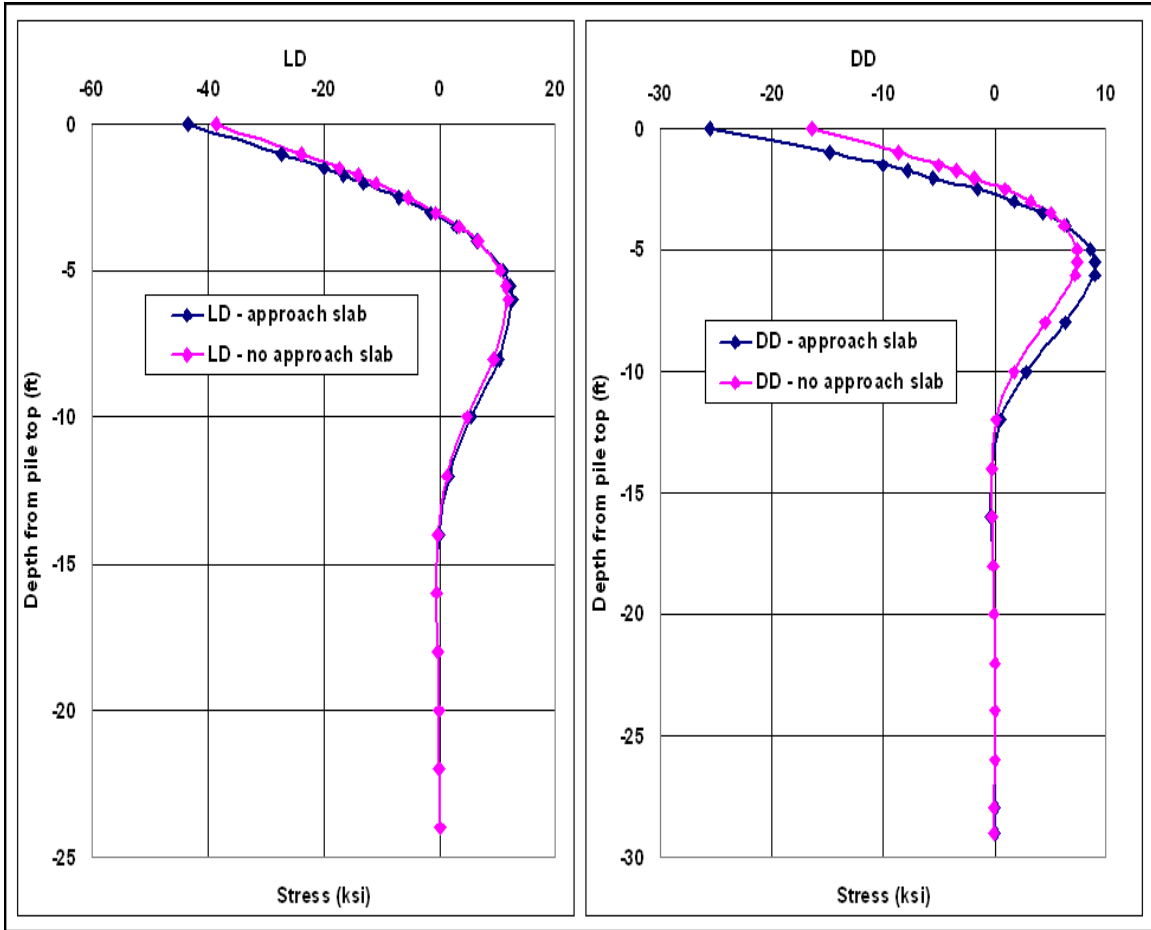
#### **4.6.3.2 Discussion**

Figure 4.38 depicts bending stresses in the central piles of the bridges with approach slabs. The observed trends are directly traceable to the corresponding bending moments (Figure 4.36).

Table 4.11 lists maximum bending stresses in the piles for several different cases. These stresses are also shown in Figure 4.39. Again, the observed trends are directly traceable to the corresponding bending moments shown in Figure 4.37. It is evident from Table 4.11 that pile head bending stresses increase by 56% and 13% in the dense and loose sands respectively due to the presence of the approach slabs.

**Table 4.11: Maximum Bending Stresses (ksi) in Central Piles**

<b>CASE</b>	<b>No Approach Slab</b>	<b>With Approach Slab</b>
	<b>(ksi)</b>	<b>(ksi)</b>
<b>LD</b>	-38.490	-43.345
<b>DD</b>	-16.363	-25.531



**Figure 4.39: Comparison of Bending Stresses (ksi) in Bridges with and without Approach Slabs**

#### 4.6.4 Soil pressure on Abutment

##### 4.6.4.1 Trends Due To Change in Soil Properties for the Particular Thermal Load

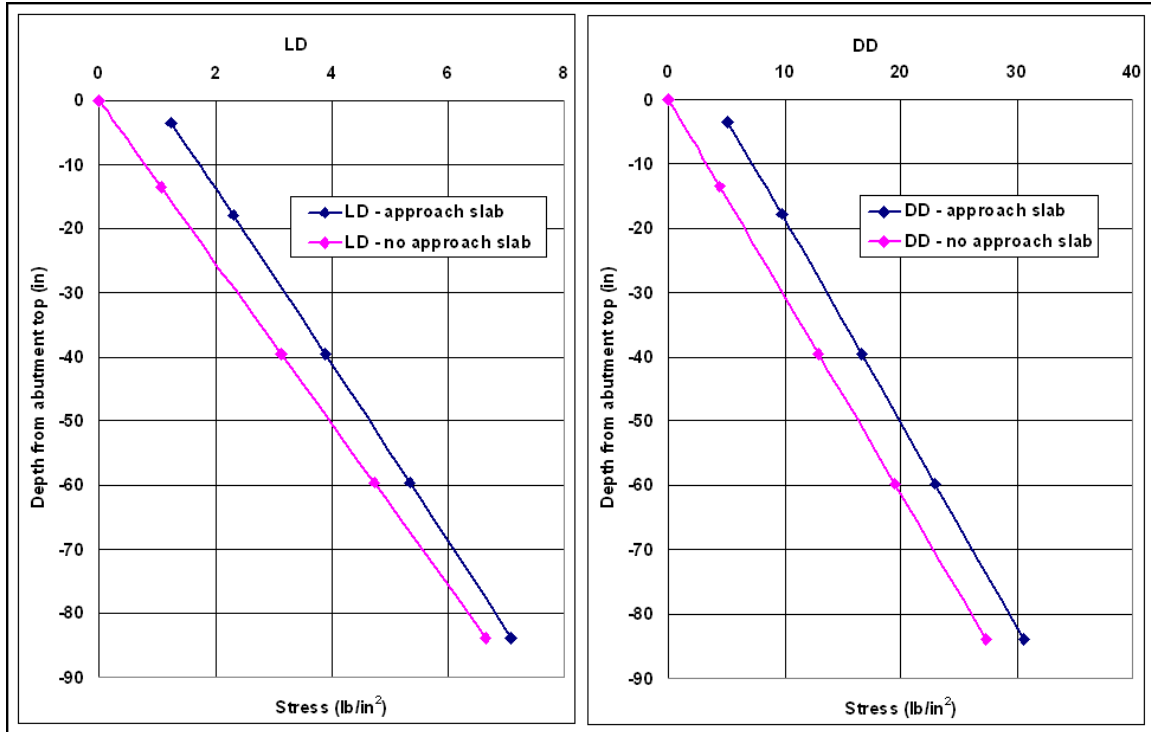


Figure 4.40: Trends in Soil Pressure on Abutment Due to Changes in Soil Properties

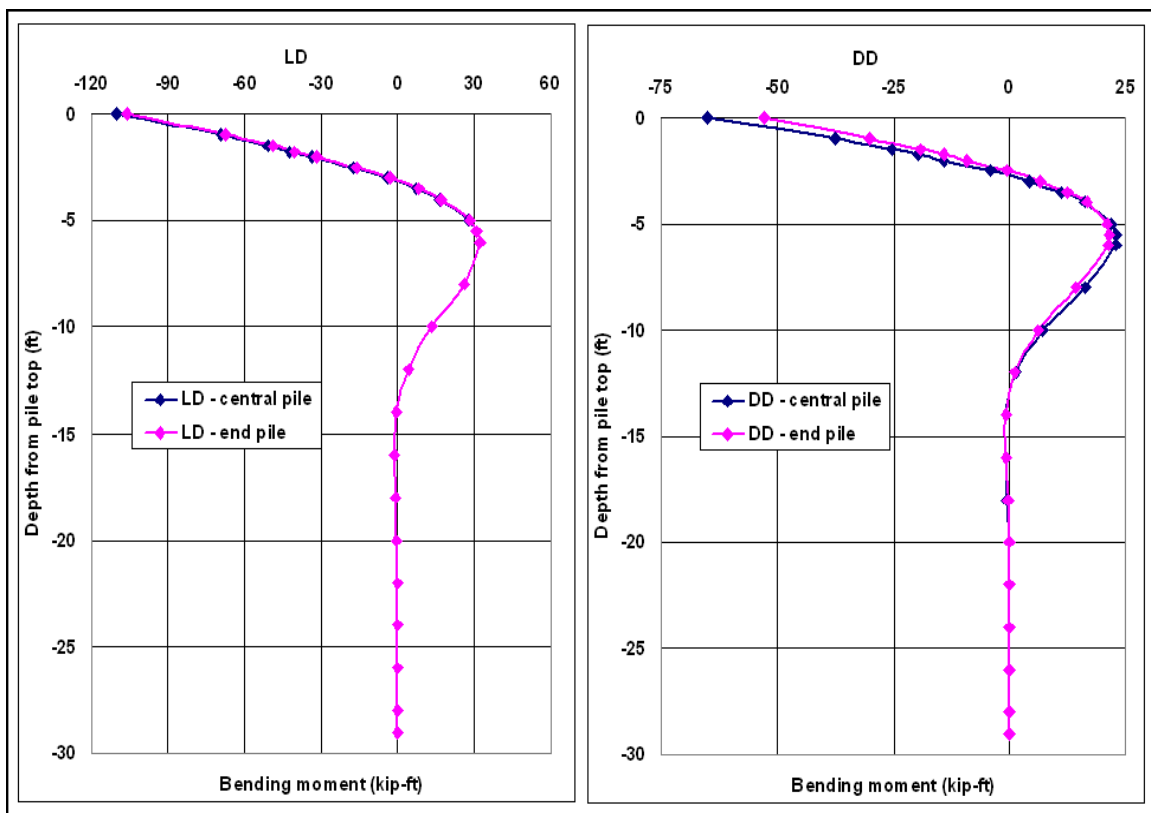
##### 4.6.4.2 Discussion

Figure 4.40 shows lateral earth pressures acting on the back faces of abutments of bridges with and without approach slabs. Distribution of the lateral earth pressure is assumed to be linear with depth. For the bridges without approach slabs, lateral earth pressure values are obtained by simply multiplying the self-weight vertical stress in sand by the corresponding value of the coefficient of lateral earth pressure reported in Table 4.3. The pressures are 4.11 times larger in the dense sand, whereby this difference accounts for different unit weights of loose and dense sands and for different coefficients of lateral earth pressures.

It is evident from Figure 4.40 that the lateral earth pressures acting on bridges with approach slabs are larger than those acting on the bridges without approach slabs regardless of the soil type. However, the increase in the lateral earth pressure is larger in the presence of the dense sand because of the larger value of the coefficient of lateral earth pressure (Table 4.7) and larger unit weight of soil.

#### **4.6.5 Comparisons between the Central Pile and End Pile**

##### **4.6.5.1 Pile Bending Moment**



**Figure 4.41: Comparison of Bending Moments (kip-ft) in Central and End Piles**

#### **4.6.5.2 Discussion**

Figure 4.41 shows bending moments in central and end piles for the two cases analyzed for the bridge with the approach slab. In both cases pile head moments are larger in central piles with the difference being larger in presence of the dense sand behind the abutment. This trend is similar to the one observed in the bridge without the approach slab shown in Figure 4.25.

#### **4.6.6 Axial Compressive Stress in Girders**

Table 4.12 provides maximum axial compressive stresses in girders. As in the bridges without approach slabs these stresses build up in the bottom part of the central girder near its connection with the abutment. In both cases the listed maximum stresses decrease by about 18.5% in the presence of the approach slab. Thus, it appears that the increased translation of the abutment decreases the restraint on girders thereby releasing the axial stresses.

**Table 4.12: Maximum Axial Stress (ksi) in the Central Girder**

<b>CASE</b>	<b>No Approach Slab</b>	<b>With Approach Slab</b>
	<b>(ksi)</b>	<b>(ksi)</b>
<b>LD</b>	-14.755	-12.079
<b>DD</b>	-24.835	-20.218

#### **4.6.7 Bending Stress in Approach Slab**

Table 4.12 provides maximum (tensile) axial stresses in the approach slab. These stresses occur only at distinct locations at the vicinity of the line, along which the approach slab connects to the back of the abutment. Although the stress value is larger in presence of the dense sand both values are rather large, thus indicating a need for

proper design and construction details that will provide the protection against cracking of the concrete.

**Table 4.13: Maximum Axial Stresses (ksi) in the Approach Slab**

CASE	Stress (ksi)
LD	1.1
DD	2.276

#### **4.6.8 Convergence of Iterations**

Equation (4.3) was used to describe the convergence of iterations obtained from the finite element analyses of the bridge with the approach slab. The coefficients  $a_r, b_r, c_r$  related to the rotation, and  $a_t, b_t, c_t$  related to the translation of the abutment top, are listed in Table 4.14. Their values are somewhat different from those provided in Table 4.5 for the corresponding case of the bridge without the approach slab.

**Table 4.14: Values of the Coefficients of Exponential Function**

	LD	DD
$a_r$	-1.4175	-1.05415
$b_r$	-2.29869	-1.4929
$c_r$	0.0554253	0.150011
$a_t$	1.83363	1.26139
$b_t$	-2.33224	-1.48501
$c_t$	0.349748	0.242049

Figure 4.42 and Figure 4.43 show convergence behaviors of the bridges with approach slabs obtained from the equivalent iterative linear finite element analyses. In addition, the Equation (4.3) with the values of coefficients listed in Table 4.14 is plotted. Overall, the analytical expression traces the convergence process very well. However, the convergence of the translational abutment displacement is described slightly better in the dense sand, unlike in the bridge without the approach slab.

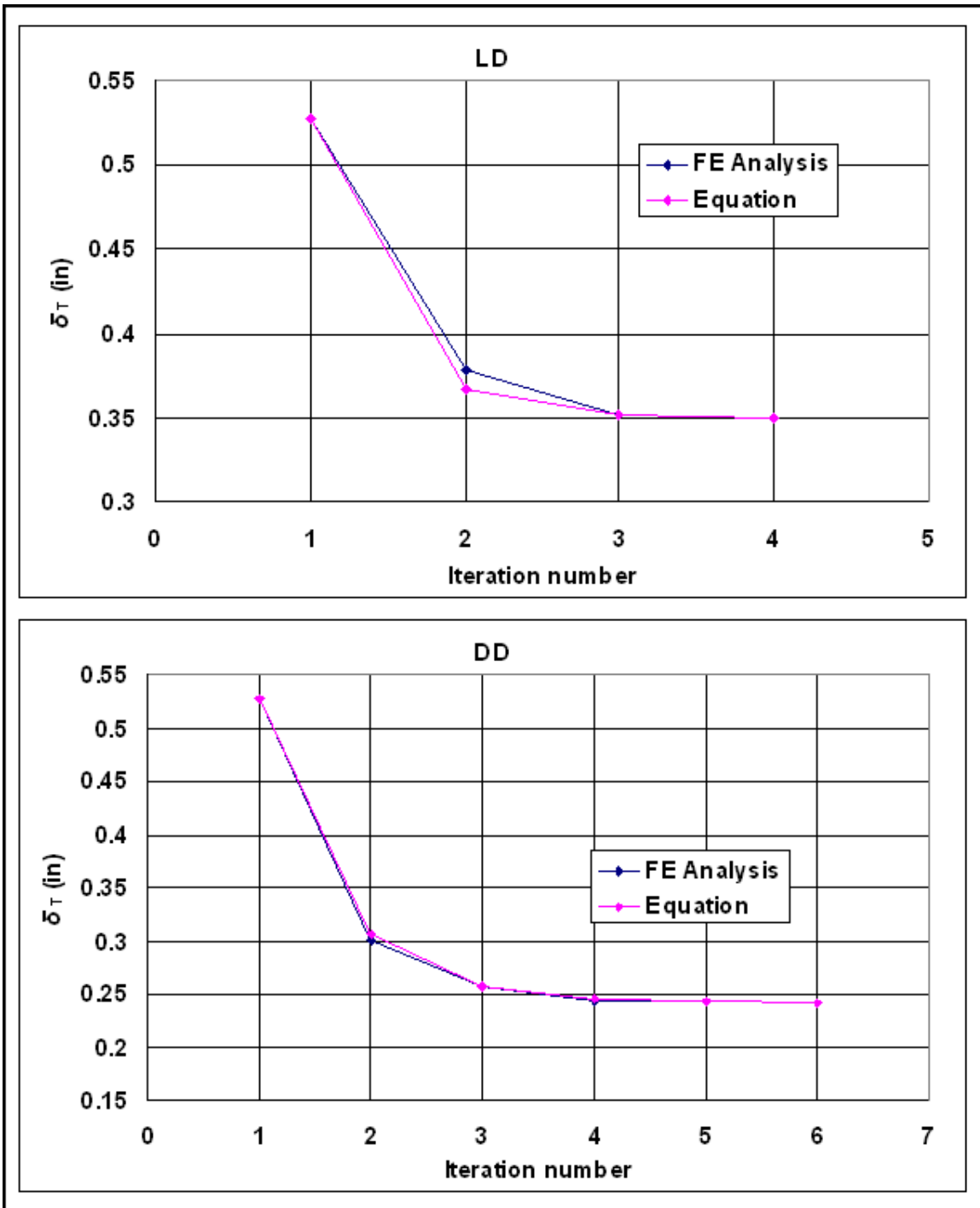


Figure 4.42: Convergence of Translational Displacement

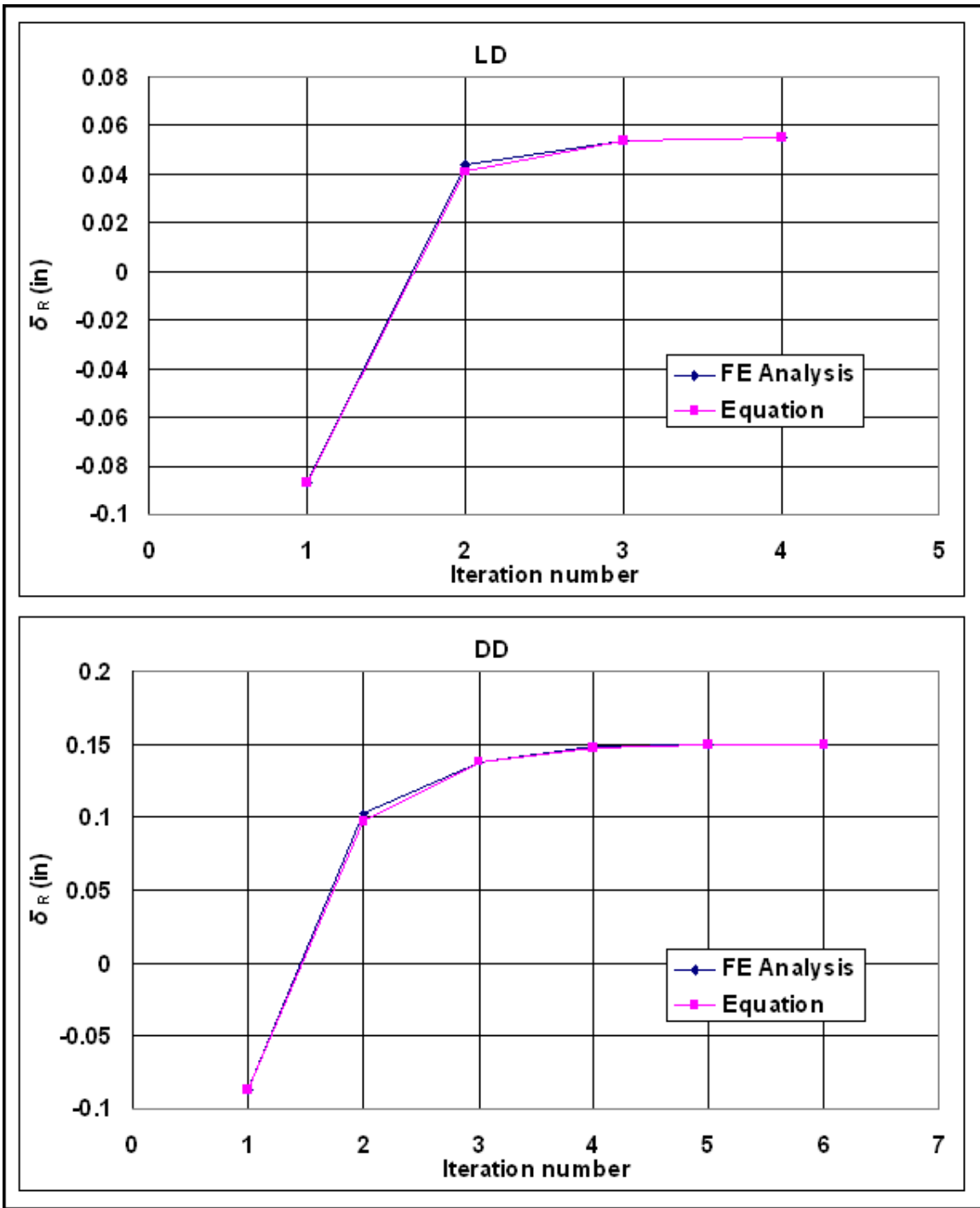


Figure 4.43: Convergence of Rotational Displacement

#### 4.6.9 Soil Pressure on Approach Slab

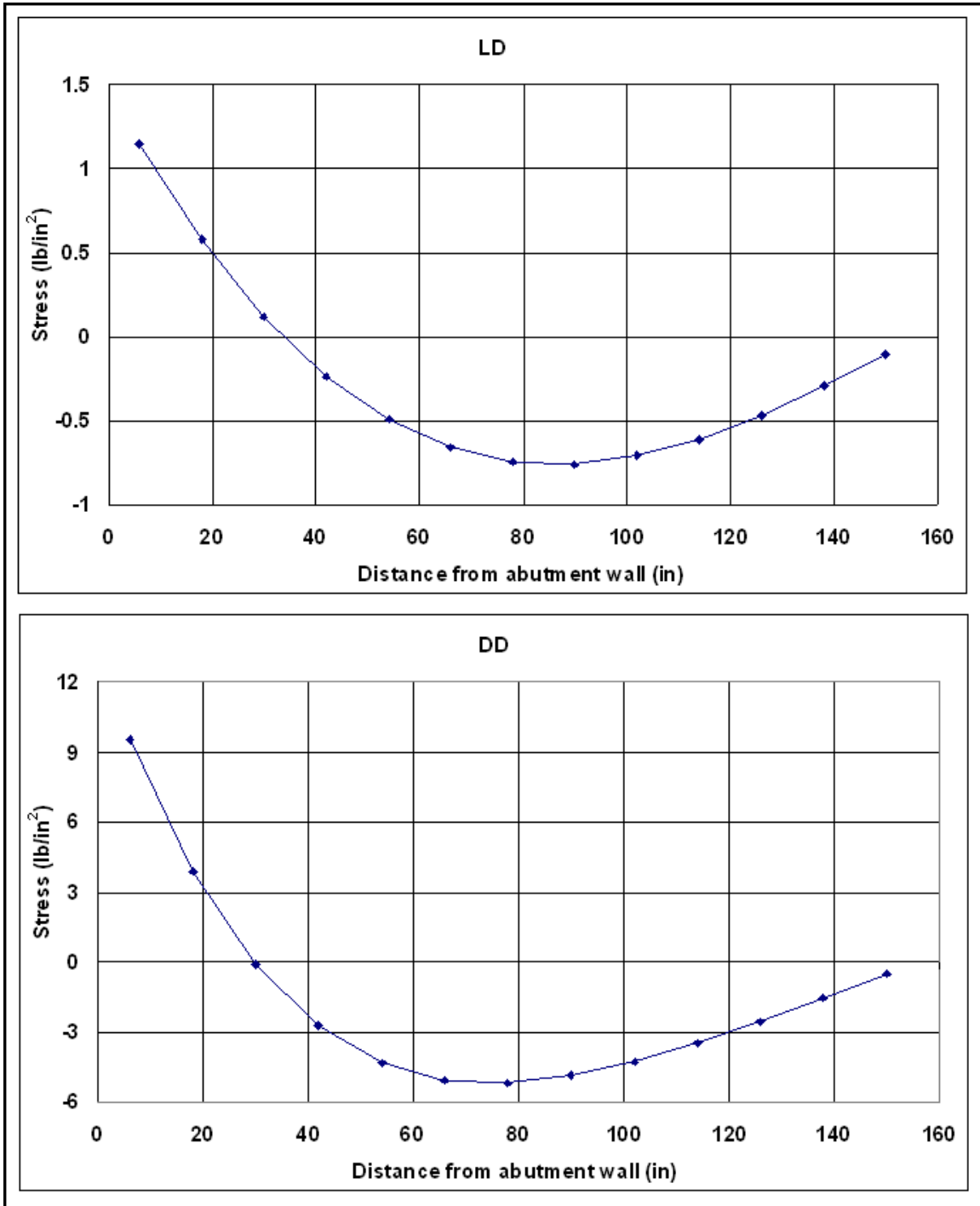


Figure 4.44: Soil Pressure on Approach Slab

Figure 4.44 shows the soil pressure exerted on the approach slab along its centerline, by loose and dense sands. In this preliminary study of the effects of the approach slab, which is beyond the initial scope of the project, the soil substituting vertical springs were assumed to be capable of sustaining tension and compression. Thus, some tensile interface stresses are generated between the approach slab and the soil near the connection of the slab and the abutment. These tensile stresses are larger in dense sand.

It is noted that the contact stress distribution shown in Figure 4.44 is not entirely realistic, because dry sand cannot sustain any tension. Thus, Figure 4.44 indicates that a separation would most likely occur between the slab and the soil within the zone of tensile stresses, followed by the adjustment of compressive interface stresses.

## CHAPTER 5 - CONCLUSIONS AND RECOMMENDATIONS

A full 3D finite element analysis of a typical 3-span IB, incorporating a nonlinear soil response, has been performed to study its response to the ambient temperature change. A sample bridge, Bemis Road Bridge: F-4-20, Fitchburg, Massachusetts, was modeled using 191,894 eight-node coupled temperature-displacement elements (C3D8T), 277,530 nodes, 12 connector elements (CONN3D2) modeling hinges, and 546 linear spring elements. Only half of the bridge was modeled due to the symmetry of its geometry and loading.

A nonlinear force-displacement relationship was used to model the contact of the bridge with soil. This was accomplished by using linear springs in conjunction with an iterative equivalent linear analysis. A stiffness of the springs attached to the abutment wall was determined based on the design recommendations given by NCHRP (1991) and CGS (1992). The stiffness of the springs attached to piles was calculated based on the recommendations by Prakash & Kumar (1996).

Although the use of springs as a substitution for soil in numerical modeling is rather an outdated approach for standard geotechnical applications, a further refinement of the bridge-soil model needs a justification in the improved accuracy of the results against incurring high computational costs. Due to a lack of a deeper understanding of the soil-structure interaction in IBs, the improved accuracy is not possible at this stage. It is the unavailability of the information about the backfill and its response that justifies the absence of a greater modeling sophistication.

The earth pressure generation is sensitive to the angle of internal friction of the backfill. NCHRP (1991) guidelines offer the values of coefficients of lateral earth

pressure for only three cohesionless soils with the internal friction angles of 30°, 37°, and 45° respectively. It should be noted that these values are based on the results of a 2D finite element analysis conducted by Clough and Duncan (1971). CGS (1992) offers design curves for the coefficients of lateral pressure that are similar to those given by NCHRP (1991), with the exception of dense sand whose design curve is significantly different. Thus, for this research, the extreme cases offered by NCHRP (1991) corresponding to internal friction angles of 30°, and 45° were adopted. This approach covered a full potential range of the actual lateral earth pressures. To provide even greater perspective the design curve recommended by CGS (1992) for the dense sand was also included in this research under the DcD case, because it differs from the one recommended by NCHRP (1991) as mentioned earlier.

It is important to note that the finite element analysis performed herein simulated only the expansion due to the thermal heating of the bridge. Thus, neither the contraction due to a thermal cooling, nor the response to a long term cyclic thermal loading that occurs during the entire service life of the bridge were modeled. These subjects are not only outside the scope of this research, but the basic knowledge about the relevant behaviors is currently almost non-existent.

## 5.1 Conclusions

The results of the 3D finite element analyses, presented in Chapter 4, clearly show that the overall response of the IB to a thermal expansion is greatly affected by the density of sand adjacent to the abutment. The following are the conclusions derived from this research:

1. The analysis shows the overall linear response with the temperature change range for given sand.
2. The properties of the soil adjacent to the abutment are a major factor governing the response of an IB to a thermal expansion:
  - a. An increase in the relative compaction (R) of the sand behind the abutment from 90% to 96% decreases the pile top displacement by 39% to 50% for temperature changes of 100 °F and 60°F respectively. The corresponding pile head bending moments decrease by 53% and 68% for temperature changes of 100 °F and 60°F respectively. In addition, the increase in the relative compaction of the sand from 90% to 96% increases the maximum compressive stresses in girders by 69% to 73% for temperature changes of 100 °F and 60°F respectively. It also increases the soil pressure on the abutment 4.4 times, regardless of the temperature change range. For the most part the influence of an increased density of the soil adjacent to the abutment is more pronounced for a smaller temperature change when the resultant change is expressed as a percentage of the initial value.



5. The analyses have also shown that adding the approach slab to the bridge causes the lateral earth pressure on the abutment to increase, especially towards the abutment top. This results in an increased translation and a decreased rotation of the abutment. The effect is more pronounced in the dense sand, in which case the pile head bending moment increases by 56 % while in the loose sand it increases by 13 % (both for  $\Delta T = 80^\circ \text{ F}$ ). However, the maximum compressive stresses in girders decrease by adding the approach slab by about 18% regardless of the soil type, due to a decreased abutment rotation.

In summary, a higher compaction level of the sand behind the abutment decreases the translation of the abutment, thus decreasing the maximum bending moments in piles. The adverse effect of denser sand is in that it increases the earth pressure, thus increasing the possibility of soil failure, but also increasing the maximum compressive stresses in girders. Consequently, design and construction measures should ensure that there is no local buckling in girders.

This study is a stepping stone to a better theoretical understanding and numerical modeling of behavior of non-skew and skew IBs. It serves as a basis for a more complete analysis accounting for different loading conditions including thermal, gravity, live and seismic loads, thus helping streamline the design process for IBs

## 5.2 Recommendations

Future work recommended in the field of IB research includes the following:

1. The results obtained herein have been successfully verified and validated against another similar numerical study. Ultimately the results need to be validated against field data collected on an actual bridge. This requires placement of instrumentation and continuous monitoring of a selected integral bridge. This is a crucial step, which will enable future use of the existing numerical IB model for various modeling purposes. The type of instrumentation, which should be used during monitoring of an IB, and its location are described as follows:
  - a. Joint meters should be installed on the exterior side of abutment(s) to record longitudinal and transversal displacements of a bridge with respect to the reference piles. Tilt-meters should be placed on the base of each abutment to measure its rotation.
  - b. Earth pressure cells should be mounted on the back side of abutment(s) at several depths along the width of abutment(s).
  - c. Vibrating wire strain gages should be mounted on the flanges of H steel piles at several depths, on end and central piles. They should also be placed on the flanges of central and end girders near their connections to abutments.
  - d. Temperature gages should be mounted at the top and bottom sides of a deck, on the front and back sides of abutment(s) and on the bottom of approach slab. In addition, each instrument usually has embedded

thermistors that provide a temperature record at the location of the instrument.

2. Nonlinear material models of concrete and steel along with the improved model for soil need to be implemented to study the long term effects of cyclic loading during the lifespan of the IB. This will help in resolving issues related to cracking of concrete decks and yielding of steel piles and girders.
3. The effect of different load combinations including dead, live, thermal and earthquake loads should be investigated.
4. The behavior of skewed IBs needs to be explored.



## REFERENCES

1. ABAQUS Inc. (2004). "ABAQUS Analysis User's Manual 6.5-1"
2. ABAQUS Inc. (2004). "ABAQUS/CAE User's Manual 6.5-1"
3. Alampalli, S and Yannotti, A.P., (1998). "In-Service Performance of Integral Bridges and Jointless Decks", Transportation Research Record 1624, Paper No. 98-0540.
4. American Petroleum Institute (API), (1993). "Recommended practice for planning, designing, and constructing fixed offshore platforms – Working stress design." 20<sup>th</sup> Ed., API RP2A-WSD, Washington, D.C.
5. Arockiasamy, M., Butrieng, N. and Sivakumar M., (2004). "State-of-the-Art of Integral Abutment Bridges: Design and Practice", Journal of Bridge Engineering, Vol. 9, No. 5
6. Arsoy, S., Barker, R.M., Duncan, J.M., (1999). "The Behavior of Integral Abutment Bridges", Final Contract Report VTRC 00-CR3, Virginia Transportation Research Council, Charlottesville, Virginia
7. Arsoy, S., (2000). "Experimental and Analytical Investigations of Piles and Abutments of Integral Bridges", PhD Thesis, Virginia Polytechnic and State University, Blacksburg, Virginia.
8. Bakeer, R.M., Mattei, N.J., Almalik, B.K., Carr, S.P., Homes, D., (2005). "Evaluation of DOTD Semi-Integral Bridge and Abutment System", Final report FHWA/LA.05/397, Louisiana Transportation Research Center, Baton Rouge, LA.
9. Canadian Geotechnical Society (CGS), (1992). Canadian foundation engineering manual, 3rd Ed., Toronto
10. Ng, C.W.W., Springman, S.M., Norrish, A.R.M., (1998). "Soil-structure interaction of spread-base integral bridge abutments", Japanese Geotechnical Society, SOIL AND FOUNDATION, Vol. 38, No. 1, pp.145-162
11. Clough, G.W., Duncan, J.M., (1971). "Finite element analyses of retaining wall behavior", Journal of the Soil Mechanics and Foundations Division, American Society of Civil Engineers, Vol. 97, No. SM12, pp. 1657-1673

12. Das, B.M., (1999). "Principles of Foundation Engineering", 4<sup>th</sup> ed., PWS Publishing, Brooks/Cole Publishing Company
13. Emerson, M., (1976). "Bridge temperatures estimated from the shade temperature", Transport and Road Research Laboratory Report 696, Transport Research Laboratory, UK
14. Faraji, S., (1997). "Behavior of integral abutment bridges in Massachusetts – Year II." Report UMTC 96-5, University of Massachusetts Transportation Center, Amherst, MA
15. Faraji, S., Ting, J.M., Crovo, D.S., Ernst, H., (2001). "Non-linear Analysis of Integral Bridges: Finite Element Model", Journal of Geotechnical and Geoenvironmental Engineering, Vol. 127, No. 5
16. Greimann, L. F., Abendroth, R. E., Johnson, D. E., and Ebner, P.B., (1987). "Pile design and tests for integral abutment bridges", Iowa State University, December 1987.
17. Hoppe E.J. and Gomez, J.P., (1996). "Field study of an integral backwall bridge", Virginia Transportation Research Council, VTRC 97-R7, October 1996.
18. Jayaram, R., Merz, P.B. and McLellan Pte Ltd, Singapore, (2001). "Integral Bridge Concept Applied to Rehabilitate an Existing Bridge and Construct a Dual-Use Bridge", Proceedings of 26<sup>th</sup> Conference on Our World in Concrete and Structures
19. KDOT Bridge Design Manual, (2007). Kansas Department of Transportation
20. Khodair, Y.A., Hassiotis, S., (2005), "Analysis of soil-pile interaction in integral abutment", Computers and Geotechnics 32, pp 201-209.
21. Lee, K.L. and Singh, A., (1971). "Relative Density and Relative Compaction", Journal of the Soil Mechanics and Foundations Division, American Society of Civil Engineers, Vol. 96, No. SM1, pp. 73-110
22. Lock, R.J., (2002). "Integral bridge abutments", M.Eng. Project Report CUED/D-SOILS/TR320, London, UK
23. Loveall, C. (1996). "Integral abutment bridges", Workshop on Integral abutment bridges, November 13-15, 1996, Pittsburg, PA.

24. Mourad, S. and Tabsh, S.W., (1999). "Deck Slab Stresses in Integral Abutment Bridges", Journal of Bridge Engineering, Vol. 4, No. 2
25. Mwindo, J.M., (1992). "Strain dependent soil modulus of horizontal subgrade reaction", MS Thesis, University of Missouri-Rolla, Rolla, MO
26. National Cooperative Highway Research Program (NCHRP), (1991). "Manuals for design of bridge foundations", Barker, R.M., Duncan, J.M., Rojiani, K.B., Ooi, P.S.K., Tan, C.K., and Kim, S.G., eds. Rep 343, Transportation Research Board, Washington, D.C.
27. Prakash, S., Kumar, S., (1996). "Nonlinear Lateral Pile Deflection Prediction in Sands", Journal of Geotechnical Engineering., Vol. 122, No. 2, pp. 130-138
28. Roman, E., Khodair, Y.A., Hassiotis, S., (2002). "Design Details on Integral Bridges", Proceedings of the Engineering Mechanics Conference, May, New York.
29. Shoukry, S.N., William, G.W., Riad, M.Y., McBride, K.C., (2006). "Field Monitoring and 3D FE Modeling of an Integral Abutment Bridge in West Virginia", TRB 2006 Annual Meeting CD-ROM
30. Soltani, A. A. and Kukreti, A. R., (1996). "Performance evaluation of integral abutment bridges" Workshop on Integral abutment bridges, November 13-15, 1996, Pittsburg, PA, 29 p.
31. Soltani, A. A. and Kukreti, A. R., (1992). "Performance evaluation of integral abutment bridges", Transportation Research Record 1371, Transportation Research Board, No. 1371, pp 17-25.
32. Ting, J.M., Faraji, S., (1998). "Streamlines analysis and design of Integral Abutment Bridges", Report UMTc 97-13, University of Massachusetts Transportation Center, Amherst, MA
33. Wasserman, E.P., (2001). "Design of Integral Abutments for Jointless Bridges", Structure, pp. 24-33
34. Wood, D.M., (2004). "Integral bridge abutment", Chapter 8, section 8.10, Geotechnical Modelling, Spon Press, Taylor and Francis Group, London, UK and New York, USA.

35. Yang, Pe-Shen, Wolde-Tinsae, A.M., and Greimann, L.F., (1985). Effects of predrilling and layered soils on piles, *Journal of Geotechnical Engineering*, ASCE, Vol. 111, No. 1.

## **APPENDIX A - TABULAR DATA OF RESULTS**

**Table A.1: Comparison of Longitudinal Displacements – Shah vs. Ting & Faraji (1998) (Refer Figure 4.7)**

<b>Depth from abutment top (ft)</b>	<b>Ting &amp; Faraji - DD 80°F</b>		<b>Depth from abutment top (ft)</b>	<b>Shah - DD 80°F</b>
<b>(ft)</b>	<b>(in)</b>		<b>(ft)</b>	<b>(in)</b>
0.76486	4.3230E-01		0.70833	0.435198
2.81790	3.8502E-01		1.83573	0.399427
4.79043	3.2615E-01		4.00667	0.32813
6.84347	2.6440E-01		5.35000	0.281844
8.81600	2.2773E-01		7.70083	0.195477
10.86904	1.4088E-01		8.70833	0.156673
12.84157	6.5617E-02		10.70833	0.085432
14.89461	1.9299E-02		12.70833	0.032563
16.86714	-1.9299E-03		14.70833	0.004911
18.92018	9.6495E-04		16.70833	-4.01E-03
20.89271	1.9299E-03		18.70833	-0.00403
22.94575	9.6495E-04		20.70833	-0.00193
24.91828	9.6495E-04		22.70833	-4.60E-04
26.97132	9.6495E-04		24.70833	8.18E-05
28.94385	0.0000E+00		26.70833	1.34E-04
30.99689	0.0000E+00		28.70833	6.32E-05
32.96942	0.0000E+00		30.70833	1.24E-05
35.02246	0.0000E+00		32.70833	-3.46E-06
			34.70833	-2.36E-06
			36.70833	2.37E-06
			37.70833	1.61E-33

**Table A.2: LD - Trends in Longitudinal Displacement Due to Changes in Thermal Load  
(Refer Figure 4-10)**

<b>Depth from abutment top</b>	<b>LD 60°F</b>	<b>LD 80°F</b>	<b>LD 100°F</b>
<b>(ft)</b>	<b>(in)</b>	<b>(in)</b>	<b>(in)</b>
-0.70833	3.1655E-01	4.2337E-01	5.3066E-01
-1.83573	2.9604E-01	3.9624E-01	4.9741E-01
-4.00667	2.6627E-01	3.5712E-01	4.4994E-01
-5.35000	2.5470E-01	3.4221E-01	4.3236E-01
-7.70083	2.4670E-01	3.3259E-01	4.2226E-01
-8.70833	2.4628E-01	3.3257E-01	4.2313E-01
-10.70833	1.8922E-01	2.5993E-01	3.3528E-01
-12.70833	1.0432E-01	1.4849E-01	1.9675E-01
-14.70833	3.9023E-02	5.9509E-02	8.2907E-02
-16.70833	5.1872E-03	1.0709E-02	1.7783E-02
-18.70833	-5.4224E-03	-6.4816E-03	-7.0671E-03
-20.70833	-5.2000E-03	-7.6019E-03	-1.0124E-02
-22.70833	-2.4916E-03	-4.1386E-03	-6.0721E-03
-24.70833	-6.0380E-04	-1.2698E-03	-2.1558E-03
-26.70833	1.0532E-04	5.9945E-06	-1.9289E-04
-28.70833	1.8275E-04	2.6361E-04	3.2752E-04
-30.70833	9.1621E-05	1.6828E-04	2.5910E-04
-32.70833	2.1502E-05	5.4979E-05	1.0314E-04
-34.70833	-2.4095E-06	3.5307E-06	1.5924E-05
-36.70833	-3.1319E-06	-5.6855E-06	-7.5571E-06
-37.70833	-1.9283E-33	-3.1971E-33	-4.4874E-33

**Table A.3: DD - Trends in Longitudinal Displacement Due to Changes in Thermal Load  
(Refer Figure 4.10)**

<b>Depth from abutment top</b>	<b>DD 60°F</b>	<b>DD 80°F</b>	<b>DD 100°F</b>
<b>(ft)</b>	<b>(in)</b>	<b>(in)</b>	<b>(in)</b>
-0.70833	2.9997E-01	4.0473E-01	5.0904E-01
-1.83573	2.6495E-01	3.6095E-01	4.5618E-01
-4.00667	2.0644E-01	2.8886E-01	3.6989E-01
-5.35000	1.7661E-01	2.5298E-01	3.2757E-01
-7.70083	1.3694E-01	2.0692E-01	2.7447E-01
-8.70833	1.2372E-01	1.9211E-01	2.5784E-01
-10.70833	7.9745E-02	1.3200E-01	1.8282E-01
-12.70833	3.6035E-02	6.5417E-02	9.5122E-02
-14.70833	9.1381E-03	2.0432E-02	3.2832E-02
-16.70833	-1.4610E-03	4.7672E-05	2.4488E-03
-18.70833	-2.9945E-03	-4.7133E-03	-6.1024E-03
-20.70833	-1.6928E-03	-3.3682E-03	-5.1117E-03
-22.70833	-4.9272E-04	-1.3046E-03	-2.2964E-03
-24.70833	1.3494E-05	-1.7728E-04	-4.9267E-04
-26.70833	9.4300E-05	1.3863E-04	1.4025E-04
-28.70833	5.0044E-05	1.1612E-04	1.8497E-04
-30.70833	1.1426E-05	4.2985E-05	8.7275E-05
-32.70833	-1.9191E-06	4.3776E-06	1.8450E-05
-34.70833	-2.6292E-06	-4.7551E-06	-4.6867E-06
-36.70833	-1.1270E-06	-3.9478E-06	-6.6869E-06
-37.70833	-1.4303E-33	-2.6206E-33	-3.7865E-33

**Table A.4: DcD - Trends in Longitudinal Displacement Due to Changes in Thermal Load (Refer Figure 4.10)**

<b>Depth from abutment top</b>	<b>DcD 60°F</b>	<b>DcD 80°F</b>	<b>DcD 100°F</b>
<b>(ft)</b>	<b>(in)</b>	<b>(in)</b>	<b>(in)</b>
-0.70833	3.0681E-01	4.1296E-01	5.1939E-01
-1.83573	2.7768E-01	3.7644E-01	4.7586E-01
-4.00667	2.3083E-01	3.1870E-01	4.0804E-01
-5.35000	2.0840E-01	2.9196E-01	3.7748E-01
-7.70083	1.8155E-01	2.6174E-01	3.4482E-01
-8.70833	1.7350E-01	2.5335E-01	3.3649E-01
-10.70833	1.2361E-01	1.8721E-01	2.5487E-01
-12.70833	6.2621E-02	1.0052E-01	1.4244E-01
-14.70833	2.0144E-02	3.6319E-02	5.5526E-02
-16.70833	5.4807E-04	3.9372E-03	8.9375E-03
-18.70833	-4.1957E-03	-5.7702E-03	-6.9178E-03
-20.70833	-3.0603E-03	-5.1942E-03	-7.5237E-03
-22.70833	-1.1854E-03	-2.4220E-03	-3.9864E-03
-24.70833	-1.5939E-04	-5.5986E-04	-1.1803E-03
-26.70833	1.2441E-04	1.2091E-04	3.5437E-05
-28.70833	1.0228E-04	1.8513E-04	2.6543E-04
-30.70833	3.6728E-05	9.0680E-05	1.6398E-04
-32.70833	3.2395E-06	2.0508E-05	5.1911E-05
-34.70833	-3.7726E-06	-3.4473E-06	1.8266E-06
-36.70833	-1.9887E-06	-4.9252E-06	-7.5294E-06
-37.70833	-1.6291E-33	-2.8661E-33	-4.1215E-33

**Table A.5; 60°F - Trends in Longitudinal Displacement Due to Changes in Soil Properties  
(Refer Figure 4.11)**

<b>Depth from abutment top</b>	<b>LD 60°F</b>	<b>DD 60°F</b>	<b>DcD 60°F</b>
<b>(ft)</b>	<b>(in)</b>	<b>(in)</b>	<b>(in)</b>
-0.70833	3.1655E-01	2.9997E-01	3.0681E-01
-1.83573	2.9604E-01	2.6495E-01	2.7768E-01
-4.00667	2.6627E-01	2.0644E-01	2.3083E-01
-5.35000	2.5470E-01	1.7661E-01	2.0840E-01
-7.70083	2.4670E-01	1.3694E-01	1.8155E-01
-8.70833	2.4628E-01	1.2372E-01	1.7350E-01
-10.70833	1.8922E-01	7.9745E-02	1.2361E-01
-12.70833	1.0432E-01	3.6035E-02	6.2621E-02
-14.70833	3.9023E-02	9.1381E-03	2.0144E-02
-16.70833	5.1872E-03	-1.4610E-03	5.4807E-04
-18.70833	-5.4224E-03	-2.9945E-03	-4.1957E-03
-20.70833	-5.2000E-03	-1.6928E-03	-3.0603E-03
-22.70833	-2.4916E-03	-4.9272E-04	-1.1854E-03
-24.70833	-6.0380E-04	1.3494E-05	-1.5939E-04
-26.70833	1.0532E-04	9.4300E-05	1.2441E-04
-28.70833	1.8275E-04	5.0044E-05	1.0228E-04
-30.70833	9.1621E-05	1.1426E-05	3.6728E-05
-32.70833	2.1502E-05	-1.9191E-06	3.2395E-06
-34.70833	-2.4095E-06	-2.6292E-06	-3.7726E-06
-36.70833	-3.1319E-06	-1.1270E-06	-1.9887E-06
-37.70833	-1.9283E-33	-1.4303E-33	-1.6291E-33

**Table A.6: 80°F - Trends in Longitudinal Displacement Due to Changes in Soil Properties (Refer Figure 4.11)**

<b>Depth from abutment top</b>	<b>LD 80°F</b>	<b>DD 80°F</b>	<b>DcD 80°F</b>
<b>(ft)</b>	<b>(in)</b>	<b>(in)</b>	<b>(in)</b>
-0.70833	4.2337E-01	4.0473E-01	4.1296E-01
-1.83573	3.9624E-01	3.6095E-01	3.7644E-01
-4.00667	3.5712E-01	2.8886E-01	3.1870E-01
-5.35000	3.4221E-01	2.5298E-01	2.9196E-01
-7.70083	3.3259E-01	2.0692E-01	2.6174E-01
-8.70833	3.3257E-01	1.9211E-01	2.5335E-01
-10.70833	2.5993E-01	1.3200E-01	1.8721E-01
-12.70833	1.4849E-01	6.5417E-02	1.0052E-01
-14.70833	5.9509E-02	2.0432E-02	3.6319E-02
-16.70833	1.0709E-02	4.7672E-05	3.9372E-03
-18.70833	-6.4816E-03	-4.7133E-03	-5.7702E-03
-20.70833	-7.6019E-03	-3.3682E-03	-5.1942E-03
-22.70833	-4.1386E-03	-1.3046E-03	-2.4220E-03
-24.70833	-1.2698E-03	-1.7728E-04	-5.5986E-04
-26.70833	5.9945E-06	1.3863E-04	1.2091E-04
-28.70833	2.6361E-04	1.1612E-04	1.8513E-04
-30.70833	1.6828E-04	4.2985E-05	9.0680E-05
-32.70833	5.4979E-05	4.3776E-06	2.0508E-05
-34.70833	3.5307E-06	-4.7551E-06	-3.4473E-06
-36.70833	-5.6855E-06	-3.9478E-06	-4.9252E-06
-37.70833	-3.1971E-33	-2.6206E-33	-2.8661E-33

**Table A.7: 100°F - Longitudinal Displacement Due to Changes in Soil Properties (Refer Figure 4.11)**

<b>Depth from abutment top</b>	<b>LD 100°F</b>	<b>DD 100°F</b>	<b>DcD 100°F</b>
<b>(ft)</b>	<b>(in)</b>	<b>(in)</b>	<b>(in)</b>
-0.70833	5.3066E-01	5.0904E-01	5.1939E-01
-1.83573	4.9741E-01	4.5618E-01	4.7586E-01
-4.00667	4.4994E-01	3.6989E-01	4.0804E-01
-5.35000	4.3236E-01	3.2757E-01	3.7748E-01
-7.70083	4.2226E-01	2.7447E-01	3.4482E-01
-8.70833	4.2313E-01	2.5784E-01	3.3649E-01
-10.70833	3.3528E-01	1.8282E-01	2.5487E-01
-12.70833	1.9675E-01	9.5122E-02	1.4244E-01
-14.70833	8.2907E-02	3.2832E-02	5.5526E-02
-16.70833	1.7783E-02	2.4488E-03	8.9375E-03
-18.70833	-7.0671E-03	-6.1024E-03	-6.9178E-03
-20.70833	-1.0124E-02	-5.1117E-03	-7.5237E-03
-22.70833	-6.0721E-03	-2.2964E-03	-3.9864E-03
-24.70833	-2.1558E-03	-4.9267E-04	-1.1803E-03
-26.70833	-1.9289E-04	1.4025E-04	3.5437E-05
-28.70833	3.2752E-04	1.8497E-04	2.6543E-04
-30.70833	2.5910E-04	8.7275E-05	1.6398E-04
-32.70833	1.0314E-04	1.8450E-05	5.1911E-05
-34.70833	1.5924E-05	-4.6867E-06	1.8266E-06
-36.70833	-7.5571E-06	-6.6869E-06	-7.5294E-06
-37.70833	-4.4874E-33	-3.7865E-33	-4.1215E-33

**Table A.8: Displacement at Abutment Top vs.  $\Delta T$  (Refer Figure 4.12)**

Temperature	LD	DD	DcD
(°F)	(in)	(in)	(in)
60	0.31655	0.29997	0.30681
80	0.42337	0.40473	0.41296
100	0.53066	0.50904	0.51939

**Table A.9:  $\delta_T$  and  $\delta_R$  vs.  $\Delta T$  (Refer Figure 4.13)**

Temperature	Translational displacement			Rotational displacement		
	LD	DD	DcD	LD	DD	DcD
(°F)	(in)	(in)	(in)	(in)	(in)	(in)
60	0.24566	0.12283	0.17272	0.07089	0.17714	0.13409
80	0.33171	0.19097	0.25233	0.09166	0.21376	0.16063
100	0.42203	0.25642	0.33523	0.10863	0.25263	0.18416

**Table A.10: LD - Comparison of Deck Displacement (Refer Figure 4.14)**

Temperature	Deck top	Pile Head	Abutment top	Analytical
(°F)	(in)	(in)	(in)	(in)
60	0.32797	0.24628	0.31655	0.32473
80	0.43847	0.33257	0.42337	0.43297
100	0.54912	0.42313	0.53066	0.54121

**Table A.11: DD - Comparison of Deck Displacement (Refer Figure 4.14)**

<b>Temperature</b>	<b>Deck top</b>	<b>Pile Head</b>	<b>Abutment top</b>	<b>Analytical</b>
<b>(°F)</b>	<b>(in)</b>	<b>(in)</b>	<b>(in)</b>	<b>(in)</b>
<b>60</b>	0.32051	0.12371	0.29997	0.32473
<b>80</b>	0.43029	0.19210	0.40473	0.43297
<b>100</b>	0.53982	0.25782	0.50904	0.54121

**Table A.12: DcD - Comparison of Deck Displacement (Refer Figure 4.14)**

<b>Temperature</b>	<b>Deck top</b>	<b>Pile Head</b>	<b>Abutment top</b>	<b>Analytical</b>
<b>(°F)</b>	<b>(in)</b>	<b>(in)</b>	<b>(in)</b>	<b>(in)</b>
<b>60</b>	0.32365	0.17349	0.30681	0.32473
<b>80</b>	0.43397	0.25334	0.41296	0.43297
<b>100</b>	0.54431	0.33649	0.51939	0.54121

**Table A.13: LD - Trends in Central Pile Bending Moment Due to Changes in Thermal Load (Refer Figure 4.15)**

<b>Depth from pile top</b>	<b>LD 60°F</b>	<b>LD 80°F</b>	<b>LD 100°F</b>
<b>(ft)</b>	<b>(kip-ft)</b>	<b>(kip-ft)</b>	<b>(kip-ft)</b>
0.00	-7.5924E+01	-9.7793E+01	-1.2037E+02
-1.00	-4.6215E+01	-6.0680E+01	-7.5799E+01
-1.50	-3.2702E+01	-4.3827E+01	-5.5589E+01
-1.75	-2.6463E+01	-3.6003E+01	-4.6168E+01
-2.00	-2.0097E+01	-2.7979E+01	-3.6469E+01
-2.50	-8.8782E+00	-1.3757E+01	-1.9205E+01
-3.00	6.3522E-01	-1.5552E+00	-4.2700E+00
-3.50	8.4161E+00	8.5700E+00	8.2537E+00
-4.00	1.4415E+01	1.6542E+01	1.8262E+01
-5.00	2.1562E+01	2.6532E+01	3.1238E+01
-5.50	2.3014E+01	2.8876E+01	3.4552E+01
-6.00	2.3313E+01	2.9742E+01	3.6065E+01
-8.00	1.7264E+01	2.3457E+01	2.9829E+01
-10.00	8.0489E+00	1.1922E+01	1.6111E+01
-12.00	1.8171E+00	3.3652E+00	5.1975E+00
-14.00	-6.5062E-01	-4.9145E-01	-1.7313E-01
-16.00	-9.0529E-01	-1.2211E+00	-1.4978E+00
-18.00	-4.8171E-01	-7.7424E-01	-1.0912E+00
-20.00	-1.2639E-01	-2.6551E-01	-4.3987E-01
-22.00	1.8121E-02	-1.0786E-02	-6.1174E-02
-24.00	3.6463E-02	4.8838E-02	5.4860E-02
-26.00	1.8094E-02	3.2791E-02	4.9105E-02
-28.00	8.0422E-04	7.5467E-03	1.8409E-02
-29.00	-4.8609E-03	-1.6135E-03	5.8189E-03

**Table A.14: DD - Trends in Central Pile Bending Moment Due to Changes in Thermal Load (Refer Figure 4.15)**

<b>Depth from pile top</b>	<b>DD 60°F</b>	<b>DD 80°F</b>	<b>DD 100°F</b>
<b>(ft)</b>	<b>(kip-ft)</b>	<b>(kip-ft)</b>	<b>(kip-ft)</b>
0.00	-2.4100E+01	-4.1578E+01	-5.6674E+01
-1.00	-1.1113E+01	-2.1890E+01	-3.1353E+01
-1.50	-5.1254E+00	-1.2856E+01	-1.9759E+01
-1.75	-2.4594E+00	-8.7635E+00	-1.4462E+01
-2.00	1.7418E-01	-4.6594E+00	-9.1105E+00
-2.50	4.6348E+00	2.4275E+00	2.1727E-01
-3.00	8.1279E+00	8.2014E+00	7.9596E+00
-3.50	1.0691E+01	1.2680E+01	1.4117E+01
-4.00	1.2342E+01	1.5861E+01	1.8666E+01
-5.00	1.3348E+01	1.8824E+01	2.3466E+01
-5.50	1.2937E+01	1.8886E+01	2.4026E+01
-6.00	1.2096E+01	1.8225E+01	2.3615E+01
-8.00	6.7604E+00	1.1618E+01	1.6208E+01
-10.00	2.1056E+00	4.5332E+00	7.0767E+00
-12.00	-9.9694E-02	5.0447E-01	1.3201E+00
-14.00	-5.4005E-01	-7.2900E-01	-7.9223E-01
-16.00	-3.2872E-01	-6.2361E-01	-8.9725E-01
-18.00	-9.5552E-02	-2.5820E-01	-4.4771E-01
-20.00	5.5571E-03	-3.6971E-02	-1.0633E-01
-22.00	2.0287E-02	2.7849E-02	2.4012E-02
-24.00	1.0034E-02	2.3237E-02	3.5917E-02
-26.00	1.7126E-03	7.7119E-03	1.6351E-02
-28.00	-1.2171E-03	-6.7336E-04	1.6135E-03
-29.00	-1.3391E-03	-1.6389E-03	-1.3086E-03

**Table A.15: DcD - Trends in Central Pile Bending Moment Due to Changes in Thermal Load (Refer Figure 4.15)**

<b>Depth from pile top</b>	<b>DcD 60°F</b>	<b>DcD 80°F</b>	<b>DcD 100°F</b>
<b>(ft)</b>	<b>(kip-ft)</b>	<b>(kip-ft)</b>	<b>(kip-ft)</b>
0.00	-4.5908E+01	-6.6796E+01	-8.7499E+01
-1.00	-2.5710E+01	-3.9131E+01	-5.2718E+01
-1.50	-1.6470E+01	-2.6511E+01	-3.6882E+01
-1.75	-1.2265E+01	-2.0711E+01	-2.9558E+01
-2.00	-8.0284E+00	-1.4818E+01	-2.2074E+01
-2.50	-6.7515E-01	-4.4837E+00	-8.8604E+00
-3.00	5.3770E+00	4.2002E+00	2.3911E+00
-3.50	1.0138E+01	1.1219E+01	1.1640E+01
-4.00	1.3600E+01	1.6536E+01	1.8824E+01
-5.00	1.7095E+01	2.2573E+01	2.7520E+01
-5.50	1.7402E+01	2.3602E+01	2.9364E+01
-6.00	1.6966E+01	2.3561E+01	2.9827E+01
-8.00	1.1058E+01	1.6844E+01	2.2747E+01
-10.00	4.3720E+00	7.6343E+00	1.1255E+01
-12.00	5.2354E-01	1.5988E+00	3.0045E+00
-14.00	-6.6270E-01	-7.1712E-01	-6.0278E-01
-16.00	-5.7156E-01	-9.0631E-01	-1.2161E+00
-18.00	-2.3384E-01	-4.6973E-01	-7.4451E-01
-20.00	-3.1633E-02	-1.1877E-01	-2.4597E-01
-22.00	2.5914E-02	2.0569E-02	-4.1799E-03
-24.00	2.0935E-02	3.6412E-02	4.8825E-02
-26.00	6.8746E-03	1.7457E-02	3.1254E-02
-28.00	-1.3505E-03	1.3086E-03	7.3689E-03
-29.00	-3.2461E-03	-3.0619E-03	-3.4303E-04

**Table A.16: 60°F - Trends in Central Pile Bending Moment Due to Changes in Soil Properties (Refer Figure 4.16)**

<b>Depth from pile top</b>	<b>LD 60°F</b>	<b>DD 60°F</b>	<b>DcD 60°F</b>
<b>(ft)</b>	<b>(kip-ft)</b>	<b>(kip-ft)</b>	<b>(kip-ft)</b>
0.00	-7.5924E+01	-2.4100E+01	-4.5908E+01
-1.00	-4.6215E+01	-1.1113E+01	-2.5710E+01
-1.50	-3.2702E+01	-5.1254E+00	-1.6470E+01
-1.75	-2.6463E+01	-2.4594E+00	-1.2265E+01
-2.00	-2.0097E+01	1.7418E-01	-8.0284E+00
-2.50	-8.8782E+00	4.6348E+00	-6.7515E-01
-3.00	6.3522E-01	8.1279E+00	5.3770E+00
-3.50	8.4161E+00	1.0691E+01	1.0138E+01
-4.00	1.4415E+01	1.2342E+01	1.3600E+01
-5.00	2.1562E+01	1.3348E+01	1.7095E+01
-5.50	2.3014E+01	1.2937E+01	1.7402E+01
-6.00	2.3313E+01	1.2096E+01	1.6966E+01
-8.00	1.7264E+01	6.7604E+00	1.1058E+01
-10.00	8.0489E+00	2.1056E+00	4.3720E+00
-12.00	1.8171E+00	-9.9694E-02	5.2354E-01
-14.00	-6.5062E-01	-5.4005E-01	-6.6270E-01
-16.00	-9.0529E-01	-3.2872E-01	-5.7156E-01
-18.00	-4.8171E-01	-9.5552E-02	-2.3384E-01
-20.00	-1.2639E-01	5.5571E-03	-3.1633E-02
-22.00	1.8121E-02	2.0287E-02	2.5914E-02
-24.00	3.6463E-02	1.0034E-02	2.0935E-02
-26.00	1.8094E-02	1.7126E-03	6.8746E-03
-28.00	8.0422E-04	-1.2171E-03	-1.3505E-03
-29.00	-4.8609E-03	-1.3391E-03	-3.2461E-03

**Table A.17: 80°F - Trends in Central Pile Bending Moment Due to Changes in Soil Properties (Refer Figure 4.16)**

<b>Depth from pile top</b>	<b>LD 80°F</b>	<b>DD 80°F</b>	<b>DcD 80°F</b>
<b>(ft)</b>	<b>(kip-ft)</b>	<b>(kip-ft)</b>	<b>(kip-ft)</b>
0.00	-9.7793E+01	-4.1578E+01	-6.6796E+01
-1.00	-6.0680E+01	-2.1890E+01	-3.9131E+01
-1.50	-4.3827E+01	-1.2856E+01	-2.6511E+01
-1.75	-3.6003E+01	-8.7635E+00	-2.0711E+01
-2.00	-2.7979E+01	-4.6594E+00	-1.4818E+01
-2.50	-1.3757E+01	2.4275E+00	-4.4837E+00
-3.00	-1.5552E+00	8.2014E+00	4.2002E+00
-3.50	8.5700E+00	1.2680E+01	1.1219E+01
-4.00	1.6542E+01	1.5861E+01	1.6536E+01
-5.00	2.6532E+01	1.8824E+01	2.2573E+01
-5.50	2.8876E+01	1.8886E+01	2.3602E+01
-6.00	2.9742E+01	1.8225E+01	2.3561E+01
-8.00	2.3457E+01	1.1618E+01	1.6844E+01
-10.00	1.1922E+01	4.5332E+00	7.6343E+00
-12.00	3.3652E+00	5.0447E-01	1.5988E+00
-14.00	-4.9145E-01	-7.2900E-01	-7.1712E-01
-16.00	-1.2211E+00	-6.2361E-01	-9.0631E-01
-18.00	-7.7424E-01	-2.5820E-01	-4.6973E-01
-20.00	-2.6551E-01	-3.6971E-02	-1.1877E-01
-22.00	-1.0786E-02	2.7849E-02	2.0569E-02
-24.00	4.8838E-02	2.3237E-02	3.6412E-02
-26.00	3.2791E-02	7.7119E-03	1.7457E-02
-28.00	7.5467E-03	-6.7336E-04	1.3086E-03
-29.00	-1.6135E-03	-1.6389E-03	-3.0619E-03

**Table A.18: 100°F - Trends in Central Pile Bending Moment Due to Changes in Soil Properties (Refer Figure 4.16)**

<b>Depth from pile top</b>	<b>LD 100°F</b>	<b>DD 100°F</b>	<b>DcD 100°F</b>
<b>(ft)</b>	<b>(kip-ft)</b>	<b>(kip-ft)</b>	<b>(kip-ft)</b>
0.00	-1.2037E+02	-5.6674E+01	-8.7638E+01
-1.00	-7.5799E+01	-3.1353E+01	-5.2844E+01
-1.50	-5.5589E+01	-1.9759E+01	-3.7003E+01
-1.75	-4.6168E+01	-1.4462E+01	-2.9675E+01
-2.00	-3.6469E+01	-9.1105E+00	-2.2186E+01
-2.50	-1.9205E+01	2.1727E-01	-8.9606E+00
-3.00	-4.2700E+00	7.9596E+00	2.3047E+00
-3.50	8.2537E+00	1.4117E+01	1.1569E+01
-4.00	1.8262E+01	1.8666E+01	1.8770E+01
-5.00	3.1238E+01	2.3466E+01	2.7501E+01
-5.50	3.4552E+01	2.4026E+01	2.9361E+01
-6.00	3.6065E+01	2.3615E+01	2.9839E+01
-8.00	2.9829E+01	1.6208E+01	2.2798E+01
-10.00	1.6111E+01	7.0767E+00	1.1307E+01
-12.00	5.1975E+00	1.3201E+00	3.0358E+00
-14.00	-1.7313E-01	-7.9223E-01	-5.9280E-01
-16.00	-1.4978E+00	-8.9725E-01	-1.2180E+00
-18.00	-1.0912E+00	-4.4771E-01	-7.4916E-01
-20.00	-4.3987E-01	-1.0633E-01	-2.4909E-01
-22.00	-6.1174E-02	2.4012E-02	-5.2725E-03
-24.00	5.4860E-02	3.5917E-02	4.8850E-02
-26.00	4.9105E-02	1.6351E-02	3.1546E-02
-28.00	1.8409E-02	1.6135E-03	7.5721E-03
-29.00	5.8189E-03	-1.3086E-03	-2.2869E-04

**Table A.19: Displacement at the Pile Top in Central Pile vs.  $\Delta T$  (Refer Figure 4.17)**

<b>Temperature</b>	<b>LD</b>	<b>DD</b>	<b>DcD</b>
<b>(°F)</b>	<b>(in)</b>	<b>(in)</b>	<b>(in)</b>
<b>60</b>	0.24628	0.12372	0.1735
<b>80</b>	0.33257	0.19211	0.25335
<b>100</b>	0.42313	0.25784	0.33649

**Table A.20: Maximum Bending Moment in Central Pile vs.  $\Delta T$  (Refer Figure 4.18)**

<b>Temperature</b>	<b>LD</b>	<b>DD</b>	<b>DcD</b>
<b>(°F)</b>	<b>(kip-ft)</b>	<b>(kip-ft)</b>	<b>(kip-ft)</b>
<b>60</b>	-75.9242	-24.0998	-45.9080
<b>80</b>	-97.7928	-41.5776	-66.7959
<b>100</b>	-120.3846	-56.6738	-87.6380

**Table A.21: LD - Trends in Central Pile Bending Stress Due to Changes in Thermal Load (Refer Figure 4.19)**

<b>Depth from pile top</b>	<b>LD 60°F</b>	<b>LD 80°F</b>	<b>LD 100°F</b>
<b>(ft)</b>	<b>(ksi)</b>	<b>(ksi)</b>	<b>(ksi)</b>
0.00	-2.9880E+01	-3.8486E+01	-4.7377E+01
-1.00	-1.8188E+01	-2.3881E+01	-2.9848E+01
-1.50	-1.2870E+01	-1.7248E+01	-2.1899E+01
-1.75	-1.0414E+01	-1.4169E+01	-1.8193E+01
-2.00	-7.9091E+00	-1.1011E+01	-1.4378E+01
-2.50	-3.4940E+00	-5.4139E+00	-7.5858E+00
-3.00	2.4999E-01	-6.1203E-01	-1.7086E+00
-3.50	3.3121E+00	3.3727E+00	3.2211E+00
-4.00	5.6731E+00	6.5103E+00	7.1620E+00
-5.00	8.4856E+00	1.0442E+01	1.2277E+01
-5.50	9.0572E+00	1.1364E+01	1.3586E+01
-6.00	9.1749E+00	1.1705E+01	1.4186E+01
-8.00	6.7942E+00	9.2315E+00	1.1749E+01
-10.00	3.1676E+00	4.6918E+00	6.3560E+00
-12.00	7.1510E-01	1.3244E+00	2.0573E+00
-14.00	-2.5605E-01	-1.9341E-01	-6.2955E-02
-16.00	-3.5628E-01	-4.8057E-01	-5.8908E-01
-18.00	-1.8957E-01	-3.0470E-01	-4.3085E-01
-20.00	-4.9742E-02	-1.0449E-01	-1.7439E-01
-22.00	7.1315E-03	-4.2450E-03	-2.4665E-02
-24.00	1.4350E-02	1.9220E-02	2.1490E-02
-26.00	7.1210E-03	1.2905E-02	1.9415E-02
-28.00	3.1650E-04	2.9700E-03	7.3500E-03
-29.00	-1.9130E-03	-6.3500E-04	2.3800E-03

**Table A.22: DD - Trends in Central Pile Bending Stress Due to Changes in Thermal Load (Refer Figure 4.19)**

<b>Depth from pile top</b>	<b>DD 60°F</b>	<b>DD 80°F</b>	<b>DD 100°F</b>
<b>(ft)</b>	<b>(ksi)</b>	<b>(ksi)</b>	<b>(ksi)</b>
0.00	-9.4845E+00	-1.6363E+01	-2.2304E+01
-1.00	-4.3734E+00	-8.6148E+00	-1.2339E+01
-1.50	-2.0171E+00	-5.0594E+00	-7.7761E+00
-1.75	-9.6789E-01	-3.4489E+00	-5.6916E+00
-2.00	6.8547E-02	-1.8337E+00	-3.5854E+00
-2.50	1.8240E+00	9.5535E-01	8.5505E-02
-3.00	3.1987E+00	3.2276E+00	3.1325E+00
-3.50	4.2073E+00	4.9903E+00	5.5556E+00
-4.00	4.8572E+00	6.2422E+00	7.3459E+00
-5.00	5.2532E+00	7.4081E+00	9.2349E+00
-5.50	5.0915E+00	7.4325E+00	9.4554E+00
-6.00	4.7603E+00	7.1726E+00	9.2937E+00
-8.00	2.6605E+00	4.5723E+00	6.3788E+00
-10.00	8.2867E-01	1.7840E+00	2.7850E+00
-12.00	-3.9235E-02	1.9854E-01	5.1954E-01
-14.00	-2.1253E-01	-2.8690E-01	-3.1178E-01
-16.00	-1.2937E-01	-2.4542E-01	-3.5311E-01
-18.00	-3.7605E-02	-1.0162E-01	-1.7620E-01
-20.00	2.1870E-03	-1.4550E-02	-4.1845E-02
-22.00	7.9840E-03	1.0960E-02	9.4500E-03
-24.00	3.9490E-03	9.1450E-03	1.4135E-02
-26.00	6.7400E-04	3.0350E-03	6.4350E-03
-28.00	-4.7900E-04	-2.6500E-04	6.3500E-04
-29.00	-5.2700E-04	-6.4500E-04	-5.1500E-04

**Table A.23: DcD - Trends in Central Pile Bending Stress Due to Changes in Thermal Load (Refer Figure 4.19)**

<b>Depth from pile top</b>	<b>DcD 60°F</b>	<b>DcD 80°F</b>	<b>DcD 100°F</b>
<b>(ft)</b>	<b>(ksi)</b>	<b>(ksi)</b>	<b>(ksi)</b>
0.00	-1.8067E+01	-2.6287E+01	-3.4490E+01
-1.00	-1.0118E+01	-1.5400E+01	-2.0797E+01
-1.50	-6.4818E+00	-1.0433E+01	-1.4562E+01
-1.75	-4.8268E+00	-8.1508E+00	-1.1679E+01
-2.00	-3.1596E+00	-5.8318E+00	-8.7313E+00
-2.50	-2.6570E-01	-1.7645E+00	-3.5264E+00
-3.00	2.1161E+00	1.6530E+00	9.0703E-01
-3.50	3.9900E+00	4.4151E+00	4.5531E+00
-4.00	5.3522E+00	6.5076E+00	7.3869E+00
-5.00	6.7278E+00	8.8838E+00	1.0823E+01
-5.50	6.8484E+00	9.2885E+00	1.1555E+01
-6.00	6.6771E+00	9.2726E+00	1.1743E+01
-8.00	4.3518E+00	6.6288E+00	8.9720E+00
-10.00	1.7206E+00	3.0045E+00	4.4497E+00
-12.00	2.0604E-01	6.2922E-01	1.1947E+00
-14.00	-2.6081E-01	-2.8222E-01	-2.3330E-01
-16.00	-2.2494E-01	-3.5668E-01	-4.7934E-01
-18.00	-9.2029E-02	-1.8486E-01	-2.9483E-01
-20.00	-1.2449E-02	-4.6740E-02	-9.8030E-02
-22.00	1.0199E-02	8.0950E-03	-2.0750E-03
-24.00	8.2390E-03	1.4330E-02	1.9225E-02
-26.00	2.7055E-03	6.8700E-03	1.2415E-02
-28.00	-5.3150E-04	5.1500E-04	2.9800E-03
-29.00	-1.2775E-03	-1.2050E-03	-9.0000E-05

**Table A.24: 60°F – Trends in Central Pile Bending Stress Due to Changes in Soil Properties (Refer Figure 4.20)**

<b>Depth from pile top</b>	<b>LD 60°F</b>	<b>DD 60°F</b>	<b>DcD 60°F</b>
<b>(ft)</b>	<b>(ksi)</b>	<b>(ksi)</b>	<b>(ksi)</b>
0.00	-2.9880E+01	-9.4845E+00	-1.8067E+01
-1.00	-1.8188E+01	-4.3734E+00	-1.0118E+01
-1.50	-1.2870E+01	-2.0171E+00	-6.4818E+00
-1.75	-1.0414E+01	-9.6789E-01	-4.8268E+00
-2.00	-7.9091E+00	6.8547E-02	-3.1596E+00
-2.50	-3.4940E+00	1.8240E+00	-2.6570E-01
-3.00	2.4999E-01	3.1987E+00	2.1161E+00
-3.50	3.3121E+00	4.2073E+00	3.9900E+00
-4.00	5.6731E+00	4.8572E+00	5.3522E+00
-5.00	8.4856E+00	5.2532E+00	6.7278E+00
-5.50	9.0572E+00	5.0915E+00	6.8484E+00
-6.00	9.1749E+00	4.7603E+00	6.6771E+00
-8.00	6.7942E+00	2.6605E+00	4.3518E+00
-10.00	3.1676E+00	8.2867E-01	1.7206E+00
-12.00	7.1510E-01	-3.9235E-02	2.0604E-01
-14.00	-2.5605E-01	-2.1253E-01	-2.6081E-01
-16.00	-3.5628E-01	-1.2937E-01	-2.2494E-01
-18.00	-1.8957E-01	-3.7605E-02	-9.2029E-02
-20.00	-4.9742E-02	2.1870E-03	-1.2449E-02
-22.00	7.1315E-03	7.9840E-03	1.0199E-02
-24.00	1.4350E-02	3.9490E-03	8.2390E-03
-26.00	7.1210E-03	6.7400E-04	2.7055E-03
-28.00	3.1650E-04	-4.7900E-04	-5.3150E-04
-29.00	-1.9130E-03	-5.2700E-04	-1.2775E-03

**Table A.25: 80°F – Trends in Central Pile Bending Stress Due to Changes in Soil Properties (Refer Figure 4.20)**

<b>Depth from pile top</b>	<b>LD 80°F</b>	<b>DD 80°F</b>	<b>DcD 80°F</b>
<b>(ft)</b>	<b>(ksi)</b>	<b>(ksi)</b>	<b>(ksi)</b>
0.00	-3.8486E+01	-1.6363E+01	-2.6287E+01
-1.00	-2.3881E+01	-8.6148E+00	-1.5400E+01
-1.50	-1.7248E+01	-5.0594E+00	-1.0433E+01
-1.75	-1.4169E+01	-3.4489E+00	-8.1508E+00
-2.00	-1.1011E+01	-1.8337E+00	-5.8318E+00
-2.50	-5.4139E+00	9.5535E-01	-1.7645E+00
-3.00	-6.1203E-01	3.2276E+00	1.6530E+00
-3.50	3.3727E+00	4.9903E+00	4.4151E+00
-4.00	6.5103E+00	6.2422E+00	6.5076E+00
-5.00	1.0442E+01	7.4081E+00	8.8838E+00
-5.50	1.1364E+01	7.4325E+00	9.2885E+00
-6.00	1.1705E+01	7.1726E+00	9.2726E+00
-8.00	9.2315E+00	4.5723E+00	6.6288E+00
-10.00	4.6918E+00	1.7840E+00	3.0045E+00
-12.00	1.3244E+00	1.9854E-01	6.2922E-01
-14.00	-1.9341E-01	-2.8690E-01	-2.8222E-01
-16.00	-4.8057E-01	-2.4542E-01	-3.5668E-01
-18.00	-3.0470E-01	-1.0162E-01	-1.8486E-01
-20.00	-1.0449E-01	-1.4550E-02	-4.6740E-02
-22.00	-4.2450E-03	1.0960E-02	8.0950E-03
-24.00	1.9220E-02	9.1450E-03	1.4330E-02
-26.00	1.2905E-02	3.0350E-03	6.8700E-03
-28.00	2.9700E-03	-2.6500E-04	5.1500E-04
-29.00	-6.3500E-04	-6.4500E-04	-1.2050E-03

**Table A.26: 100°F – Trends in Central Pile Bending Stress Due to Changes in Soil Properties (Refer Figure 4.20)**

<b>Depth from pile top</b>	<b>LD 100°F</b>	<b>DD 100°F</b>	<b>DcD 100°F</b>
<b>(ft)</b>	<b>(ksi)</b>	<b>(ksi)</b>	<b>(ksi)</b>
0.00	-4.7377E+01	-2.2304E+01	-3.4490E+01
-1.00	-2.9848E+01	-1.2339E+01	-2.0797E+01
-1.50	-2.1899E+01	-7.7761E+00	-1.4562E+01
-1.75	-1.8193E+01	-5.6916E+00	-1.1679E+01
-2.00	-1.4378E+01	-3.5854E+00	-8.7313E+00
-2.50	-7.5858E+00	8.5505E-02	-3.5264E+00
-3.00	-1.7086E+00	3.1325E+00	9.0703E-01
-3.50	3.2211E+00	5.5556E+00	4.5531E+00
-4.00	7.1620E+00	7.3459E+00	7.3869E+00
-5.00	1.2277E+01	9.2349E+00	1.0823E+01
-5.50	1.3586E+01	9.4554E+00	1.1555E+01
-6.00	1.4186E+01	9.2937E+00	1.1743E+01
-8.00	1.1749E+01	6.3788E+00	8.9720E+00
-10.00	6.3560E+00	2.7850E+00	4.4497E+00
-12.00	2.0573E+00	5.1954E-01	1.1947E+00
-14.00	-6.2955E-02	-3.1178E-01	-2.3330E-01
-16.00	-5.8908E-01	-3.5311E-01	-4.7934E-01
-18.00	-4.3085E-01	-1.7620E-01	-2.9483E-01
-20.00	-1.7439E-01	-4.1845E-02	-9.8030E-02
-22.00	-2.4665E-02	9.4500E-03	-2.0750E-03
-24.00	2.1490E-02	1.4135E-02	1.9225E-02
-26.00	1.9415E-02	6.4350E-03	1.2415E-02
-28.00	7.3500E-03	6.3500E-04	2.9800E-03
-29.00	2.3800E-03	-5.1500E-04	-9.0000E-05

**Table A.27: Maximum Bending Stress in Central Pile vs.  $\Delta T$  (Refer Figure 4.21)**

Temperature	LD	DD	DcD
°F	(ksi)	(ksi)	(ksi)
60	-29.8799	-9.4845	-18.0670
80	-38.4862	-16.3628	-26.2874
100	-47.3772	-22.3039	-34.4898

**Table A.28: LD – Trends in Soil Pressure on Abutment Due to Changes in Thermal Load (Refer Figure 4.22)**

Depth from Abutment Top	60°F	80°F	100°F
(in)	lb/in <sup>2</sup>	lb/in <sup>2</sup>	lb/in <sup>2</sup>
0.00	0.0000	0.0000	0.0000
13.53	0.9064	1.0728	1.1398
39.58	2.6516	3.1383	3.3344
55.70	3.7315	4.4165	4.6924
83.91	5.6213	6.6533	7.0690
96.00	6.4313	7.6119	8.0875

**Table A.29: DD – Trends in Soil Pressure on Abutment Due to Changes in Thermal Load (Refer Figure 4.22)**

Depth from Abutment Top	60°F	80°F	100°F
(in)	lb/in <sup>2</sup>	lb/in <sup>2</sup>	lb/in <sup>2</sup>
0.00	0.0000	0.0000	0.0000
13.53	3.9791	4.4142	5.0380
39.58	11.6404	12.9130	14.7381
55.70	16.3812	18.1721	20.7405
83.91	24.6777	27.3756	31.2448
96.00	28.2333	31.3200	35.7467

**Table A.30: DcD – Trends in Soil Pressure on Abutment Due to Changes in Thermal Load (Refer Figure 4.22)**

<b>Depth from Abutment Top</b>	<b>60°F</b>	<b>80°F</b>	<b>100°F</b>
<b>(in)</b>	<b>lb/in<sup>2</sup></b>	<b>lb/in<sup>2</sup></b>	<b>lb/in<sup>2</sup></b>
0.00	0.0000	0.0000	0.0000
13.53	2.6806	2.9381	3.1672
39.58	7.8418	8.5949	9.2653
55.70	11.0356	12.0954	13.0388
83.91	16.6247	18.2213	19.6425
96.00	19.0200	20.8467	22.4727

**Table A.31: 60°F – Trends in Soil Pressure on Abutment Due to Changes in Soil Properties (Refer Figure 4.23)**

<b>Depth from Abutment Top</b>	<b>LD</b>	<b>DD</b>	<b>DcD</b>
<b>(in)</b>	<b>lb/in<sup>2</sup></b>	<b>lb/in<sup>2</sup></b>	<b>lb/in<sup>2</sup></b>
0.00	0.0000	0.0000	0.0000
13.53	0.9064	3.9791	2.6806
39.58	2.6516	11.6404	7.8418
55.70	3.7315	16.3812	11.0356
83.91	5.6213	24.6777	16.6247
96.00	6.4313	28.2333	19.0200

**Table A.32: 80°F – Trends in Soil Pressure on Abutment Due to Changes in Soil Properties (Refer Figure 4.23)**

<b>Depth from Abutment Top</b>	<b>LD</b>	<b>DD</b>	<b>DcD</b>
<b>(in)</b>	<b>lb/in<sup>2</sup></b>	<b>lb/in<sup>2</sup></b>	<b>lb/in<sup>2</sup></b>
0.00	0.0000	0.0000	0.0000
13.53	1.0728	4.4142	2.9381
39.58	3.1383	12.9130	8.5949
55.70	4.4165	18.1721	12.0954
83.91	6.6533	27.3756	18.2213
96.00	7.6119	31.3200	20.8467

**Table A.33: 100°F – Trends in Soil Pressure on Abutment Due to Changes in Soil Properties (Refer Figure 4.23)**

<b>Depth from Abutment Top</b>	<b>LD</b>	<b>DD</b>	<b>DcD</b>
<b>(in)</b>	<b>lb/in<sup>2</sup></b>	<b>lb/in<sup>2</sup></b>	<b>lb/in<sup>2</sup></b>
0.00	0.0000	0.0000	0.0000
13.53	1.1398	5.0380	3.1672
39.58	3.3344	14.7381	9.2653
55.70	4.6924	20.7405	13.0388
83.91	7.0690	31.2448	19.6425
96.00	8.0875	35.7467	22.4727

**Table A.34: LD - Longitudinal Displacement Comparison of Central Pile vs. End Pile (Refer Figure 4.24)**

	Central pile			End pile		
Depth from pile top	LD 60°F	LD 80°F	LD 100°F	LD 60°F	LD 80°F	LD 100°F
(ft)	(in)	(in)	(in)	(in)	(in)	(in)
0	2.463E-01	3.326E-01	4.231E-01	2.528E-01	3.450E-01	4.414E-01
-2	1.892E-01	2.599E-01	3.353E-01	1.916E-01	2.665E-01	3.461E-01
-4	1.043E-01	1.485E-01	1.968E-01	1.050E-01	1.516E-01	2.024E-01
-6	3.902E-02	5.951E-02	8.291E-02	3.915E-02	6.077E-02	8.544E-02
-8	5.187E-03	1.071E-02	1.778E-02	5.231E-03	1.110E-02	1.864E-02
-10	-5.422E-03	-6.482E-03	-7.067E-03	-5.382E-03	-6.436E-03	-6.964E-03
-12	-5.200E-03	-7.602E-03	-1.012E-02	-5.170E-03	-7.656E-03	-1.025E-02
-14	-2.492E-03	-4.139E-03	-6.072E-03	-2.478E-03	-4.192E-03	-6.202E-03
-16	-6.038E-04	-1.270E-03	-2.156E-03	-6.042E-04	-1.300E-03	-2.228E-03
-18	1.053E-04	5.994E-06	-1.929E-04	9.732E-05	-8.921E-06	-2.213E-04
-20	1.827E-04	2.636E-04	3.275E-04	1.723E-04	2.536E-04	3.167E-04
-22	9.162E-05	1.683E-04	2.591E-04	8.243E-05	1.595E-04	2.520E-04
-24	2.150E-05	5.498E-05	1.031E-04	1.697E-05	5.053E-05	1.002E-04
-26	-2.410E-06	3.531E-06	1.592E-05	2.588E-06	1.100E-05	2.668E-05
-28	-3.132E-06	-5.686E-06	-7.557E-06	1.511E-05	1.902E-05	2.378E-05
-29	-1.928E-33	-3.197E-33	-4.487E-33	8.504E-33	1.056E-32	1.260E-32

**Table A.35: DD - Longitudinal Displacement Comparison of Central Pile vs. End Pile  
(Refer Figure 4.24)**

Depth from pile top (ft)	Central pile			End pile		
	DD 60°F (in)	DD 80°F (in)	DD 100°F (in)	DD 60°F (in)	DD 80°F (in)	DD 100°F (in)
0	1.237E-01	1.921E-01	2.578E-01	1.023E-01	1.704E-01	2.418E-01
-2	7.975E-02	1.320E-01	1.828E-01	5.835E-02	1.085E-01	1.628E-01
-4	3.603E-02	6.542E-02	9.512E-02	2.283E-02	4.974E-02	8.072E-02
-6	9.138E-03	2.043E-02	3.283E-02	3.867E-03	1.336E-02	2.575E-02
-8	-1.461E-03	4.767E-05	2.449E-03	-2.250E-03	-1.576E-03	4.614E-04
-10	-2.994E-03	-4.713E-03	-6.102E-03	-2.329E-03	-4.175E-03	-5.813E-03
-12	-1.693E-03	-3.368E-03	-5.112E-03	-1.056E-03	-2.569E-03	-4.371E-03
-14	-4.927E-04	-1.305E-03	-2.296E-03	-2.149E-04	-8.588E-04	-1.810E-03
-16	1.349E-05	-1.773E-04	-4.927E-04	5.849E-05	-5.030E-05	-3.178E-04
-18	9.430E-05	1.386E-04	1.402E-04	6.618E-05	1.249E-04	1.483E-04
-20	5.004E-05	1.161E-04	1.850E-04	2.373E-05	7.838E-05	1.476E-04
-22	1.143E-05	4.298E-05	8.727E-05	2.470E-07	1.986E-05	5.726E-05
-24	-1.919E-06	4.378E-06	1.845E-05	-3.478E-06	-2.196E-06	7.124E-06
-26	-2.629E-06	-4.755E-06	-4.687E-06	3.547E-06	3.224E-06	4.318E-06
-28	-1.127E-06	-3.948E-06	-6.687E-06	1.662E-05	2.054E-05	2.424E-05
-29	-1.430E-33	-2.621E-33	-3.786E-33	9.258E-33	1.144E-32	1.359E-32

**Table A.36: DcD - Longitudinal Displacement Comparison of Central Pile vs. End Pile  
(Refer Figure 4.24)**

Depth from pile top	Central pile			End pile		
	DcD 60°F	DcD 80°F	DcD 100°F	DcD 60°F	DcD 80°F	DcD 100°F
(ft)	(in)	(in)	(in)	(in)	(in)	(in)
0	1.735E-01	2.533E-01	3.365E-01	1.637E-01	2.482E-01	3.359E-01
-2	1.236E-01	1.872E-01	2.549E-01	1.117E-01	1.781E-01	2.485E-01
-4	6.262E-02	1.005E-01	1.424E-01	5.442E-02	9.337E-02	1.365E-01
-6	2.014E-02	3.632E-02	5.553E-02	1.641E-02	3.267E-02	5.220E-02
-8	5.481E-04	3.937E-03	8.938E-03	-3.017E-04	2.885E-03	7.828E-03
-10	-4.196E-03	-5.770E-03	-6.918E-03	-3.898E-03	-5.625E-03	-6.884E-03
-12	-3.060E-03	-5.194E-03	-7.524E-03	-2.631E-03	-4.802E-03	-7.184E-03
-14	-1.185E-03	-2.422E-03	-3.986E-03	-9.496E-04	-2.161E-03	-3.726E-03
-16	-1.594E-04	-5.599E-04	-1.180E-03	-9.534E-05	-4.655E-04	-1.069E-03
-18	1.244E-04	1.209E-04	3.544E-05	1.136E-04	1.235E-04	4.980E-05
-20	1.023E-04	1.851E-04	2.654E-04	7.924E-05	1.614E-04	2.440E-04
-22	3.673E-05	9.068E-05	1.640E-04	2.222E-05	7.065E-05	1.410E-04
-24	3.240E-06	2.051E-05	5.191E-05	-1.306E-06	1.229E-05	4.108E-05
-26	-3.773E-06	-3.447E-06	1.827E-06	1.817E-06	3.480E-06	1.034E-05
-28	-1.989E-06	-4.925E-06	-7.529E-06	1.616E-05	1.967E-05	2.356E-05
-29	-1.629E-33	-2.866E-33	-4.121E-33	8.947E-33	1.104E-32	1.313E-32

**Table A.37: LD – Bending Moment Comparison of Central Pile vs. End Pile (Refer Figure 4.25)**

Depth from pile top  (ft)	Central pile			End pile		
	LD 60°F (kip-ft)	LD 80°F (kip-ft)	LD 100°F (kip-ft)	LD 60°F (kip-ft)	LD 80°F (kip-ft)	LD 100°F (kip-ft)
0	-7.59E+01	-9.78E+01	-1.20E+02	-7.28E+01	-9.50E+01	-1.18E+02
-1	-4.62E+01	-6.07E+01	-7.58E+01	-4.43E+01	-5.91E+01	-7.45E+01
-1.5	-3.27E+01	-4.38E+01	-5.56E+01	-3.09E+01	-4.22E+01	-5.41E+01
-1.75	-2.65E+01	-3.60E+01	-4.62E+01	-2.47E+01	-3.43E+01	-4.46E+01
-2	-2.01E+01	-2.80E+01	-3.65E+01	-1.85E+01	-2.64E+01	-3.50E+01
-2.5	-8.88E+00	-1.38E+01	-1.93E+01	-7.45E+00	-1.23E+01	-1.77E+01
-3	6.35E-01	-1.56E+00	-4.34E+00	1.86E+00	-1.74E-01	-2.83E+00
-3.5	8.42E+00	8.57E+00	8.18E+00	9.44E+00	9.83E+00	9.64E+00
-4	1.44E+01	1.65E+01	1.82E+01	1.53E+01	1.77E+01	1.96E+01
-5	2.16E+01	2.65E+01	3.12E+01	2.21E+01	2.74E+01	3.24E+01
-5.5	2.30E+01	2.89E+01	3.45E+01	2.34E+01	2.97E+01	3.57E+01
-6	2.33E+01	2.97E+01	3.60E+01	2.37E+01	3.05E+01	3.71E+01
-8	1.73E+01	2.35E+01	2.99E+01	1.74E+01	2.39E+01	3.06E+01
-10	8.05E+00	1.19E+01	1.62E+01	8.12E+00	1.22E+01	1.66E+01
-12	1.82E+00	3.37E+00	5.23E+00	1.88E+00	3.53E+00	5.51E+00
-14	-6.51E-01	-4.91E-01	-1.60E-01	-5.97E-01	-4.05E-01	-2.68E-02
-16	-9.05E-01	-1.22E+00	-1.50E+00	-8.68E-01	-1.18E+00	-1.44E+00
-18	-4.82E-01	-7.74E-01	-1.09E+00	-4.60E-01	-7.54E-01	-1.08E+00
-20	-1.26E-01	-2.66E-01	-4.43E-01	-1.16E-01	-2.55E-01	-4.33E-01
-22	1.81E-02	-1.08E-02	-6.27E-02	2.23E-02	-4.01E-03	-5.43E-02
-24	3.65E-02	4.88E-02	5.46E-02	3.91E-02	5.42E-02	6.26E-02
-26	1.81E-02	3.28E-02	4.93E-02	1.92E-02	3.46E-02	5.21E-02
-28	8.04E-04	7.55E-03	1.87E-02	-1.12E-02	-9.25E-03	-2.54E-03
-29	-4.86E-03	-1.61E-03	6.05E-03	-3.07E-02	-3.58E-02	-3.60E-02

**Table A.38: DD – Bending Moment Comparison of Central Pile vs. End Pile (Refer Figure 4.25)**

Depth from pile top  (ft)	Central pile			End pile		
	DD 60°F (kip-ft)	DD 80°F (kip-ft)	DD 100°F (kip-ft)	DD 60°F (kip-ft)	DD 80°F (kip-ft)	DD 100°F (kip-ft)
0	-2.41E+01	-4.16E+01	-5.67E+01	-8.51E+00	-2.48E+01	-4.09E+01
-1	-1.11E+01	-2.19E+01	-3.14E+01	-1.10E+00	-1.09E+01	-2.09E+01
-1.5	-5.13E+00	-1.29E+01	-1.98E+01	2.87E+00	-3.85E+00	-1.10E+01
-1.75	-2.46E+00	-8.76E+00	-1.45E+01	4.58E+00	-6.98E-01	-6.51E+00
-2	1.74E-01	-4.66E+00	-9.11E+00	6.16E+00	2.34E+00	-2.09E+00
-2.5	4.63E+00	2.43E+00	2.17E-01	8.74E+00	7.53E+00	5.56E+00
-3	8.13E+00	8.20E+00	7.96E+00	1.06E+01	1.16E+01	1.18E+01
-3.5	1.07E+01	1.27E+01	1.41E+01	1.17E+01	1.45E+01	1.65E+01
-4	1.23E+01	1.59E+01	1.87E+01	1.22E+01	1.64E+01	1.99E+01
-5	1.33E+01	1.88E+01	2.35E+01	1.16E+01	1.75E+01	2.29E+01
-5.5	1.29E+01	1.89E+01	2.40E+01	1.07E+01	1.70E+01	2.29E+01
-6	1.21E+01	1.82E+01	2.36E+01	9.57E+00	1.59E+01	2.20E+01
-8	6.76E+00	1.16E+01	1.62E+01	4.54E+00	9.23E+00	1.42E+01
-10	2.11E+00	4.53E+00	7.08E+00	1.03E+00	3.17E+00	5.80E+00
-12	-9.97E-02	5.04E-01	1.32E+00	-3.21E-01	9.24E-02	8.62E-01
-14	-5.40E-01	-7.29E-01	-7.92E-01	-4.27E-01	-6.71E-01	-7.83E-01
-16	-3.29E-01	-6.24E-01	-8.97E-01	-1.99E-01	-4.71E-01	-7.57E-01
-18	-9.56E-02	-2.58E-01	-4.48E-01	-3.58E-02	-1.62E-01	-3.40E-01
-20	5.56E-03	-3.70E-02	-1.06E-01	1.54E-02	-5.84E-03	-6.09E-02
-22	2.03E-02	2.78E-02	2.40E-02	1.48E-02	2.84E-02	3.29E-02
-24	1.00E-02	2.32E-02	3.59E-02	7.66E-03	2.03E-02	3.56E-02
-26	1.71E-03	7.71E-03	1.64E-02	4.68E-03	8.59E-03	1.61E-02
-28	-1.22E-03	-6.73E-04	1.61E-03	-8.84E-03	-1.29E-02	-1.61E-02
-29	-1.34E-03	-1.64E-03	-1.31E-03	-2.63E-02	-3.30E-02	-4.07E-02

**Table A.39: DcD – Bending Moment Comparison of Central Pile vs. End Pile (Refer Figure 4.25)**

Depth from pile top	Central pile			End pile		
	DcD 60°F	DcD 80°F	DcD 100°F	DcD 60°F	DcD 80°F	DcD 100°F
(ft)	(kip-ft)	(kip-ft)	(kip-ft)	(kip-ft)	(kip-ft)	(kip-ft)
0	-4.59E+01	-6.68E+01	-8.76E+01	-3.60E+01	-5.72E+01	-7.81E+01
-1	-2.57E+01	-3.91E+01	-5.28E+01	-1.93E+01	-3.29E+01	-4.67E+01
-1.5	-1.65E+01	-2.65E+01	-3.70E+01	-1.11E+01	-2.12E+01	-3.16E+01
-1.75	-1.23E+01	-2.07E+01	-2.97E+01	-7.44E+00	-1.58E+01	-2.46E+01
-2	-8.03E+00	-1.48E+01	-2.22E+01	-3.81E+00	-1.04E+01	-1.76E+01
-2.5	-6.75E-01	-4.48E+00	-8.96E+00	2.46E+00	-1.06E+00	-5.27E+00
-3	5.38E+00	4.20E+00	2.30E+00	7.52E+00	6.74E+00	5.18E+00
-3.5	1.01E+01	1.12E+01	1.16E+01	1.14E+01	1.30E+01	1.37E+01
-4	1.36E+01	1.65E+01	1.88E+01	1.41E+01	1.76E+01	2.02E+01
-5	1.71E+01	2.26E+01	2.75E+01	1.65E+01	2.26E+01	2.79E+01
-5.5	1.74E+01	2.36E+01	2.94E+01	1.65E+01	2.32E+01	2.94E+01
-6	1.70E+01	2.36E+01	2.98E+01	1.58E+01	2.29E+01	2.96E+01
-8	1.11E+01	1.68E+01	2.28E+01	9.81E+00	1.59E+01	2.21E+01
-10	4.37E+00	7.63E+00	1.13E+01	3.67E+00	7.00E+00	1.08E+01
-12	5.24E-01	1.60E+00	3.04E+00	3.26E-01	1.38E+00	2.84E+00
-14	-6.63E-01	-7.17E-01	-5.93E-01	-6.15E-01	-6.93E-01	-5.76E-01
-16	-5.72E-01	-9.06E-01	-1.22E+00	-4.80E-01	-8.18E-01	-1.13E+00
-18	-2.34E-01	-4.70E-01	-7.49E-01	-1.78E-01	-4.04E-01	-6.77E-01
-20	-3.16E-02	-1.19E-01	-2.49E-01	-1.37E-02	-8.96E-02	-2.11E-01
-22	2.59E-02	2.06E-02	-5.27E-03	2.64E-02	2.77E-02	8.51E-03
-24	2.09E-02	3.64E-02	4.89E-02	1.97E-02	3.76E-02	5.35E-02
-26	6.87E-03	1.75E-02	3.15E-02	7.94E-03	1.79E-02	3.19E-02
-28	-1.35E-03	1.31E-03	7.57E-03	-1.09E-02	-1.36E-02	-1.27E-02
-29	-3.25E-03	-3.06E-03	-2.29E-04	-2.77E-02	-3.57E-02	-4.13E-02

**Table A.40: LD – Bending Stress Comparison of Central Pile vs. End Pile (Refer Figure 4.26)**

Depth from pile top	Central pile			End pile		
	LD 60°F	LD 80°F	LD 100°F	LD 60°F	LD 80°F	LD 100°F
(ft)	(ksi)	(ksi)	(ksi)	(ksi)	(ksi)	(ksi)
0	-2.99E+01	-3.85E+01	-4.74E+01	-2.86E+01	-3.74E+01	-4.64E+01
-1	-1.82E+01	-2.39E+01	-2.98E+01	-1.74E+01	-2.32E+01	-2.93E+01
-1.5	-1.29E+01	-1.72E+01	-2.19E+01	-1.22E+01	-1.66E+01	-2.13E+01
-1.75	-1.04E+01	-1.42E+01	-1.82E+01	-9.72E+00	-1.35E+01	-1.76E+01
-2	-7.91E+00	-1.10E+01	-1.44E+01	-7.27E+00	-1.04E+01	-1.38E+01
-2.5	-3.49E+00	-5.41E+00	-7.59E+00	-2.93E+00	-4.82E+00	-6.97E+00
-3	2.50E-01	-6.12E-01	-1.71E+00	7.31E-01	-6.85E-02	-1.11E+00
-3.5	3.31E+00	3.37E+00	3.22E+00	3.72E+00	3.87E+00	3.79E+00
-4	5.67E+00	6.51E+00	7.16E+00	6.01E+00	6.96E+00	7.71E+00
-5	8.49E+00	1.04E+01	1.23E+01	8.70E+00	1.08E+01	1.28E+01
-5.5	9.06E+00	1.14E+01	1.36E+01	9.23E+00	1.17E+01	1.40E+01
-6	9.17E+00	1.17E+01	1.42E+01	9.31E+00	1.20E+01	1.46E+01
-8	6.79E+00	9.23E+00	1.17E+01	6.84E+00	9.41E+00	1.21E+01
-10	3.17E+00	4.69E+00	6.36E+00	3.19E+00	4.80E+00	6.55E+00
-12	7.15E-01	1.32E+00	2.06E+00	7.39E-01	1.39E+00	2.17E+00
-14	-2.56E-01	-1.93E-01	-6.30E-02	-2.35E-01	-1.59E-01	-1.06E-02
-16	-3.56E-01	-4.81E-01	-5.89E-01	-3.42E-01	-4.64E-01	-5.68E-01
-18	-1.90E-01	-3.05E-01	-4.31E-01	-1.81E-01	-2.97E-01	-4.23E-01
-20	-4.97E-02	-1.04E-01	-1.74E-01	-4.57E-02	-1.00E-01	-1.71E-01
-22	7.13E-03	-4.24E-03	-2.47E-02	8.77E-03	-1.58E-03	-2.14E-02
-24	1.44E-02	1.92E-02	2.15E-02	1.54E-02	2.13E-02	2.46E-02
-26	7.12E-03	1.29E-02	1.94E-02	7.56E-03	1.36E-02	2.05E-02
-28	3.17E-04	2.97E-03	7.35E-03	-4.41E-03	-3.64E-03	-1.00E-03
-29	-1.91E-03	-6.35E-04	2.38E-03	-1.21E-02	-1.41E-02	-1.41E-02

**Table A.41: DD – Bending Stress Comparison of Central Pile vs. End Pile (Refer Figure 4.26)**

Depth from pile top  (ft)	Central pile			End pile		
	DD 60°F  (ksi)	DD 80°F  (ksi)	DD 100°F  (ksi)	DD 60°F  (ksi)	DD 80°F  (ksi)	DD 100°F  (ksi)
0	-9.48E+00	-1.64E+01	-2.23E+01	-3.35E+00	-9.75E+00	-1.61E+01
-1	-4.37E+00	-8.61E+00	-1.23E+01	-4.32E-01	-4.29E+00	-8.24E+00
-1.5	-2.02E+00	-5.06E+00	-7.78E+00	1.13E+00	-1.51E+00	-4.33E+00
-1.75	-9.68E-01	-3.45E+00	-5.69E+00	1.80E+00	-2.75E-01	-2.56E+00
-2	6.85E-02	-1.83E+00	-3.59E+00	2.42E+00	9.23E-01	-8.24E-01
-2.5	1.82E+00	9.55E-01	8.55E-02	3.44E+00	2.96E+00	2.19E+00
-3	3.20E+00	3.23E+00	3.13E+00	4.16E+00	4.55E+00	4.63E+00
-3.5	4.21E+00	4.99E+00	5.56E+00	4.60E+00	5.72E+00	6.51E+00
-4	4.86E+00	6.24E+00	7.35E+00	4.79E+00	6.47E+00	7.83E+00
-5	5.25E+00	7.41E+00	9.23E+00	4.55E+00	6.90E+00	9.02E+00
-5.5	5.09E+00	7.43E+00	9.46E+00	4.20E+00	6.69E+00	9.00E+00
-6	4.76E+00	7.17E+00	9.29E+00	3.77E+00	6.27E+00	8.66E+00
-8	2.66E+00	4.57E+00	6.38E+00	1.79E+00	3.63E+00	5.59E+00
-10	8.29E-01	1.78E+00	2.79E+00	4.05E-01	1.25E+00	2.28E+00
-12	-3.92E-02	1.99E-01	5.20E-01	-1.26E-01	3.64E-02	3.39E-01
-14	-2.13E-01	-2.87E-01	-3.12E-01	-1.68E-01	-2.64E-01	-3.08E-01
-16	-1.29E-01	-2.45E-01	-3.53E-01	-7.82E-02	-1.85E-01	-2.98E-01
-18	-3.76E-02	-1.02E-01	-1.76E-01	-1.41E-02	-6.37E-02	-1.34E-01
-20	2.19E-03	-1.46E-02	-4.18E-02	6.05E-03	-2.30E-03	-2.39E-02
-22	7.98E-03	1.10E-02	9.45E-03	5.81E-03	1.12E-02	1.29E-02
-24	3.95E-03	9.14E-03	1.41E-02	3.02E-03	7.97E-03	1.40E-02
-26	6.74E-04	3.04E-03	6.43E-03	1.84E-03	3.38E-03	6.35E-03
-28	-4.79E-04	-2.65E-04	6.35E-04	-3.48E-03	-5.07E-03	-6.35E-03
-29	-5.27E-04	-6.45E-04	-5.15E-04	-1.04E-02	-1.30E-02	-1.60E-02

**Table A.42: DcD – Bending Stress Comparison of Central Pile vs. End Pile (Refer Figure 4.26)**

Depth from pile top	Central pile			End pile		
	DcD 60°F	DcD 80°F	DcD 100°F	DcD 60°F	DcD 80°F	DcD 100°F
(ft)	(ksi)	(ksi)	(ksi)	(ksi)	(ksi)	(ksi)
0	-1.81E+01	-2.63E+01	-3.45E+01	-1.42E+01	-2.25E+01	-3.08E+01
-1	-1.01E+01	-1.54E+01	-2.08E+01	-7.58E+00	-1.30E+01	-1.84E+01
-1.5	-6.48E+00	-1.04E+01	-1.46E+01	-4.38E+00	-8.33E+00	-1.24E+01
-1.75	-4.83E+00	-8.15E+00	-1.17E+01	-2.93E+00	-6.22E+00	-9.70E+00
-2	-3.16E+00	-5.83E+00	-8.73E+00	-1.50E+00	-4.11E+00	-6.94E+00
-2.5	-2.66E-01	-1.76E+00	-3.53E+00	9.68E-01	-4.17E-01	-2.07E+00
-3	2.12E+00	1.65E+00	9.07E-01	2.96E+00	2.65E+00	2.04E+00
-3.5	3.99E+00	4.42E+00	4.55E+00	4.49E+00	5.10E+00	5.39E+00
-4	5.35E+00	6.51E+00	7.39E+00	5.56E+00	6.93E+00	7.97E+00
-5	6.73E+00	8.88E+00	1.08E+01	6.51E+00	8.88E+00	1.10E+01
-5.5	6.85E+00	9.29E+00	1.16E+01	6.49E+00	9.14E+00	1.16E+01
-6	6.68E+00	9.27E+00	1.17E+01	6.23E+00	9.02E+00	1.16E+01
-8	4.35E+00	6.63E+00	8.97E+00	3.86E+00	6.25E+00	8.69E+00
-10	1.72E+00	3.00E+00	4.45E+00	1.44E+00	2.76E+00	4.24E+00
-12	2.06E-01	6.29E-01	1.19E+00	1.28E-01	5.45E-01	1.12E+00
-14	-2.61E-01	-2.82E-01	-2.33E-01	-2.42E-01	-2.73E-01	-2.27E-01
-16	-2.25E-01	-3.57E-01	-4.79E-01	-1.89E-01	-3.22E-01	-4.46E-01
-18	-9.20E-02	-1.85E-01	-2.95E-01	-7.00E-02	-1.59E-01	-2.67E-01
-20	-1.24E-02	-4.67E-02	-9.80E-02	-5.38E-03	-3.53E-02	-8.31E-02
-22	1.02E-02	8.10E-03	-2.08E-03	1.04E-02	1.09E-02	3.35E-03
-24	8.24E-03	1.43E-02	1.92E-02	7.76E-03	1.48E-02	2.10E-02
-26	2.71E-03	6.87E-03	1.24E-02	3.13E-03	7.04E-03	1.25E-02
-28	-5.32E-04	5.15E-04	2.98E-03	-4.31E-03	-5.35E-03	-5.00E-03
-29	-1.28E-03	-1.20E-03	-9.00E-05	-1.09E-02	-1.40E-02	-1.63E-02

**Table A.43: Maximum Axial Stress in the Central Girder vs.  $\Delta T$  (Refer Figure 4.27)**

Temperature	LD	DD	DcD
°F	(ksi)	(ksi)	(ksi)
60	-11.921	-20.635	-17.125
80	-14.729	-24.836	-20.382
100	-17.255	-29.031	-23.440

**Table A.44: LD 60°F - Convergence of Displacement (Refer Figure 4.28, 4.29)**

Iteration number	$\delta_R$ (in)	$\delta_T$ (in)
1	-0.07921	0.406998
2	0.053599	0.264671
3	0.068331	0.248467
4	0.070553	0.246024
5	0.070888	0.245657

**Table A.45: DD 60°F - Convergence of Displacement (Refer Figure 4-28, 4-29)**

Iteration number	$\delta_R$ (in)	$\delta_T$ (in)
1	-0.07921	0.406998
2	0.113627	0.194366
3	0.153794	0.149109
4	0.167546	0.13363
5	0.173385	0.127047
6	0.176034	0.124067
7	0.177139	0.122831

**Table A.46: DcD 60°F - Convergence of Displacement (Refer Figure 4.28, 4.29)**

<b>Iteration number</b>	<b><math>\delta_R</math> (in)</b>	<b><math>\delta_T</math> (in)</b>
<b>1</b>	-0.07921	0.406998
<b>2</b>	0.091306	0.220633
<b>3</b>	0.121915	0.186321
<b>4</b>	0.130577	0.176636
<b>5</b>	0.133277	0.173621
<b>6</b>	0.134086	0.172722

**Table A.47: LD 80°F - Convergence of Displacement (Refer Figure 4.30, 4.31)**

<b>Iteration number</b>	<b><math>\delta_R</math> (in)</b>	<b><math>\delta_T</math> (in)</b>
<b>1</b>	-0.09226	0.529168
<b>2</b>	0.071107	0.354317
<b>3</b>	0.089139	0.334475
<b>4</b>	0.091659	0.33171
<b>5</b>	0.091927	0.331421

**Table A.48: DD 80°F - Convergence of Displacement (Refer Figure 4.30, 4.31)**

<b>Iteration number</b>	<b><math>\delta_R</math> (in)</b>	<b><math>\delta_T</math> (in)</b>
<b>1</b>	-0.09226	0.529168
<b>2</b>	0.145376	0.267649
<b>3</b>	0.19152	0.215859
<b>4</b>	0.205701	0.199989
<b>5</b>	0.210976	0.19408
<b>6</b>	0.213025	0.191788
<b>7</b>	0.213761	0.190968

**Table A.49: DcD 80°F - Convergence of Displacement (Refer Figure 4.30, 4.31)**

Iteration number	$\delta_R$ (in)	$\delta_T$ (in)
1	-0.09226	0.529168
2	0.113991	0.304394
3	0.148324	0.266079
4	0.157349	0.255992
5	0.159963	0.253071
6	0.16063	0.252332

**Table A.50: LD 100°F - Convergence of Displacement (Refer Figure 4.32, 4.33)**

Iteration number	$\delta_R$ (in)	$\delta_T$ (in)
1	-0.1053	0.651337
2	0.086982	0.445738
3	0.106212	0.424673
4	0.108634	0.422026
5	0.108945	0.421686

**Table A.51: DD 100°F - Convergence of Displacement (Refer Figure 4.32, 4.33)**

Iteration number	$\delta_R$ (in)	$\delta_T$ (in)
1	-0.1053	0.651337
2	0.170029	0.34911
3	0.225668	0.286628
4	0.24306	0.267136
5	0.249465	0.259949
6	0.251836	0.257296
7	0.252627	0.256417

**Table A.52: DcD 100°F - Convergence of Displacement (Refer Figure 4.32, 4.33)**

<b>Iteration number</b>	<b><math>\delta_R</math> (in)</b>	<b><math>\delta_T</math> (in)</b>
<b>1</b>	-0.1053	0.651337
<b>2</b>	0.134238	0.390856
<b>3</b>	0.172604	0.348115
<b>4</b>	0.181786	0.337871
<b>5</b>	0.184163	0.335228
<b>6</b>	0.18471	0.334622

**Table A.53: Trends in Longitudinal Displacement Due to Changes in Soil Properties – Bridge with Approach Slab (Refer Figure 4.34)**

<b>Depth from abutment top</b>	<b>LD 80°F – Approach Slab</b>	<b>DD 80°F – Approach Slab</b>
<b>(ft)</b>	<b>(in)</b>	<b>(in)</b>
-0.70833	4.2555E-01	4.0013E-01
-1.83573	4.0292E-01	3.6504E-01
-4.00667	3.7168E-01	3.0801E-01
-5.35000	3.6171E-01	2.8158E-01
-7.70083	3.6050E-01	2.5148E-01
-8.70833	3.6397E-01	2.4335E-01
-10.70833	2.8907E-01	1.7927E-01
-12.70833	1.6806E-01	9.5722E-02
-14.70833	6.9266E-02	3.4208E-02
-16.70833	1.3786E-02	3.4492E-03
-18.70833	-6.5897E-03	-5.5951E-03
-20.70833	-8.5402E-03	-4.9201E-03
-22.70833	-4.8679E-03	-2.2522E-03
-24.70833	-1.5998E-03	-4.9910E-04
-26.70833	-6.4881E-05	1.2542E-04
-28.70833	2.8880E-04	1.7510E-04
-30.70833	2.0151E-04	8.3315E-05
-32.70833	7.1628E-05	1.7253E-05
-34.70833	6.4818E-06	-7.1164E-06
-36.70833	-8.9518E-06	-1.3165E-05
-37.70833	-5.0649E-33	-7.0620E-33

**Table A.54: Displacement Comparison – Bridge with and without Approach Slab (Refer Figure 4.35)**

<b>Depth from abutment top</b>	<b>LD 80°F</b>	<b>LD 80°F – Approach Slab</b>	<b>DD 80°F</b>	<b>DD 80°F – Approach Slab</b>
<b>(ft)</b>	<b>(in)</b>	<b>(in)</b>	<b>(in)</b>	<b>(in)</b>
-0.70833	4.2335E-01	4.2555E-01	4.0013E-01	4.0473E-01
-1.83573	3.9618E-01	4.0292E-01	3.6504E-01	3.6095E-01
-4.00667	3.5699E-01	3.7168E-01	3.0801E-01	2.8886E-01
-5.35000	3.4204E-01	3.6171E-01	2.8158E-01	2.5298E-01
-7.70083	3.3234E-01	3.6050E-01	2.5148E-01	2.0692E-01
-8.70833	3.3229E-01	3.6397E-01	2.4335E-01	1.9211E-01
-10.70833	2.5957E-01	2.8907E-01	1.7927E-01	1.3200E-01
-12.70833	1.4814E-01	1.6806E-01	9.5722E-02	6.5417E-02
-14.70833	5.9263E-02	6.9266E-02	3.4208E-02	2.0432E-02
-16.70833	1.0592E-02	1.3786E-02	3.4492E-03	4.7672E-05
-18.70833	-6.5035E-03	-6.5897E-03	-5.5951E-03	-4.7133E-03
-20.70833	-7.5813E-03	-8.5402E-03	-4.9201E-03	-3.3682E-03
-22.70833	-4.1137E-03	-4.8679E-03	-2.2522E-03	-1.3046E-03
-24.70833	-1.2553E-03	-1.5998E-03	-4.9910E-04	-1.7728E-04
-26.70833	1.0509E-05	-6.4881E-05	1.2542E-04	1.3863E-04
-28.70833	2.6325E-04	2.8880E-04	1.7510E-04	1.1612E-04
-30.70833	1.6692E-04	2.0151E-04	8.3315E-05	4.2985E-05
-32.70833	5.4133E-05	7.1628E-05	1.7253E-05	4.3776E-06
-34.70833	3.2664E-06	6.4818E-06	-7.1164E-06	-4.7551E-06
-36.70833	-5.6996E-06	-8.9518E-06	-1.3165E-05	-3.9478E-06
-37.70833	-3.1958E-33	-5.0649E-33	-7.0620E-33	-2.6206E-33

**Table A.55: Trends in Central Pile Bending Moment Due to Changes in Soil Properties  
(Refer Figure 4.36)**

<b>Depth from pile top (ft)</b>	<b>LD 80°F – Approach Slab (kip-ft)</b>	<b>DD 80°F – Approach Slab (kip-ft)</b>
0	-1.1014E+02	-6.4874E+01
-1	-6.9199E+01	-3.7576E+01
-1.5	-5.0717E+01	-2.5352E+01
-1.75	-4.2112E+01	-1.9737E+01
-2	-3.3263E+01	-1.4032E+01
-2.5	-1.7535E+01	-4.0400E+00
-3	-3.9675E+00	4.3400E+00
-3.5	7.3687E+00	1.1096E+01
-4	1.6382E+01	1.6196E+01
-5	2.7938E+01	2.1930E+01
-5.5	3.0815E+01	2.2869E+01
-6	3.2057E+01	2.2777E+01
-8	2.6042E+01	1.6135E+01
-10	1.3666E+01	7.2166E+00
-12	4.1336E+00	1.4485E+00
-14	-3.5386E-01	-7.1999E-01
-16	-1.3288E+00	-8.6634E-01
-18	-8.9775E-01	-4.3824E-01
-20	-3.3194E-01	-1.0583E-01
-22	-2.9170E-02	2.1573E-02
-24	5.1214E-02	3.2830E-02
-26	3.8470E-02	1.3963E-02
-28	1.2286E-02	4.3070E-03
-29	3.3160E-03	6.6447E-03

**Table A.56: Pile Bending Moment Comparison – Bridge with and without Approach Slab (Refer Figure 4.37)**

Depth from pile top	LD 80°F	LD 80°F – Approach Slab	DD 80°F	DD 80°F – Approach Slab
(ft)	(kip-ft)	(kip-ft)	(kip-ft)	(kip-ft)
0	-9.7802E+01	-1.1014E+02	-4.1578E+01	-6.4874E+01
-1	-6.0651E+01	-6.9199E+01	-2.1890E+01	-3.7576E+01
-1.5	-4.3781E+01	-5.0717E+01	-1.2856E+01	-2.5352E+01
-1.75	-3.5950E+01	-4.2112E+01	-8.7635E+00	-1.9737E+01
-2	-2.7920E+01	-3.3263E+01	-4.6594E+00	-1.4032E+01
-2.5	-1.3688E+01	-1.7535E+01	2.4275E+00	-4.0400E+00
-3	-1.4835E+00	-3.9675E+00	8.2014E+00	4.3400E+00
-3.5	8.6407E+00	7.3687E+00	1.2680E+01	1.1096E+01
-4	1.6608E+01	1.6382E+01	1.5861E+01	1.6196E+01
-5	2.6578E+01	2.7938E+01	1.8824E+01	2.1930E+01
-5.5	2.8909E+01	3.0815E+01	1.8886E+01	2.2869E+01
-6	2.9762E+01	3.2057E+01	1.8225E+01	2.2777E+01
-8	2.3433E+01	2.6042E+01	1.1618E+01	1.6135E+01
-10	1.1883E+01	1.3666E+01	4.5332E+00	7.2166E+00
-12	3.3370E+00	4.1336E+00	5.0447E-01	1.4485E+00
-14	-5.0253E-01	-3.5386E-01	-7.2900E-01	-7.1999E-01
-16	-1.2208E+00	-1.3288E+00	-6.2361E-01	-8.6634E-01
-18	-7.7041E-01	-8.9775E-01	-2.5820E-01	-4.3824E-01
-20	-2.6257E-01	-3.3194E-01	-3.6971E-02	-1.0583E-01
-22	-9.6430E-03	-2.9170E-02	2.7849E-02	2.1573E-02
-24	4.8889E-02	5.1214E-02	2.3237E-02	3.2830E-02
-26	3.2537E-02	3.8470E-02	7.7119E-03	1.3963E-02
-28	7.3434E-03	1.2286E-02	-6.7336E-04	4.3070E-03
-29	-1.7406E-03	3.3160E-03	-1.6389E-03	6.6447E-03

**Table A.57: Trends in Central Pile Bending Stress Due to Changes in Soil Properties – Bridge with Approach Slab (Refer Figure 4.38)**

<b>Depth from pile top (ft)</b>	<b>LD 80°F – Approach Slab (ksi)</b>	<b>DD 80°F – Approach Slab (ksi)</b>
0	-4.3345E+01	-2.5531E+01
-1	-2.7233E+01	-1.4788E+01
-1.5	-1.9960E+01	-9.9774E+00
-1.75	-1.6573E+01	-7.7675E+00
-2	-1.3091E+01	-5.5224E+00
-2.5	-6.9008E+00	-1.5899E+00
-3	-1.5614E+00	1.7080E+00
-3.5	2.8999E+00	4.3669E+00
-4	6.4470E+00	6.3739E+00
-5	1.0995E+01	8.6306E+00
-5.5	1.2127E+01	9.0002E+00
-6	1.2616E+01	8.9639E+00
-8	1.0249E+01	6.3497E+00
-10	5.3782E+00	2.8401E+00
-12	1.6268E+00	5.7005E-01
-14	-1.3926E-01	-2.8335E-01
-16	-5.2295E-01	-3.4095E-01
-18	-3.5331E-01	-1.7247E-01
-20	-1.3064E-01	-4.1650E-02
-22	-1.1480E-02	8.4900E-03
-24	2.0155E-02	1.2920E-02
-26	1.5140E-02	5.4950E-03
-28	4.8350E-03	1.6950E-03
-29	1.3050E-03	2.6150E-03

**Table A.58: Pile Bending Stress Comparison – Bridge with and without Approach Slab  
(Refer Figure 4.39)**

<b>Depth from pile top</b>	<b>LD 80°F</b>	<b>LD 80°F – Approach Slab</b>	<b>DD 80°F</b>	<b>DD 80°F – Approach Slab</b>
<b>(ft)</b>	<b>(ksi)</b>	<b>(ksi)</b>	<b>(ksi)</b>	<b>(ksi)</b>
0	-9.7802E+01	-4.3345E+01	-4.1578E+01	-2.5531E+01
-1	-6.0651E+01	-2.7233E+01	-2.1890E+01	-1.4788E+01
-1.5	-4.3781E+01	-1.9960E+01	-1.2856E+01	-9.9774E+00
-1.75	-3.5950E+01	-1.6573E+01	-8.7635E+00	-7.7675E+00
-2	-2.7920E+01	-1.3091E+01	-4.6594E+00	-5.5224E+00
-2.5	-1.3688E+01	-6.9008E+00	2.4275E+00	-1.5899E+00
-3	-1.4835E+00	-1.5614E+00	8.2014E+00	1.7080E+00
-3.5	8.6407E+00	2.8999E+00	1.2680E+01	4.3669E+00
-4	1.6608E+01	6.4470E+00	1.5861E+01	6.3739E+00
-5	2.6578E+01	1.0995E+01	1.8824E+01	8.6306E+00
-5.5	2.8909E+01	1.2127E+01	1.8886E+01	9.0002E+00
-6	2.9762E+01	1.2616E+01	1.8225E+01	8.9639E+00
-8	2.3433E+01	1.0249E+01	1.1618E+01	6.3497E+00
-10	1.1883E+01	5.3782E+00	4.5332E+00	2.8401E+00
-12	3.3370E+00	1.6268E+00	5.0447E-01	5.7005E-01
-14	-5.0253E-01	-1.3926E-01	-7.2900E-01	-2.8335E-01
-16	-1.2208E+00	-5.2295E-01	-6.2361E-01	-3.4095E-01
-18	-7.7041E-01	-3.5331E-01	-2.5820E-01	-1.7247E-01
-20	-2.6257E-01	-1.3064E-01	-3.6971E-02	-4.1650E-02
-22	-9.6430E-03	-1.1480E-02	2.7849E-02	8.4900E-03
-24	4.8889E-02	2.0155E-02	2.3237E-02	1.2920E-02
-26	3.2537E-02	1.5140E-02	7.7119E-03	5.4950E-03
-28	7.3434E-03	4.8350E-03	-6.7336E-04	1.6950E-03
-29	-1.7406E-03	1.3050E-03	-1.6389E-03	2.6150E-03

**Table A.59: LD 80°F – Soil Pressure on Abutment Comparison – Bridge with and without Approach Slab (Refer Figure 4.40)**

<b>Depth from abutment top</b>	<b>LD 80°F</b>	<b>Depth from abutment top</b>	<b>LD 80°F – Approach Slab</b>
<b>(in)</b>	<b>(ksi)</b>	<b>(in)</b>	<b>(ksi)</b>
0	0.0000	-3.5	1.2364
-13.53	1.0728	-17.775	2.3112
-39.58	3.1383	-39.58	3.8876
-59.73	4.7360	-59.73	5.3445
-83.91	6.6533	-83.91	7.0926

**Table A.60: DD 80°F – Soil Pressure on Abutment Comparison – Bridge with and without Approach Slab (Refer Figure 4.40)**

<b>Depth from abutment top</b>	<b>DD 80°F</b>	<b>Depth from abutment top</b>	<b>DD 80°F – Approach Slab</b>
<b>(in)</b>	<b>(ksi)</b>	<b>(in)</b>	<b>(ksi)</b>
0	0.0000	-3.5	5.0465
-13.53	4.4142	-17.775	9.7313
-39.58	12.9130	-39.58	16.6229
-59.73	19.4869	-59.73	22.9914
-83.91	27.3756	-83.91	30.6336

**Table A.61: Pile Bending Moment Comparison – Central Pile vs. End (Refer Figure 4.41)**

<b>Depth from pile top</b>	<b>LD 80°F – Central Pile</b>	<b>LD 80°F – End Pile</b>	<b>DD 80°F – Central Pile</b>	<b>DD 80°F – End Pile</b>
<b>(ft)</b>	<b>(kip-ft)</b>	<b>(kip-ft)</b>	<b>(kip-ft)</b>	<b>(kip-ft)</b>
0	-1.1014E+02	-1.0627E+02	-6.4874E+01	-52.80723
-1	-6.9199E+01	-6.7233E+01	-3.7576E+01	-30.075959
-1.5	-5.0717E+01	-4.8907E+01	-2.5352E+01	-19.163016
-1.75	-4.2112E+01	-4.0377E+01	-1.9737E+01	-14.175932
-2	-3.3263E+01	-3.1686E+01	-1.4032E+01	-9.1981447
-2.5	-1.7535E+01	-1.6216E+01	-4.0400E+00	-0.5056303
-3	-3.9675E+00	-2.9051E+00	4.3400E+00	6.68575984
-3.5	7.3687E+00	8.1936E+00	1.1096E+01	12.3909922
-4	1.6382E+01	1.6994E+01	1.6196E+01	16.5936139
-5	2.7938E+01	2.8213E+01	2.1930E+01	2.10E+01
-5.5	3.0815E+01	3.0965E+01	2.2869E+01	21.5037471
-6	3.2057E+01	3.2108E+01	2.2777E+01	21.1112859
-8	2.6042E+01	2.5927E+01	1.6135E+01	1.43E+01
-10	1.3666E+01	1.3593E+01	7.2166E+00	6.10E+00
-12	4.1336E+00	4.1441E+00	1.4485E+00	1.05E+00
-14	-3.5386E-01	-2.9690E-01	-7.1999E-01	-7.16E-01
-16	-1.3288E+00	-1.2684E+00	-8.6634E-01	-7.53E-01
-18	-8.9775E-01	-8.5514E-01	-4.3824E-01	-3.52E-01
-20	-3.3194E-01	-3.0900E-01	-1.0583E-01	-7.05E-02
-22	-2.9170E-02	-1.8651E-02	2.1573E-02	2.79E-02
-24	5.1214E-02	5.7007E-02	3.2830E-02	3.28E-02
-26	3.8470E-02	4.0313E-02	1.3963E-02	0.01505533
-28	1.2286E-02	-5.5902E-03	4.3070E-03	-0.0091602
-29	3.3160E-03	-3.3427E-02	6.6447E-03	-0.0255115

**Table A.62: LD 80°F - Convergence of Displacement (Refer Figure 4.42, 4.43)**

<b>Iteration number</b>	<b><math>\delta_R</math> (in)</b>	<b><math>\delta_T</math> (in)</b>
<b>1</b>	-0.08688	0.527753
<b>2</b>	0.044541	0.378162
<b>3</b>	0.053991	0.351426
<b>4</b>	0.055281	0.349911

**Table A.63: DD 80°F - Convergence of Displacement (Refer Figure 4.42, 4.43)**

<b>Iteration number</b>	<b><math>\delta_R</math> (in)</b>	<b><math>\delta_T</math> (in)</b>
<b>1</b>	-0.08688	0.527753
<b>2</b>	0.102767	0.300232
<b>3</b>	0.138048	0.256706
<b>4</b>	0.148698	0.243559
<b>5</b>	0.149542	0.242641
<b>6</b>	0.149875	0.242219

**Table A.64: Soil Pressure on Approach (Refer Figure 4.44)**

<b>Distance from abutment top (in)</b>	<b>LD 80°F (ksi)</b>	<b>DD 80°F (ksi)</b>
6	1.1514	9.5174
18	0.5813	3.9052
30	0.1213	-0.0979
42	-0.2342	-2.7543
54	-0.4917	-4.3271
66	-0.6589	-5.0660
78	-0.7448	-5.1897
90	-0.7585	-4.8784
102	-0.7099	-4.2722
114	-0.6091	-3.4739
126	-0.4666	-2.5547
138	-0.2934	-1.5622
150	-0.1017	-0.5296

# K - TRAN

KANSAS TRANSPORTATION RESEARCH  
AND  
NEW - DEVELOPMENTS PROGRAM



A COOPERATIVE TRANSPORTATION RESEARCH PROGRAM BETWEEN:

KANSAS DEPARTMENT OF TRANSPORTATION



THE UNIVERSITY OF KANSAS



KANSAS STATE UNIVERSITY

